Fibre Bridging in Composite Laminates

Methods for the exclusion of the fibre bridging effect in composite structures under cyclic Mode I loading

Master's Thesis Report

Idriss Boul Boul

Delft University of Technology

TU Delft

Fibre Bridging in Composite Laminates

Methods for the exclusion of the fibre bridging effect in composite structures under cyclic Mode I loading

by

Idriss Boul Boul

to obtain the degree of Master of Science
at the Delft University of Technology,
to be defended publicly on Wednesday July 5, 2023 at 13:30.

Student number: 4591682
Project duration: September, 2022 - July, 2023
Thesis committee: Dr. ir. R.C. Alderliesten, TU Delft, chair
Dr. ir. J.A. Pascoe, TU Delft, supervisor
Dr. ing. S.G.P. Castro, TU Delft

Cover: Large-scale fibre bridging in a composite DCB specimen

TU Delft

Preface

These pages contain the research I conducted over the past months as part of my graduation project at the Delft University of Technology. This project marks the end of my time as a student of this wonderful institution. After completing my BSc degree at 3mE, I decided to pursue my childhood dream of studying Aerospace Engineering. I have not felt a moment of regret regarding this decision. Better yet, I have a tremendous feeling of gratitude for being able to develop myself at this university, which is only an hour's worth of cycling from my home town.

During my time at the Aerospace Engineering faculty, I formed meaningful friendships. I want to express my gratitude to my fellow MSc students, PhDs, AML colleagues, and others, for creating a joyful work environment. I couldn't have completed this project without a few key individuals, and I'd like to thank them now.

Firstly, I wish to extend a feeling of gratitude to my thesis supervisor, John-Alan Pascoe. Our weekly meetings and your active involvement have shaped this research into what it has become. Your expertise and mentorship have greatly contributed to both my academic and personal growth.

Furthermore, I would like to express my heartfelt appreciation to the technical staff at DASML (Victor, Johan, Alexander, Chantal and Dave) for their invaluable support in conducting my experiments. I also have to thank Dr Rafiullah Khan of the International Islamic University in Islamabad, Pakistan for the useful discussions regarding the thesis topic.

In humble appreciation of my origins as a student, I extend heartfelt gratitude to my cherished friends and esteemed colleagues at the IWS at 3mE. In particular, my dear friends Jurrian, Tjitze Karel and Daniel with whom I have shared great memories so far.

Last but certainly not least, I am deeply grateful to my loving family, my parents, my brother, and my sayang Vira, whose unwavering love and unconditional support have been my source of motivation.

Idriss Boul Boul
's-Gravenzande, June 2023

Abstract

In composite structures, delamination damage is typically the most common failure mechanism. Accurately characterizing the delamination behaviour of composite laminates is therefore crucial for predicting the fatigue safe-life of such structures. To this end, double-cantilever beam (DCB) composite specimens are used to measure the interlaminar fracture toughness and delamination growth rate under cyclic Mode I loading.

In unidirectional (UD) composite laminates, delamination planes may exhibit fibre nesting, leading to the development of the fibre bridging effect during delamination growth. This effect, which resists delamination, significantly increases the apparent fracture toughness of the laminate. However, fibre bridging is usually insignificant in multidirectional (MD) laminates, where delamination occurs between plies with different fibre orientations. Nesting typically does not happen in MD laminates. As a result, MD laminates should not be designed using fatigue resistance data obtained from UD specimens without first accounting for the fibre bridging effect. Neglecting fibre bridging exclusion can result in an overestimation of delamination resistance, leading to unsafe failure predictions.

This research investigated methods to exclude the fibre bridging effect in cyclic Mode I experiments with UD composite specimens. Existing literature suggested different approaches to account for this effect, aiming to create a ”zero-bridging” fatigue delamination resistance curve. The study examined methods such as cutting bridging fibres in-situ, constant-SERR experiments, specimen-specific extrapolation, and utilizing the Hartman-Schijve equation to describe fatigue delamination.

By examining different exclusion methods and understanding their limitations, this work contributed to enhancing the reliability of fatigue delamination predictions in composite specimens under laboratory conditions. This study compared methods to exclude the fibre bridging effect and assessed their merits in terms of ease of use, accuracy, and conservative predictions of delamination resistance. The results of this study suggest that a specimen-specific extrapolation method is a suitable approach to account for fibre bridging.

Keywords: composites, delamination, fatigue, mechanical testing, fibre bridging effect

Contents

Nomenclature

Abbreviations

Abbreviation	Definition
ASTM	American Society for Testing and Materials
DASML	Delft Aerospace Structures and Materials Laboratory
DCB	Double-cantilever beam
FRP	Fibre-reinforced polymer
ISO	International Organization for Standardization
LVDT	Linear variable differential transformer
MCC	Modified compliance calibration
MD	Multidirectional
PAN	Polyacrylonitrile
PTFE	Polytetrafluoroethylene (= Teflon)
R-curve	Delamination resistance curve
SERR	Strain energy release rate
UD	Unidirectional

Symbols

Symbol	Definition	Unit
$2h$	Specimen thickness	[mm]
α_i	Curve fitting coefficient	[-]
δ	Opening displacement	[mm]
δ_{max}	Maximum displacement during fatigue loading	[mm]
δ_{min}	Minimum displacement during fatigue loading	[mm]
a	Delamination length	[mm]
a_c	Cutting thread position	[mm]
$a - a_0$	Pre-crack delamination length	[mm]
a_0	Length of initial delamination, i.e. length of starter crack film	[mm]
a_{spec}	Distance between piano hinge axis and front specimen	[mm]
A	Constant in the Hartman-Schijve equation	[N/m]
A_0	Value of A when $a - a_0$ is zero	[N/m]
B	Specimen width	[mm]
C_i	Surface fitting coefficient	[-]
C	Compliance	[mm/N]
da/dN	Crack growth rate	[mm/cycle]
F	Large-displacement correction factor	[-]
G	SERR	[N/m]
G_{max}	Maximum value of SERR during a fatigue cycle	[N/m]
G_{min}	Minimum value of SERR during a fatigue cycle	[N/m]
G_{IC}	Interlaminar fracture toughness	[N/m]
$\Delta\sqrt{G}$	SERR range $\left(=\left(\sqrt{G_{\mathrm{max}}}-\sqrt{G_{\mathrm{min}}}\right)^2\right)$	[$\sqrt{}$(N/m)]
$\Delta\sqrt{G_{thr}}$	Constant in the Hartman-Schijve equation	[$\sqrt{}$(N/m)]
$\Delta\sqrt{G_{thr,0}}$	Value of $\Delta\sqrt{G_{thr}}$ when $a - a_0$ is zero	[$\sqrt{}$(N/m)]
L	Specimen length	[mm]
l_1	Distance from piano hinge axis to midplane	[mm]
N	Number of cycles	[cycle]
P	Load	[N]
R	Stress ratio	[-]
R_d	Displacement ratio	[-]

List of Figures

List of Tables

1 Introduction

Background

Since the start of the aviation era, the path to lightweight aircraft has seen the rise of new materials and structures [18, 36]. Fibre-reinforced polymer (FRP) laminated structures have become the standard choice in the aerospace industry due to their excellent mechanical properties and weight-saving capabilities [38]. Further development of aerospace composite materials can be found in multiple aspects, from the ease of certification [12] to manufacturing process improvements [37].

Historically, for laminated composite materials, the interlaminar and out-of-plane mechanical properties are considered major weak points in the design [68, 8]. A great obstacle to the application of composite materials is the relatively low interlaminar fracture toughness [52]. As a result, delamination is the most frequently occurring type of life-limiting failure mode for composite structures [4]. Whilst delaminations may develop during manufacturing, they may also result from impact damage and/or in-plane loading of the structure [17]. This leads to a reduction of the interlaminar mechanical properties of the structure. The inability to mitigate compressive forces gives rise to local or global buckling when the interlaminar stresses overcome the corresponding strength which is decreased as a result of the delaminations [57].

To measure the interlaminar fracture toughness a double-cantilever beam (DCB) composite specimen consisting of multiple plies is typically used [43]. At the mid-plane of this DCB specimen, the delamination propagates along the longest dimension of the specimen. The two adjacent plies at the mid-plane, which is the delamination interface, are of particular interest as their orientation influences the delamination behaviour [7]. The plies at the delamination interface might consist of different fibre orientations, which is known as a multidirectional (MD) interface. In the case of a unidirectional (UD) delamination interface, the fibre orientations of the two plies at the mid-plane, are the same.

Multidirectional composite laminates may introduce a bend-twist coupling causing the test to not be purely Mode I (opening tensile) [19]. This is undesirable as the to-be-measured properties are typically assigned for a single failure mode, denoted by either Mode I (opening tensile), Mode II (sliding) or Mode III (tearing). Unidirectional laminates with zero-degree fibre orientation do not have this unwanted bend-twist coupling. Therefore, UD laminates with zero-degree fibre orientations are used for measuring the Mode I interlaminar fracture toughness of a given composite material [10].

Delamination in such UD laminates however brings with it an effect which is prone to altering the data obtained in delamination experiments. In the wake of the delamination tip, fibres of the adjacent mid-plane plies may bridge the crack surface [33]. These bridging fibres are able to transfer considerable amounts of stress across the delamination plane [25]. Thereby disproving the classical notion that no loads are transferred in the wake of a delamination tip. The fibre bridging effect leads to an increase in the apparent Mode I interlaminar fracture toughness. Whilst this increase in a critical mechanical property might seem desirable, it is typically attributed to the experimental setup and not being reflective of in-service composites which are generally made of multidirectional (MD) laminates [55, 5].

Therefore, a composite structure with an MD laminate should not make use of fatigue data which is obtained with UD specimens without first excluding the contribution of the fibre bridging effect. Designing with unrealistic data due to fibre bridging should be avoided as it can lead to unconservative and unsafe designs. Methods are found in the relevant literature for excluding the fibre bridging effect. They range from altering the experimental setup to processing data to account for the bridging effect. All of them have the goal of reducing the obtained fatigue data to a case where the fibre bridging has no contribution, i.e. a ”zero-bridging” scenario. Up to now, these methods have not been directly compared to each other. Nor has an understanding been established of which method for the fibre exclusion methods provides the most conservative ”zero-bridging” depiction.

The present thesis attempts to unambiguously compare these methods for the exclusion of the fibre bridging effect by means of performing experiments on UD specimens made from the same composite material. In this way, scatter related to material properties is reduced. The resulting ”zero-bridging” fatigue delamination resistance curves obtained by employing various fibre briding exclusion methods are evaluated based on their respective abilities to reflect a ”zero-bridging” case. This evaluation will consist of determining not only the accuracy and conservativeness of the results but also the ease of use and straightforwardness of the different methods.

Report Outline

This thesis report is split into multiple chapters. Firstly, the prevailing literature concerning the topic will be explored and summarised in the Literature Study, Chapter 2. A research gap is identified and subsequently, a plan is provided with relevant research questions with the intent of answering said questions in Chapter 3. The path towards an answer to the posed research question is paved in the section on Methodologies, Chapter 4. Methods for analyzing the obtained data and presenting the finding can be found in the Data Analysis (Chapter 5). Next, the results of this research are presented along with a discussion in Chapter 6. Conclusions are drawn based on the results in Chapter 7 followed by recommendations for future research concerning the topic in Chapter 8.

2

Literature Study

This chapter provides a review of the relevant literature regarding the fibre bridging effect. The chapter explains what the fibre bridging effect signifies and how it influences data obtained in fatigue delamination experiments. Furthermore, this chapter presents the various methods which may be used to mitigate its impact, establishing a groundwork for the research presented in this thesis.

2.1. The Fibre Bridging Effect

In laminated fibre-reinforced composite materials, the phenomenon of fibre bridging occurs when the fibres of neighbouring plies bridge the crack plane in the wake of a delamination front [33]. The main result of this phenomenon is that bridging fibres may behave as crack-shielding entities, increasing the overall delamination resistance of the material during prolonged crack extension. This section contains background information about the fibre bridging effect, in particular its origin and influence in fatigue delamination experiments.

2.1.1. Origins of Fibre Bridging

To understand the influence of fibre bridging on fatigue delamination propagation of composite structures, its origin is first briefly discussed. Historically the onset of fibre bridging has been attributed to nesting which occurs during the manufacturing of a composite laminate [28]. During the nesting (Figure 2.1a), fibres of adjacent plies intermingle between their corresponding layers. As a result, for the delamination to propagate, the nested fibres must be pulled from the neighbouring layer [27], see Figure 2.1b. However, this explanation for the onset of the fibre bridging effect only relates to UD composite laminates according to Liu and Chen [35]. In their view, a second source of fibre bridging is related to the weak fibre/matrix interface or larger crack tip yield zone [50, 28]. This explanation may be more suitable for most instances of the fibre bridging effect. Whether or not the fibre bridging effect is an accurate term for the crack-shielding phenomenon occurring in MD composite laminates remains unclear. Nonetheless, the relevant standard regarding quasi-static delamination of composites [55] overlooks the second explanation for the origin of the fibre bridging effect.

Hu et al. [23] investigated the influence that the curing cycle has on the amount of fibre bridging which is observed during delamination growth. In their research, it was found that extending the curing time at elevated temperatures tends to reduce the amount of fibre bridging observed during fatigue delamination. A possible explanation for this effect is that the prolonged curing of the composite structures causes a decrease in heterogeneity in the strength of the fibre/matrix interface.

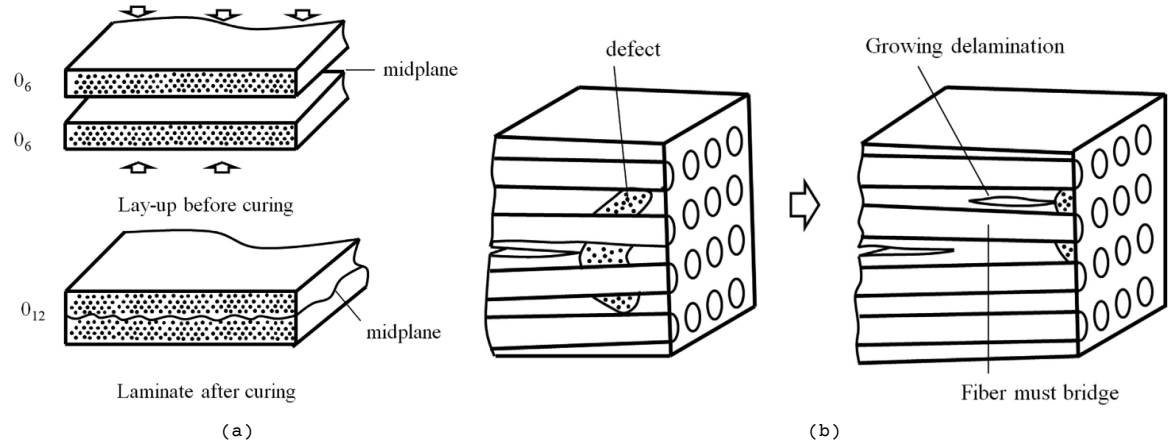

Figure 2.1: Schematic of nesting of fibres in adjacent plies causing the fibre bridging effect and a schematic of delamination migration leading to a bridging fibre [28].

2.1.2. R-curve Effect

Now that it is established what fibre bridging means and how it typically occurs, the next part would be understanding the consequences it has on material properties. The bridging mechanism changes the delamination resistance of a composite specimen. This means that the fracture toughness will increase for extended delamination propagation [56], resulting in a different delamination resistance curve (R-curve). The fibre bridging effect is said to cause this R-curve effect. Sørensen and Jacobsen [54] showed this behaviour and made a model to describe the effect, the results of which can be seen in Figure 2.2.

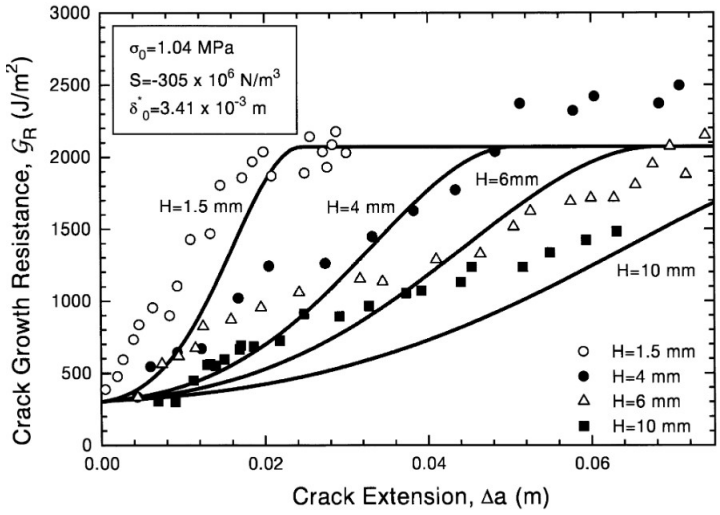

Figure 2.2: Crack growth resistance curves (R-curves) for materials which show fibre bridging with different specimen thickness [54].

The data points found by Sørensen and Jacobsen [54] show that after a certain delamination length a, a saturation of the fibre bridging effect occurs where the increase in fracture toughness is halted. A plateau is created and this represents the state where new bridging fibres are created near the crack tip at the same amount as they are broken when the crack opening displacement becomes too large. This occurs at the very left in

Figure 2.4 for instance.

Furthermore, Yao et al. [63] showed how the crack shielding effect of bridging fibres translates to adjusted fatigue data. Two specimens are considered, where in one specimen the bridging fibres are cut away, as per a method devised by Khan et al. [34]. The other specimen still has fibre bridging. In this manner, the fibre bridging effect becomes evident in Figure 2.3, where the bridging fibres cause the data of one of the specimens to shift to the right in the delamination resistance curve, meaning a higher resistance against delamination growth. The same fatigue loading ΔG will lead to a smaller crack growth rate, da/dN.

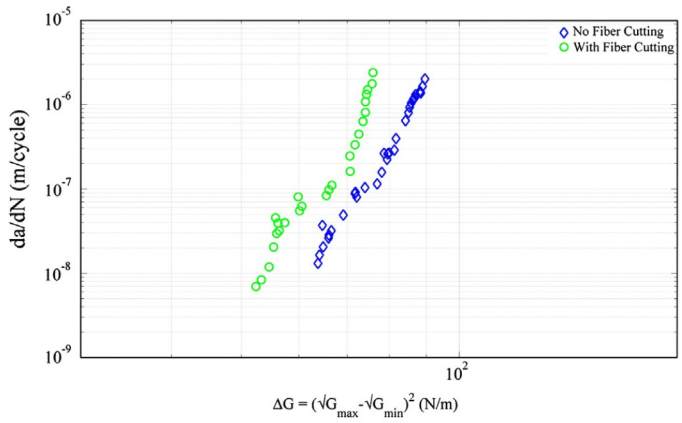

Figure 2.3: Fatigue delamination resistance curves for two specimens. One where the bridging fibres were removed and one where the fibres were not cut [63].

2.1.3. A Unidirectional Assumption

An early paper by Johnson et al. [28] on the topic of fibre bridging states that the effect of fibre bridging should be looked at in two ways. Firstly, the increased toughness properties due to fibre bridging may be representative of how fibre bridging could influence the properties of an actual composite structure given that fibre bridging also occurs in the structures. Since increased mechanical properties are almost always desired, the effect of fibre bridging should be predictable and quantifiable in order to make use of the increased resistance against delamination growth during the design phase. In cases where fibre bridging does not occur in structures, fatigue data related to laboratory tests where fibre bridging did occur might give the designer an unconservative and unsafe result. Moreover, in prevailing literature related to the topic of fibre bridging, there seems to be a consensus that fibre bridging is an artefact of Mode I testing of unidirectional specimen [40, 5, 55] and is rarely reported to occur under in-service conditions [2, 64, 9, 39]. ISO 15024 [55] and ASTM D5528 [5] leave no room for uncertainty on this topic. According to these standards, fibre bridging is considered to be an artefact of the DCB test on unidirectional laminates.

The second viewpoint that Johnson et al. [28] put forward is that fibre bridging is not desired when the interlaminar fracture toughness of a material is analyzed. Because of the lack of real-world occurrences of fibre bridging, efforts are made to develop methods for the exclusion of fibre bridging in testing conditions. These methods will be introduced and explored experimentally in this research.

The assumption that the fibre bridging effect might be an artefact of

laboratory conditions and that it is exclusive to unidirectional laminates might be short-sighted. To support this view a recent MSc thesis [44] on the topic of fibre orientations of the interface on fatigue delamination growth showed that the statement made in the ATSM D5528 standard [5] is unfounded. In his research, van der Panne [44] performed DCB tests on multiple specimens with dissimilar fibre orientations at the crack interface and found that fibre bridging is in fact not necessarily an artefact of the DCB test on unidirectional materials. Moreover, in all of the tested fibre orientations (including a 0//90 orientation), fibre bridging was reported resulting in an increase in the delamination resistance. In Figure 2.4, an example is shown of a multidirectional DCB specimen which clearly shows fibre bridging occurring. De Carvalho and Murri [13] claim that the fibre bridging effect is ”less predominant” in generic, multidirectional ply interfaces than in unidirectional specimens.

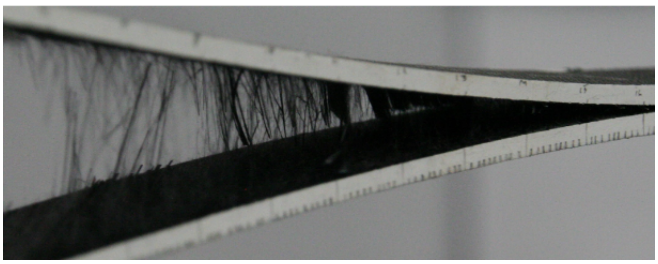

Figure 2.4: Image of a DCB test specimen with a multidirectional layup showing clear signs of fibre bridging [44].

It seems that the overall notion that fibre bridging is an artefact of the DCB testing of unidirectional specimens stems from the assumption that composite structures generally consist of multidirectional laminates and therefore show little to no fibre bridging. Firstly, as shown from recent literature [44], fibre bridging does occur in multidirectional laminates. Secondly, fibre bridging may occur in composite structures which do not consist of multidirectional laminates. Such unidirectional laminates can be found in large composite structures, for instance in wind turbine rotor blades. Sørensen et al. [53] considered the failure of bridged fibres for a unidirectional laminate which is typically used in wind turbine blades.

In summary, it may be concluded that the fibre bridging effect does not solely occur in UD composite laminates tested in laboratory conditions. This notion, put forward by multiple sources [40, 5, 55] is too simplistic. However, the influence of the fibre bridging effect in UD composite laminates on the corresponding delamination resistance is still of a high order. If the assumption that in-service composite components will fail to produce bridging fibres in the same order as UD composite laminates tested in laboratory conditions holds true, then an effort must be made to exclude the fibre bridging effect in the UD laminates. The increase in the apparent fracture toughness is then not reflective of the in-service delamination characteristics of the composite structures. Efforts are therefore made to exclude the fibre bridging effect from fatigue delamination experiments conducted on UD composite specimens.

2.2. Methodology for Fibre Bridging Exclusion

The effect of fibre bridging can be seen in data obtained in a Mode I fatigue testing campaign (see Figure 2.3). In cases where fibre bridging is not expected to occur in real-life composite structures, it would be unsafe to use fatigue delamination data where the effect does occur during the design phase. This indicates that there should be an effort to exclude or quantify the additional stresses related to fibre bridging. In this chapter, approaches for the exclusion of the fibre bridging effect are discussed.

2.2.1. Method I: Cutting Bridging Fibres

The fibre bridging effect is a physical phenomenon which can be visually observed during the fatigue delamination experiments. Because the bridging fibres tend to be accessible when the composite laminate is held open it is possible to remove them in-situ. This approach of removing the bridging fibres physically is explored in this section.

Huang and Hull [26] explored the possibility of removing bridging fibres in a composite specimen by submerging a specimen in a solution of hydrochloric acid (HCl). In their research, a DCB specimen was held open by the two loading points and a glass rod with a diameter of 5 mm was inserted into the delamination plane to open the specimen and expose the bridging fibres. A schematic of this setup is displayed in figure 2.5. After about eight hours of submerging the specimen in the HCl solution, microscopic examination showed that 95 % of the crack length is free of bridging fibres [26]. The material used for the DCB specimens in this study consisted of a unidirectional E-glass/epoxy composite. The method of removing the bridging fibres was based on the fact unprotected E-glass fibres typically fracture at lower stress levels when they are exposed to an acid such as HCl, whilst the matrix material remains unscathed [6, 46, 16]. This method of removing the bridging fibres and therefore also the fibre bridging effect proved to be a reasonable procedure to halt the increase in Mode I fracture toughness increase due to fibre bridging.

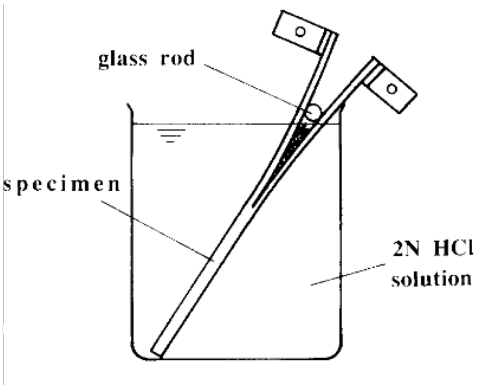

Figure 2.5: Schematic depiction of the removal of bridging glass fibres of a DCB composite specimen using an acid bath [26].

Bridging fibres may also be removed during the experiments by cutting them in order to physically exclude them from contributing to the experimental data. Hu et al. [24] give an experimental approach to quantify the stress caused by bridging fibres. In their paper, the change of compliance of the specimen by the step-wise saw cutting of the fibres is measured. A limiting factor in an approach such as this is that the saw blade is not able to reach the crack tip because of the increasingly tight margin. Khan et al. [34]

also used the approach of removing bridging fibres physically. Their method comprises a glass fibre thread which can be smaller than the saw of the previously mentioned approach. The glass fibre thread was made by twisting multiple glass fibres and forming them into a tow that had a diameter of 0.1 mm. An image of the setup can be seen in Figure 2.6. According to the authors, the glass cutting thread either broke the bridging fibres or in other cases, forced bridging fibres to pull out of the material. Both occurrences have the same result, being that the bridging fibres no longer fulfil a crack shielding role. In spite of the smaller cutting dimension, the cutting thread was still removed from the crack tip at a distance of 3-5 mm. Khan et al. [34] opted to remove the remaining load carried by the uncut bridging fibres by means of extrapolation. This way the effect of the remaining bridging fibres may also be excluded. Thus the contribution of fibre bridging may not be completely removed by this cutting procedure without performing extrapolation to a "zero-bridging"-case.

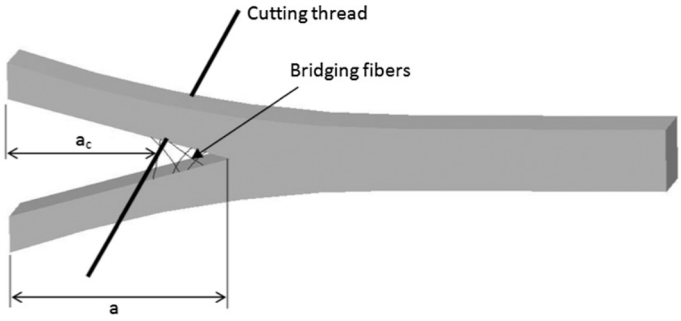

Figure 2.6: Depiction of the glass cutting thread used for the removal of the bridging fibres by Khan et al. [34].

Khan et al. [34] performed fatigue delamination experiments where the test was intermittently paused and with the DCB specimen held open, the bridging fibres were cut using the cutting thread. By storing the loads measured on the composite specimen before and after the cutting procedure, a load where all the bridging fibres are hypothetically removed, can be calculated using Equation 2.1. Because the cutting thread can only reach up to 3 mm behind the delamination tip it is essential to perform this extrapolation. The region where the cutting thread is not able to reach due to the size of the cutting thread typically contains the highest density of bridging fibres which also contribute the most to the increase in the apparent fracture toughness due to the fibre bridging effect. The equation for calculating the theoretical load on the specimen where all the bridging fibres have been removed is given:

$$P_a = P_{ac}\left(\frac{a}{a_c}\right)^m \tag{2.1}$$

where P_a is the load where all the bridging fibres are hypothetically removed, P_{ac} and a_c are the post-cutting load and the last cutting thread position and a is the total delamination length. The power law exponent m is determined in Figure 2.7. Here, the post-cutting load and the cutting thread position are plotted and a power law is fitted through the data points.

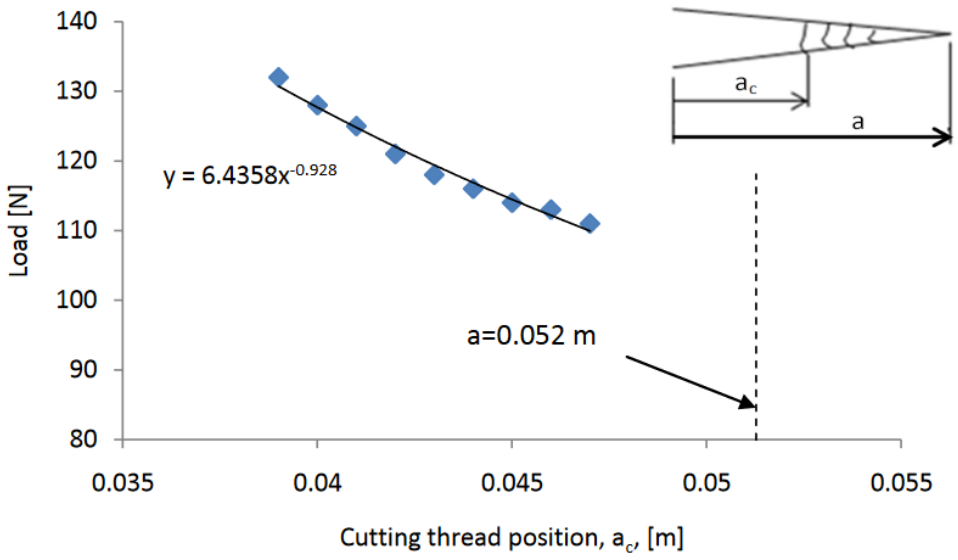

Figure 2.7: Post fibre-cutting load versus the cutting thread position. The exponent m of Equation 2.1 is equal to the slope of the fitted power law [32].

The obtained load values for the hypothetical ”zero-bridging” case can be used to calculate corresponding SERR values which in turn may be used to construct a fatigue delamination resistance curve where the fibre bridging effect is removed. Because the calculated ”zero-bridging” load, using Equation 2.1, is typically lower than the load measured after cutting bridging, the SERR value associated with this load is also lower. A fatigue delamination resistance curve would thus shift towards the left for the ”zero-bridging” curve, towards a more conservative line.

2.2.2. Method II: Constant-$\Delta\sqrt{G}$

Even though the fibre bridging effect is a physical phenomenon which may be removed by physically removing the bridging fibres as can be seen in the previous section, the cutting method still requires some extrapolation. Another method for excluding the fibre bridging effect from fatigue data involves changing the experimental setup.

Russell and Street [49] proposed to load a typical DCB specimen in series with a linear elastic spring to provide control of the strain energy release rate range, $\Delta\sqrt{G}$. The goal with this is to keep the $\Delta\sqrt{G}$ constant during the crack propagation. The authors argue that, unlike in the quasi-static loading case, the effects of fibre bridging on the crack growth rate (da/dN) are not easy to quantify. The reason given is that strain energy release rate G changes as the crack propagates throughout the specimen and the decrease of the crack growth rate, da/dN, due to fibre bridging is obscured by a change due to $\Delta\sqrt{G}$.

Russell and Street [49] used the conventional DCB setup with the addition of a helical spring to achieve the constant $\Delta\sqrt{G}$ during the fatigue testing. The purpose of the elastic spring in this setup is to not have an immediate reduction in $\Delta\sqrt{G}$ during testing. This can be achieved by taking a spring compliance which is twice the compliance of the initial specimen. After a sufficient crack length, the displacement can be gradually increased by the displacement ram, in order to maintain constant $\Delta\sqrt{G}$.

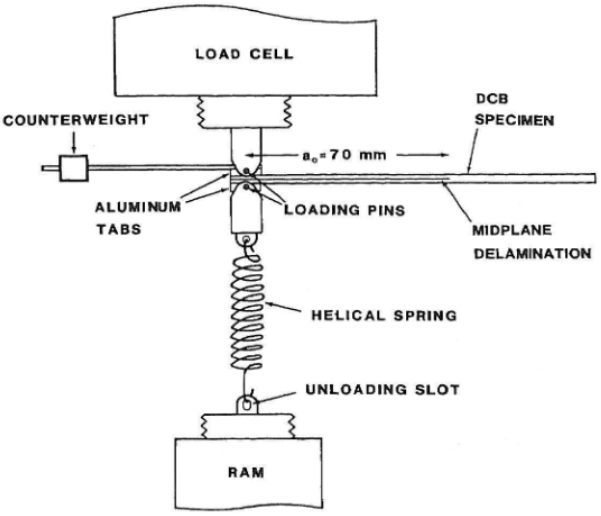

Figure 2.8: Diagram of the experimental setup used to achieve a constant ΔG for a DCB specimen [49].

In the initial stages of the research done by Russell and Street [49], it was found that the relationship derived in the paper was invalid. Large bridging fibres resulted in upward curvature of the load-displacement curves and had also an effect on the measured compliance. This made it difficult to maintain a constant $\Delta\sqrt{G}$, the authors chose to use an adhesively bonded composite which showed less fibre bridging. In this manner, the constant-$\Delta\sqrt{G}$ test could be performed.

Where Russell and Street did not seem to account for the fibre bridging effect in the initial design of their experimental setup but later on accounted for it by choosing a specimen material which showed practically none of the

effect, a similar method was proposed by Hojo and Aoki [21] and Donough et al. [15].

In the research of Hojo and Aoki [21], the goal was to determine Mode I fatigue data that allows for extrapolation to a fatigue data curve without the influence of fibre bridging [9]. A method for DCB testing under a constant maximum energy release rate, G_{max} is presented, because the "true" growth law which is not affected by fibre bridging is desired. A series of tests were performed with the G_{max} kept constant and by taking the growth rate at zero-increment of the crack length, the "true" growth law is extrapolated.

Composite laminates are loaded in Mode I fatigue according to a typical DCB setup. In order to keep the maximum energy release rate, G_{max}, constant, the maximum load applied to the specimen is adjusted during the test. Crack lengths during the fatigue testing are computed by measuring the compliance using the modified compliance calibration (MCC) equation [22]. The left diagram of figure 2.9 shows a relationship found between the crack growth rate, da/dN, and the delamination length, a. For a constant G_{max} of 500 N/m, the crack growth rate decreases almost linearly when the crack length is shorter than about 10 mm. The authors conclude that the initial inconsistency for values where the crack length is very small is related to the difference between the crack length and the crack growth rate along the crack front in the width direction of the specimen [21]. As the slope of Figure 2.9 becomes more or less horizontal, the crack growth rate does not seem to be decreasing with a further extension of the crack length. This indicates that there is some kind of saturation point after which fibre bridging does not attain additional influence of the fatigue data anymore. The authors do not make a conclusion on why this saturation occurs, but Chapter 2.1.2 covers this phenomenon where a plateau is observed in the delamination resistance curves of the work of Sørensen and Jacobsen [54].

The desired value for which no fibre bridging occurs should be located at the point where the pre-crack delamination length $a - a_0$ is zero because in this state there is no possibility for fibres to bridge the crack surface. The method used in the research by Hojo and Aoki [21] is to extrapolate the straight, decreasing line to the crack growth rate value for which $a - a_0$ = 0 mm. This gives the growth rate, for a given G_{max}, where no fibre bridging occurs. A fatigue diagram can be constructed by taking multiple values for the G_{max}, doing the experiments, and extrapolating toward the zero-crack values. A Paris-type power law can then be fitted for the found values which would represent the situation where no fibre bridging occurs, this is done in Figure 2.10.

In the same year, and with a similar method, Donough et al. [15] put forward a method to account for the effect of fibre bridging by means of an inverse method which determines the tractions stresses related to the bridging effect. Similar to the previously discussed work, the authors also elected to make use of a constant G_{max} testing approach. The two studies show unison when considering the found fatigue data curves, see Figure 2.9. Whilst Hojo and Aoki [21] do not conclude that the line becoming somewhat horizontal stems from the saturation due to fully developed fibre bridging, Donough et al. [15] point out this steady-state where bridging fibres nucleate at the same rate as they dissipate, which is supported by the research performed by Yao et al. [65].

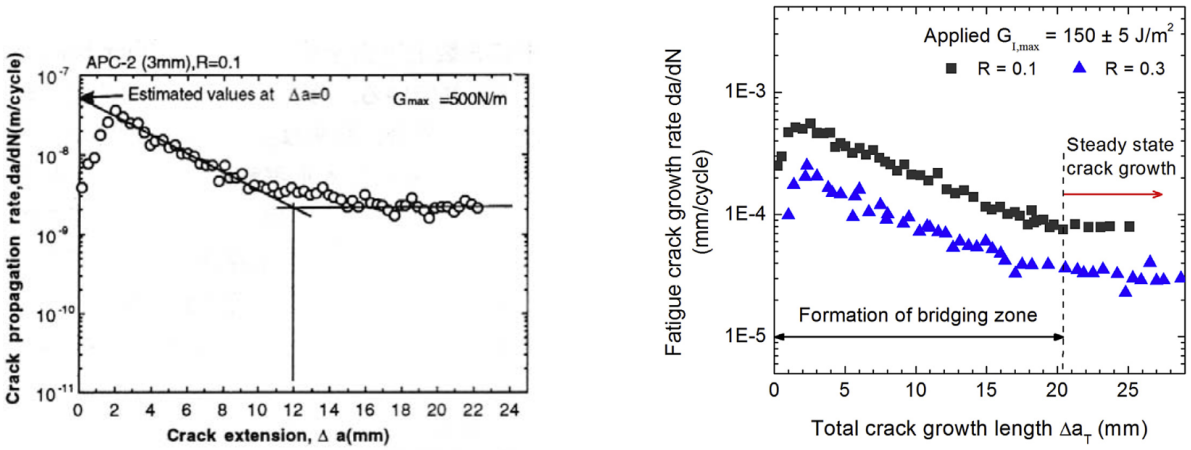

Figure 2.9: Crack growth rates versus the crack length for two constant-G_{max} testing methods (left: Hojo et al. [21] and right: Donough et al. [15]).

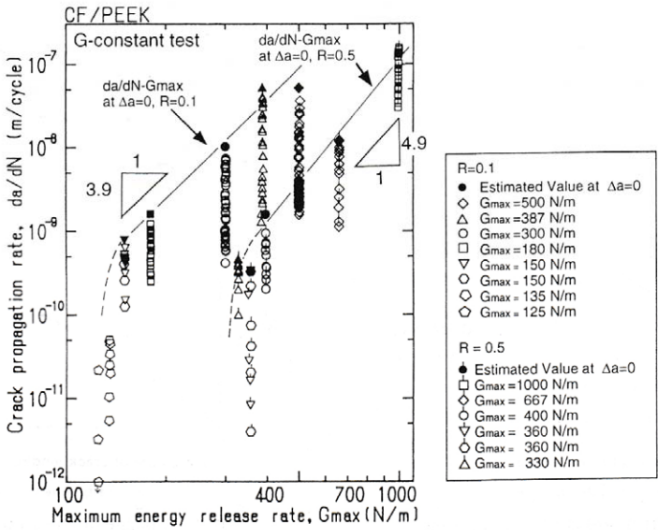

Figure 2.10: The relationship found between the crack growth rate and the maximum energy release rate for fatigue tests with a constant G_{max} [21].

There seems to be uncertainty about the choice of similitude parameter for fatigue delamination testing of composites [47]. The method described by Hojo and Aoki [21] describe a method for constant-G_{max} testing. According to a discussion [47] about the similitude parameter for characterizing delamination growth, to represent cyclic loading $\Delta\sqrt{G} = \left(\sqrt{G_{\max}} - \sqrt{G_{\min}}\right)^2$ should be used. Research about a method where this similitude parameter is kept constant during delamination experiments has not been found. Thus, a method with constant-$\Delta\sqrt{G}$ could be a better approach for this method.

2.2.3. Method III: Specimen Specific Extrapolation

Alderliesten [2] states that approaches towards fibre bridging exclusion often make use of theoretical models or dissimilar fatigue delamination mechanics [39] to quantify the fibre bridging effect. The result is that a reported outcome of experimental data depends on the theoretical model used for the fibre bridging analysis and the validity of the results could be contested based on inaccurate models and unfounded assumptions. Therefore, Alderliesten [2] and Yao [61] describe a method for the elimination of fibre bridging in fatigue delamination resistance curves of composite DCB experiments using solely experimental data and no additional theoretical models. The central concept is that the elimination of the fibre bridging effect should only require the data from the same specimen, as in literature [28] fibre bridging is historically said to be a specimen-specific artefact.

To this end, multiple fatigue delamination tests are performed on the same DCB specimens, generating multiple fatigue delamination resistance curves. By analyzing the obtained curves and evaluating them against the effective delamination length at which the data was obtained, the data may then be translated to a situation where the pre-crack delamination length is equal to zero. This procedure involves performing regression of the obtained delamination resistance curves and should be performed for each composite specimen individually.

Figure 2.11 shows how multiple fatigue delamination resistance curves can be obtained by performing fatigue delamination tests on a single composite specimen. In between the tests, the delamination tip is quasi-statically extended by "a few" millimetres according to the method as described by Alderliesten [2]. Whether or not this delamination tip extension is needed remains uncertain according to the paper. It could be possible that performing quasi-static delamination propagation introduces excessive fibre bridging development as compared to cyclic loading. De Carvalho and Murri [13] state that the amount of fibre bridging in quasi-static tests does not typically relate to the fibre bridging in fatigue loading.

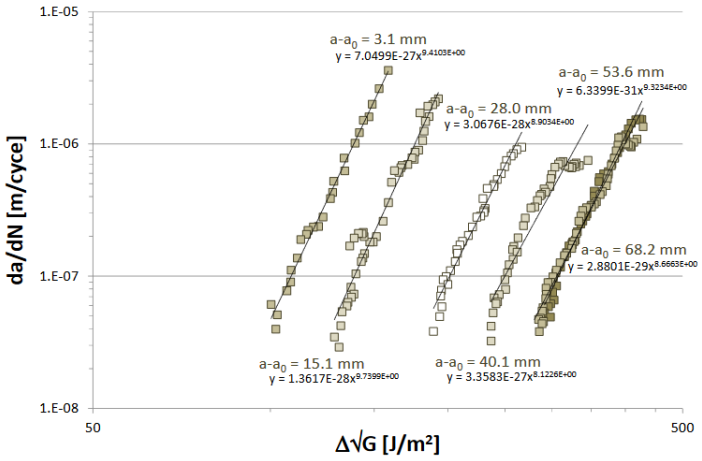

Figure 2.11: Six consecutive delamination resistance curves generated from a single DCB specimen according to the method described by Alderliesten [2].

A Paris-type power law relationship is fitted through the data points of

each individual fatigue test, according to:

$$\frac{da}{dN} = c(\Delta\sqrt{G})^n = c\left[\left(\sqrt{G_{max}} - \sqrt{G_{min}}\right)^2\right]^n \tag{2.2}$$

For each of the obtained curves, the data points are translated along the slope of Equation 2.2, which is the exponent n, to a chosen value of the crack growth rate, da/dN_T. The choice for the value of da/dN_T is arbitrary but it should lay within the range of all the fatigue delamination resistance curves. The slope n is slightly different for each fatigue delamination resistance curve and the translation to the chosen da/dN_T therefore be done individually for each curve, which is illustrated in Figure 2.12 for the first three curves of Figure 2.11. The chosen value for the delamination growth rate, da/dN_T is equal to 4.5×10^{-7} m/cycle.

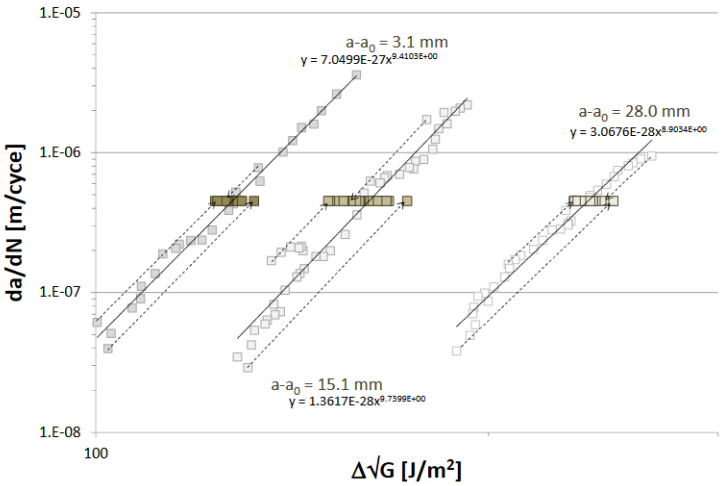

Figure 2.12: The translation of the first three fatigue delamination resistance curves of Figure 2.11 along their corresponding slope n to a selected value of $da/dN_T = 4.5 \times 10^{-7}$ m/cycle.

The equation which is used for determining the translated value of the SERR at the selected crack growth rate, $\Delta\sqrt{G_T}$, is:

$$\log_{10}\left(\Delta_{\sqrt{}}G_T\right) = \frac{1}{n}\left[\log_{10}\left(\frac{da}{dN_T}\right) - \log_{10}\left(\frac{da}{dN}\right)\right] + \log_{10}(\Delta_{\sqrt{}}G) \tag{2.3}$$

where da/dN_T is the selected crack growth rate, equal to 4.5×10^{-7} m/cycle in the case of Figure 2.12. da/dN and $\Delta\sqrt{G}$ are the crack growth rate and the SERR value of the to-be translated fatigue data points.

A range of $\Delta\sqrt{G_T}$ values is found for each of the fatigue delamination resistance curves and an average of each of these ranges can be calculated. These values of $\Delta\sqrt{G_T, avg}$ can be plotted against the corresponding pre-crack delamination lengths $a - a_0$, again for each of the delamination resistance curves individually. In this manner, it can be determined whether or not a saturation point for the development of bridging fibres has been reached.

In Figure 2.13 the values of $\Delta\sqrt{G_T, avg}$ are plotted against $a - a_0$ and the saturation of the fibre bridging effect is indeed visualized by the fitted line becoming horizontal. This nonlinear relationship can be approximated by using a second-order polynomial (Figure 2.13) or with a bi-linear expression [62].

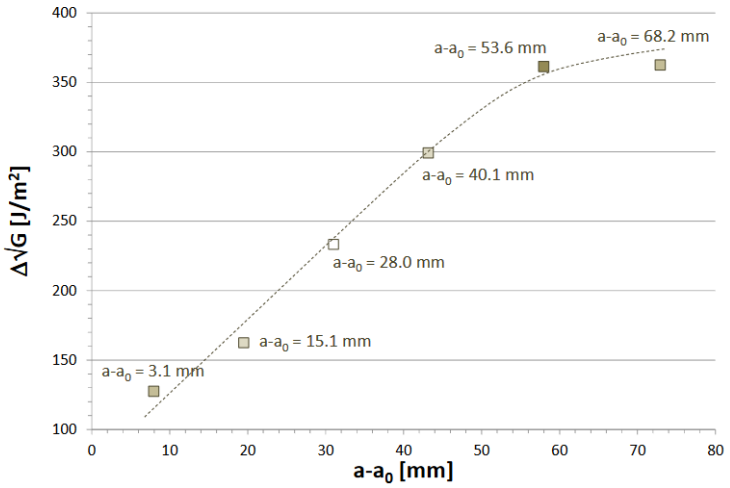

Figure 2.13: $\Delta\sqrt{G_{T,avg}}$ as a function of the pre-crack delamination length, $a - a_0$ for the delamination resistance curves of Figure 2.11.

The fatigue data points of Figure 2.11 each have a distinctive value for the pre-crack delamination length, $a - a_0$. Regression can therefore be performed through $\Delta\sqrt{G}$, da/dN and $a - a_0$. This regression analysis can be performed on all the data points if the found relationship of Figure 2.13 indeed indicates saturation of fibre bridging. If this is established, the following equation provides a suitable expression for regression:

$$\log(\Delta\sqrt{G}) = C_0 + C_1\,(a - a_0) + C_2 \log\left(\frac{da}{dN}\right) + C_3\,(a - a_0)^2 + C_4\left[\log\left(\frac{da}{dN}\right)\right]^2 \qquad (2.4)$$

where C_i are constants obtained by fitting this expression to the fatigue data.

This surface fit of the data allows for determining a fatigue delamination resistance curve in the absence of the fibre bridging effect. This may be achieved by assuming that no fibre bridging occurs when $a - a_0$ is equal to zero. At this pre-crack delamination length, it is assumed that no bridging fibres are able to have been formed. By setting $a - a_0$ to zero in Equation 2.4 an average zero-bridging curve can be constructed using the following expression:

$$\log(\Delta\sqrt{G})_{avg,thr} = C_0 + C_2 \log\left(\frac{da}{dN}\right) + C_4\left[\log\left(\frac{da}{dN}\right)\right]^2 \qquad (2.5)$$

The curve obtained with this expression lies to the left of the original fatigue delamination resistance curves. This means that it is more conservative than the original curves. This is expected as the "zero-bridging" curve does not exhibit delamination retardation due to the fibre bridging effect.

One must still consider the inherent scatter which is associated with the original delamination resistance curves. The resulting "zero-bridging" curve must not ignore this relevant information. The deviation between the SERR value of a given fatigue data point and the SERR value of the fitted Paris-type power law at the same crack growth rate, da/dN, can be stored. This deviation described the degree of scatter, i.e. if it is higher then it will deviate more from the Paris-type power law fitting. Next, this stored deviation value may be displayed again by plotting a data point with the same offset from the newly constructed "zero-bridging" fatigue delamination resistance curve. In such a manner, the inherent scatter of the original

delamination resistance curves is not ignored. In the end, a ”zero-bridging” curve is obtained along with the transformed fatigue data points where their scatter is preserved, see Figure 2.14.

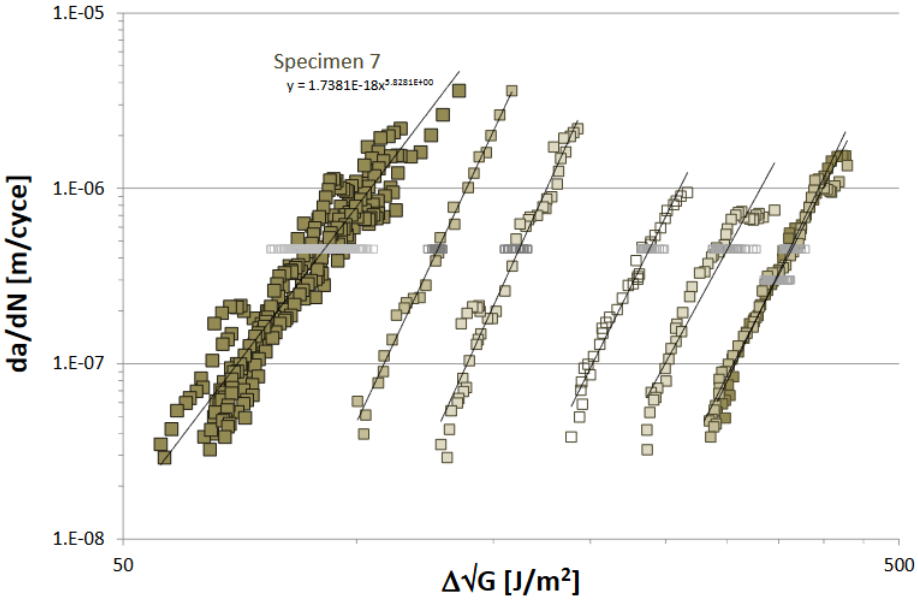

Figure 2.14: The initial delamination curves and the translated curve obtained by excluding fibre bridging [2, 59].

2.2.4. Method IV: Hartman-Schijve Equation

The exact same data gathered over the course of a DCB testing campaign [66, 67] during which the method [2] described above was first used, also has been applied to an approach for the representation of fatigue data based on the Hartman-Schijve equation in the manner of Jones et al. [31]. The method described by Jones et al. [31] can be used to determine an "upper-bound" fatigue delamination curve. The authors observed significant crack growth retardation due to large-scale fibre bridging.

Jones et al. [31] propose an empirical methodology to fit the fatigue data to the Hartman-Schijve variant of the NASGRO equation [41] which can be used for describing delamination growth in composites [29] and was first derived by Andersons et al. [4]:

$$\frac{da}{dN} = D\left[\frac{\Delta\sqrt{G} - \Delta\sqrt{G_{thr}}}{\sqrt{\left\{1 - \sqrt{G_{\max}}/\sqrt{A}\right\}}}\right]^n \tag{2.6}$$

where D, n, A and $\sqrt{G_{thr}}$ are constants. The value of A can either be assumed to be equal to the fracture energy, $G_{c,0}$, taken from quasi-static testing [29] or it can be fitted empirically [8]. $\sqrt{G_{thr}}$ represents the SERR value at a fatigue threshold, below which no significant crack growth occurs.

In a 2018 paper of Yao et al. [64] the values of A and $\sqrt{G_{thr}}$ are chosen such that, for the used data set of multiple fatigue tests, the logarithmic da/dN versus logarithmic $\left[\frac{\Delta\sqrt{G}-\Delta\sqrt{G_{thr}}}{\sqrt{\left\{1-\sqrt{G_{\max}}/\sqrt{A}\right\}}}\right]$ collapse onto each other and become almost linear. By combining multiple relationships described by Equation 2.6 from different tests, a single, linear relationship is determined.

Through fitting of the parameters A and $\sqrt{G_{thr}}$ for the different fatigue tests a so-called "master" Hartman-Schijve representation is indeed obtained which is seen in Figure 2.15. Each line here represents a unique fatigue test performed on a composite DCB specimen. The advantage of using this method for the representation of delamination growth in composites is the fact that it includes varying specimen parameters such as the effect of the pre-crack delamination length of the specimens, the inherent scatter observed in fatigue testing of composites due to for instance manufacturing defects, the effect of varying the stress ratio and the effect of varying the thickness. One could consider that the fitting parameters A and $\sqrt{G_{thr}}$ are used for compensating the aforementioned effects. The resulting "master" relationship should have a high coefficient of determination, R^2, which will be an indication of a proper selection of the curve fitting parameters A and $\sqrt{G_{thr}}$.

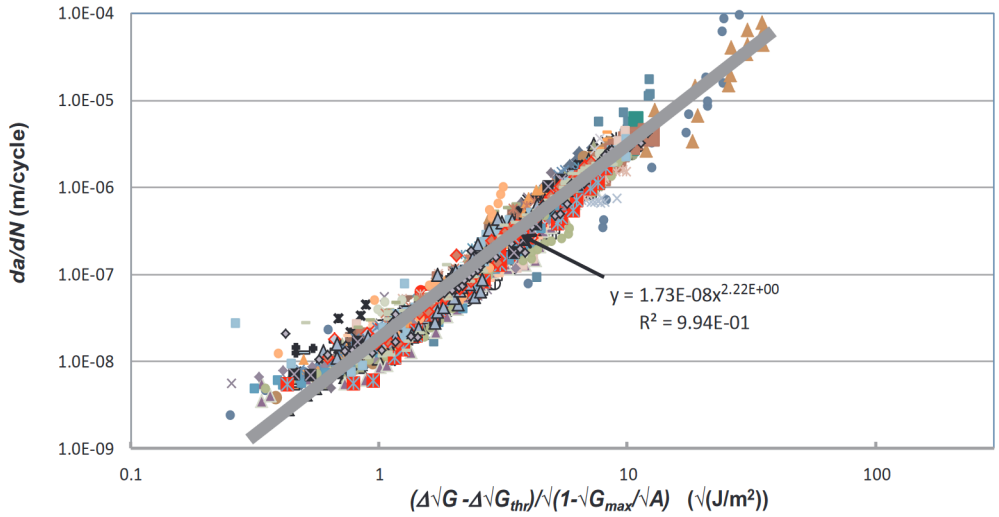

Figure 2.15: A linear, "master" relationship obtained for multiple fatigue tests on composite specimens with varying testing parameters. For information about the nature of each specimen and its testing parameters, the reader is referred to the relevant paper [64].

For design purposes and to exclude the fibre bridging effect from the data which is represented using the Hartman-Schijve equation, a methodology is described to find the curve fitting parameters A_0 and $\sqrt{G_{thr,0}}$ which are the "zero-bridging" variants of the original values of A and $\sqrt{G_{thr}}$. These values represent the case where the pre-crack delamination length, $a - a_0$, of the fatigue test, is equal to zero, i.e. the point at which the composite specimen sees little to no delamination growth retardation due to fibre bridging. This hypothesis is supported by the argument that the fibre bridging phenomenon requires a specific level of delamination propagation to initiate any noticeable changes in fatigue data. Consequently, a "zero-bridging" scenario would indicate the absence of observable crack growth.

Yao et al. [64] describe two ways to obtain a lower-bound value for the fatigue threshold, $\sqrt{G_{thr,0}}$. In the first method, the values for $\sqrt{G_{thr}}$ which were found in the previous step are plotted against the corresponding value for the pre-crack extension length, $a-a_0$. The value for $\sqrt{G_{thr,0}}$ can be extrapolated by fitting a polynomial function through the plotted data points and determining the value by setting the pre-crack extension as equal to zero. An example of this method is displayed in Figure 2.16. The fit to these data points is typically of a high degree, but not exact. The authors [64] mention this shortcoming in the paper but also state that this method can be used as an elementary and straightforward procedure to determine the value of $\sqrt{G_{thr,0}}$ with at least some degree of certainty. The second deficiency of this fitting method, which the authors fail to mention in the article, is the choice of the degree of the fitting polynomial. A lower-order polynomial typically fails to accurately represent the data points with a low R^2 as a result. When employing a higher-order polynomial, the process of extrapolating to a zero-bridging value becomes less reliable due to the polynomial's tendency to abruptly change direction in order to closely align with the leftmost data point. This unpredictable behaviour in the extrapolated region can lead to either underestimated or overestimated values for the "zero-bridging" parameter, $\sqrt{G_{thr,0}}$, resulting in overly cautious or overly optimistic outcomes in the fatigue delamination resistance curves.

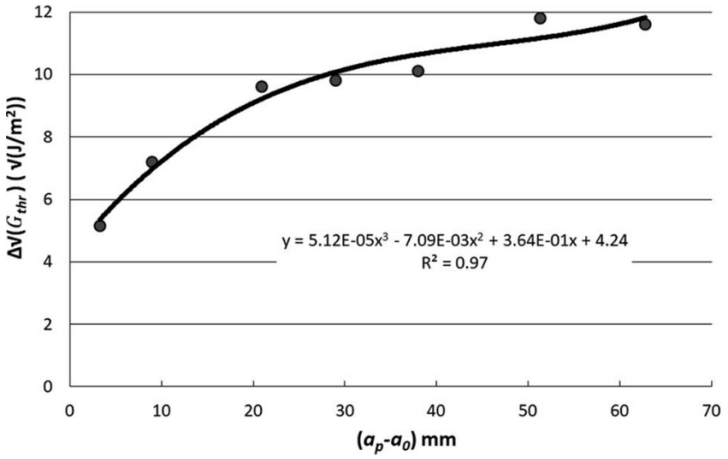

Figure 2.16: $\sqrt{G_{thr}}$ versus the pre-crack extension length, $a - a_0$. The fitted polynomial may be used for obtaining a value at $\sqrt{G_{thr}}$ for $a - a_0$ equal to zero, i.e. $\sqrt{G_{thr,0}}$.

The second method which may be used to estimate $\sqrt{G_{thr,0}}$ is based on an earlier paper of Yao [62]. In this method, an expression is given for the SERR, G where the effect of bridging fibres is accounted for. The value of G at the tip of the delamination with the absence of bridging fibres, G_{tip} is expressed as:

$$G_{tip} = G \cdot \left[\frac{A_0}{A}\right] \tag{2.7}$$

The used curve fitting parameters A and $\sqrt{G_{thr}}$ can be used in this equation along with A_0 to calculate $\sqrt{G_{thr,0}}$. $\sqrt{G_{thr,0}}$ is assumed to be the same as $\sqrt{G_{tip}}$ as it is defined as the zero-bridging SERR range. A_0 can be found by plotting the found values along with their corresponding pre-crack lengths, fitting a polynomial and extrapolating to the case where the pre-crack extension is equal to zero which is analogous to the first method described for determining $\sqrt{G_{thr,0}}$.

Next, a statistical approach is used to obtain an "upper-bound" curve for design purposes. From the variety of specimens of which the zero-bridging parameters A_0 and $\sqrt{G_{thr,0}}$ can be determined, a set of values follows from which a mean and standard deviation can be determined assuming that these zero-bridging values are spread along a normal distribution. By adopting designing rules for composite structures [48, 42], conservative design values can be calculated for A_0 and $\sqrt{G_{thr,0}}$ by using their mean value minus three standard deviations. In this manner, an "A-basis"-approach [48, 42] is adopted where the values determined are expected to fall below at least 99% of the population of values with a confidence of 95%. This methodology is typically used for primary structures in aircraft where the failure of a component would result in loss of structural integrity [11].

The Paris' law which is fitted through the variety of fatigue data obtained from a multitude of experiments according to Equation 2.6 has two fitting parameters D and n. They may be used along with the obtained values of A_0 and $\sqrt{G_{thr,0}}$ and the appropriate statistical approach [48, 42] to construct an "upper-bound" fatigue delamination growth curve. This curve represents a worst-case for the obtained fatigue data and may be appropriate to use for designing primary structures in a composite design. A range of values for both $\Delta\sqrt{G}$ and G_{max} can be constructed with the maximum for G_{max} being equal to A_0, above this value quasi-static delamination growth is assumed to occur. For the minimum bound for $\Delta\sqrt{G}$, $\sqrt{G_{thr,0}}$ can be used, below which now

delamination growth is assumed to occur. To find the minimum and maximum bound for G_{max} and $\Delta\sqrt{G}$ respectively, the following equation is used where R is the stress ratio:

$$\Delta G = G_{max} \cdot (1 - R)^2 \tag{2.8}$$

In Figure 2.17, the resulting upper-bound fatigue delamination growth curve is presented by Yao et al. [64]. It is shown that the predicted curve encompasses all experimental data, resulting in a more conservative design curve than the curve one would get from simply averaging the experimental data.

The method used for obtaining a design curve which represents the case with little crack retardation, i.e. zero-bridging, assumes that the constants in Equation 2.6 are distributed along a Gaussian distribution. This makes it possible to take the mean value minus either three or two times the standard deviation to obtain an "A-basis" or "B-basis" of the lower-bound respectively. To support this viewpoint, Jones et al. [31] paraphrase Rouchon and Bos [48], who state that if sufficient data points exist for the accurate determination of a true mean value of $\sqrt{G_{thr,0}}$, the mean value minus two standard deviations may be used. If there are not sufficient data points, then it should be the mean value minus three standard deviations of said parameters. Jones does not comment on the question of when "sufficient data points" are obtained. Nor do the authors make a statement on the choice for a Gaussian distribution as opposed to for instance a Weibull distribution which Rouchon and Bos [48] also cover in their statistical analysis. This assumption must be emphasized when considering this method for the exclusion of the fibre bridging effect from fatigue delamination data.

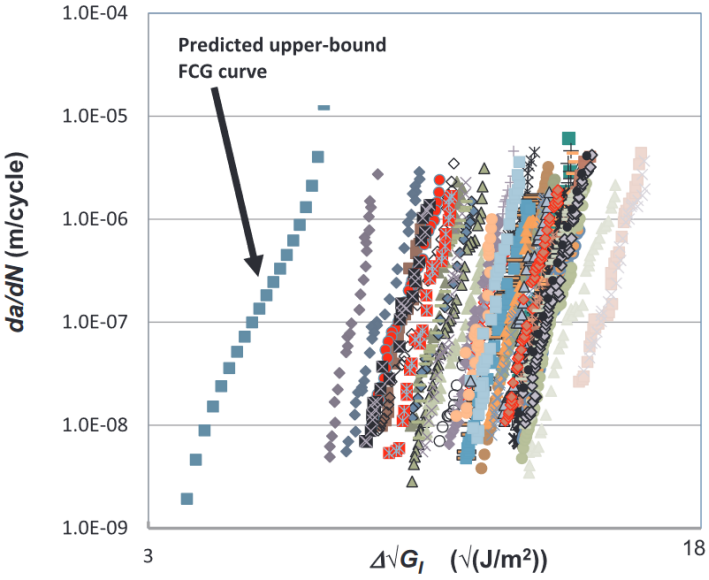

Figure 2.17: Fatigue experiment results in values of logarithmic da/dN versus logarithmic $\Delta\sqrt{G}$ and the upper-bound fatigue delamination curve using values of A_0 and $\sqrt{G_{thr,0}}$ with their mean value minus three standard deviations.

3

Research Scope

As described in Chapter 2, the fibre bridging effect introduces a resistance against delamination which is assumed to only exist in delamination tests of UD composite specimens. Mechanical properties of composites are typically found through experiments with UD specimens. The increase in delamination resistance does not offer an accurate representation of what happens when in-service composite structures show delamination, however. Therefore, prior to using data associated with experiments where the fibre bridging occurs, it must first be excluded or accounted for.

Multiple methods and techniques [34, 21, 2, 31] with the goal of excluding the fibre bridging effect from the conventional DCB test are discussed in Section 2.2. Up until now, these methods have not been compared which each other in a direct manner. The conservativeness of the different methods could be different based on the underlying procedure. Furthermore, no conclusive evidence is present on which of these methods most accurately describes a zero-bridging delamination case. As a result, there is no agreement on a standard to obtain Mode I fatigue delamination data of composite specimens [2] as of the time of writing this report. A better understanding of the methods [34, 21, 2, 31] for the accounting of fibre bridging is therefore desired before such a standard on Mode I fatigue delamination propagation can exist [9].

3.1. Research Questions

Based on the findings of the Literature Study and the subsequently found research gap, the main research question follows:

”How can the fibre bridging effect be excluded in a suitable manner from data obtained during the cyclic Mode I loading of UD composite specimens?”

To support the main research question, several subquestions are:

1. Which method for the exclusion of the fibre bridging effect in cyclic Mode I loading of UD composite laminates is feasible to be integrated into a standardized framework for describing fatigue delamination growth in composite specimens?

2. Which method for the exclusion of the fibre bridging effect in cyclic Mode I loading achieves a ”zero-bridging” fatigue delamination scenario that is regarded as the most conservative?

3. Which method for the exclusion of the fibre bridging effect in cyclic Mode I accurately represents a fatigue delamination scenario in the absence of the fibre bridging effect?

4

Experimental Methodologies

This chapter contains the experimental procedures which were followed over the course of the project. It includes a manufacturing plan for the composite DCB specimens and a discussion of the experimental setups which were used for providing results.

4.1. Specimen Manufacturing

The goal of the project is to perform fatigue delamination experiments using the methods described in the literature study of this report. Naturally, this means that specimens should be manufactured. This section describes the process of manufacturing specimens that have been shown to produce the fibre bridging effect in earlier research projects [44, 64].

The material for the specimens came from a roll of a partially cured polymer matrix with pre-impregnated carbon fibres, i.e. a pre-preg. The product name of the roll is M30S/DT120, which is produced by Delta-Preg. To prevent the polymer matrix of the prepreg from curing prematurely when it is not in use, the roll was kept inside a freezer. The polymer matrix is the product DT120 which is a high-viscosity thermosetting epoxy resin capable of being used in a vacuum bag autoclave curing cycle. The unidirectional carbon fibres inside the roll of pre-preg are oriented in the longest dimension of the roll. The M30S carbon fibres are from the brand Torayca and polyacrylonitrile (PAN) is the precursor for these fibres.

Each of the specimens should have the exact same geometry. The length L is 200 mm, the width b is 25 mm and the thickness $2h$ will depend on the number of prepreg plies used, but this will be in the vicinity of 5 mm. A large panel was built using the entire width of the roll of prepreg material, which is 600 mm. Afterwards, specimens were cut to size from this composite panel. A composite plate with this width allowed for the production of at least 20 specimens when considering the thickness of a saw blade.

A large aluminium mould was used for the production of the composite panel. After the mould was thoroughly cleaned, a release agent (Marbocote 227) was applied to prevent the prepreg material from sticking to the mould after curing. An initial pre-preg layer was cut to size from the roll and placed onto the mould. The dimensions of the layers were 600 mm by 250 mm, this will leave a sufficient margin around the edges.

A debulking process using a vacuum suction table was then applied to ensure proper adherence of the first ply to the mould. Subsequent pre-preg layers were then cut to size and were placed onto each other, whilst making sure to debulk the product every three layers for at least three minutes per layer.

(a)

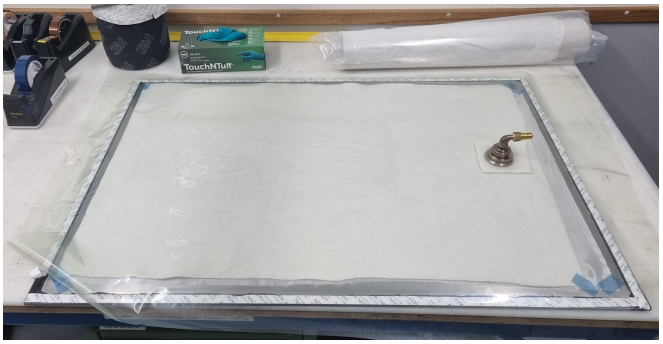

(b)

Figure 4.1: The mid-plane of the composite panel shows the location of the PTFE insert and the product ready for the curing cycle.

After applying 16 layers and arriving at the mid-plane, a length of non-adhesive polytetrafluoroethylene (PTFE) was applied to one side of the product as seen in Figure 4.1a and schematically in Figure 4.2. The PTFE insert creates a starter crack on one side of the specimen. The PTFE insert was placed so that once the specimen was cut out of the panel, the insert would reach up to 50 mm inside the mid-plane of the specimen. Since there was 25 mm of excess material around the edge of the panel, the PTFE insert was placed 75 mm away from the top of the panel.

After the PTFE insert was placed uniformly across the length of the composite panel the remaining prepreg plies were laid up until a total of 32 plies was reached. A release film was put on top of the prepreg material to prevent it from sticking to the peel ply which was then positioned over the release film. A large breather film was placed onto the whole and a vacuum bag was stuck to the mould using sealant tape. The vacuum bag contained a hole through which a vacuum connector was installed. The product was then checked for any leaks by pulling a vacuum through the connector using a pump, any leaks were shown by loss of pressure over time.

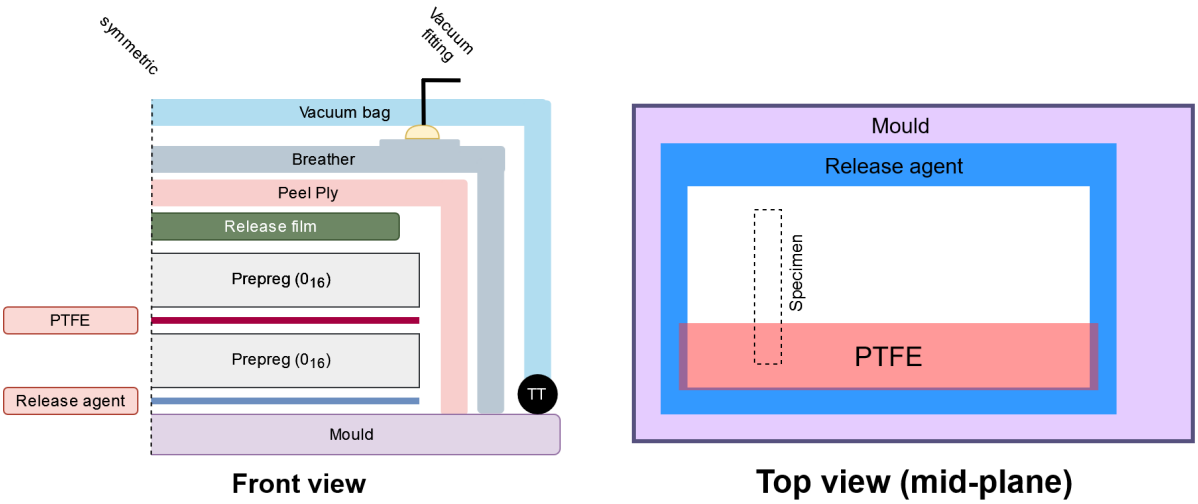

Figure 4.2: Schematic for the manufacturing of the prepreg specimens.

After a vacuum inspection was done to ensure no leaks were present, the panel was placed into the autoclave for the curing of the resin. The supplier of the resin material specified the curing cycle parameters. While multiple curing cycles were possible for this particular epoxy resin, the recommended cure cycle was followed. A curing temperature of 120 °C was maintained inside the autoclave for 90 minutes. The initial heating ramp rate was 3 °C/min starting from room temperature and up to the curing temperature of 120 °C. During the entire process, a vacuum was applied to the bagged product, and an additional 6 bars of curing pressure was applied inside the autoclave. The temperature and pressure of the curing cycle were given in Figures 4.3a and 4.3b.

To transform the cured composite panel into usable specimens, the specimens were cut with a Proth cutting machine. From one single composite panel, twenty specimens were collected. Aluminium tabs were bonded to the composite specimens to make them quickly attachable to the DCB testing machine. The surfaces of the specimens where the tabs were to be bonded and the aluminium tabs themselves were sanded and subsequently bonded together using 3M Scotch-Weld epoxy adhesive EC-2216 B/A. A two-piece Teflon mould was used for ensuring proper alignment of the tabs to the specimens, see Figure 4.4. After 24 hours of curing, the adhesive bond between the aluminium tabs and the specimen was strong enough for subsequent testing in the testing machine. ISO 15024 [55] stated that either load blocks or piano hinges should be used for introducing load into the specimen. The setup in this study used piano hinges. The specimens were labelled and catalogued using a unique name for each individual specimen.

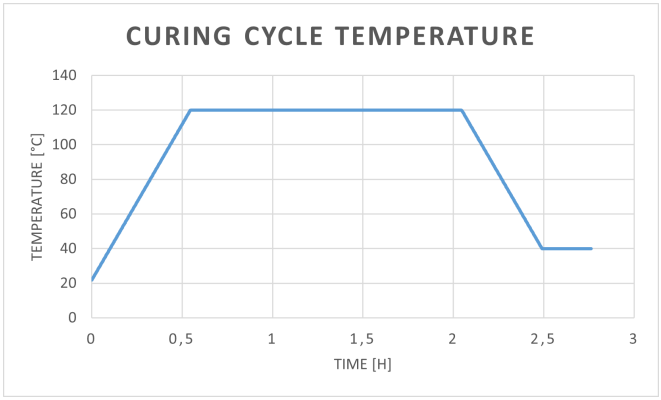

(a)

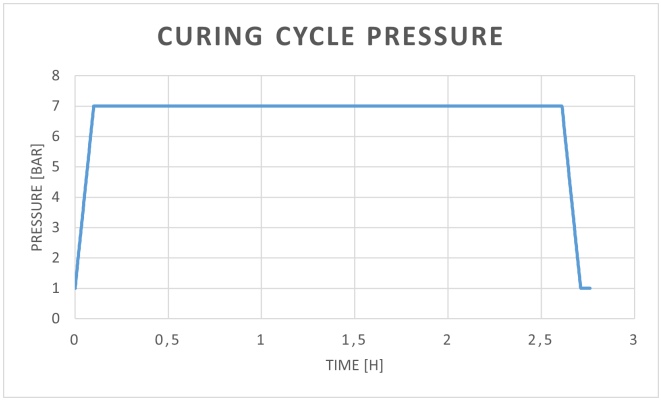

(b)

Figure 4.3: The curing temperature and pressure inside of the autoclave during the curing cycle.

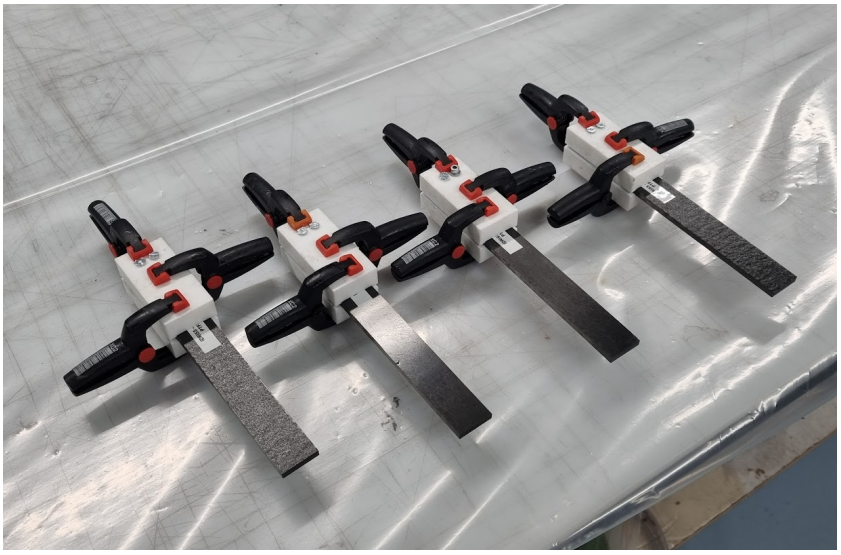

Figure 4.4: Using a Teflon mould for precise alignment, the aluminium tabs were bonded to the composite specimens.

In order to track the delamination length during experiments, a long side of each specimen is polished using fine sandpaper and lightly coated with a water-based, brittle white fluid. Regular correction fluid was used in this case. A very narrow strip of grid paper with a precision of 1 mm is glued onto the side at either the top or bottom of the specimen. The grid paper should not cover the mid-plane of the specimen so as not to obstruct the view of the crack tip. The centimetre intervals are marked on the whitened surface of the side of the specimens, to make crack length determination easy. A finished specimen, which is seen in Figure 4.5, is now ready to be used in the fatigue test machine, with the DCB setup.

To track delamination length during experiments, one side of each specimen was polished, coated with correction fluid, and a narrow strip of 1mm grid paper was attached. The grid paper was positioned to avoid obstructing the delamination plane. Centimetre intervals were marked on the whitened surface for crack length determination. The prepared specimens were then ready for use in the fatigue test machine with the DCB setup (see Figure 4.5).

Figure 4.5: Ready composite specimen for DCB fatigue delamination experiment.

4.2. Experimental Setup

The double cantilevered beam (DCB) test is used in all the fibre exclusion methods mentioned in the literature study. This setup is typically used to evaluate the interlaminar fracture toughness of composite materials. The fatigue load is applied perpendicular to the largest surface of the composite specimens at the location of the bonded aluminium tabs. The applied load causes the crack to propagate through the specimen.

For Mode I fatigue loading, the Delft Aerospace Structures and Materials Laboratory (DASML) has several machines available. The fatigue machine used in the present thesis project is an MTS Landmark 100 kN machine. Due to inertial limitation at high (>5 mm) displacements, the testing frequency is limited to 2 Hz for all fatigue experiments using this machine. The selected stress ratio R for all experiments is equal to 0.1.

The displacement values needed for data analysis of the fatigue data are obtained through an internal linear variable differential transformer (LVDT). This electrical transformer is able to accurately measure the linear displacement and position of the piston onto which the specimen is attached. The load associated with a given displacement is measured using a 1 kN load cell which is mounted onto the fatigue machine. This load cell is more accurate at lower load values (< 200 N) than the internal load cell of the 100 kN fatigue rig which has a much broader range and therefore a higher resolution.

Naturally, the delamination length or crack length is essential in data acquisition of fatigue testing. To accurately record this variable, a camera is used which can record the crack length at any given point during the fatigue cycle. The software which actuates the fatigue machine can also send a signal to the camera, triggering an image capture. The picture is saved onto a PC. To ensure proper lighting, an LED lamp is used. The entire setup with its components labelled is shown in Figure 4.6.

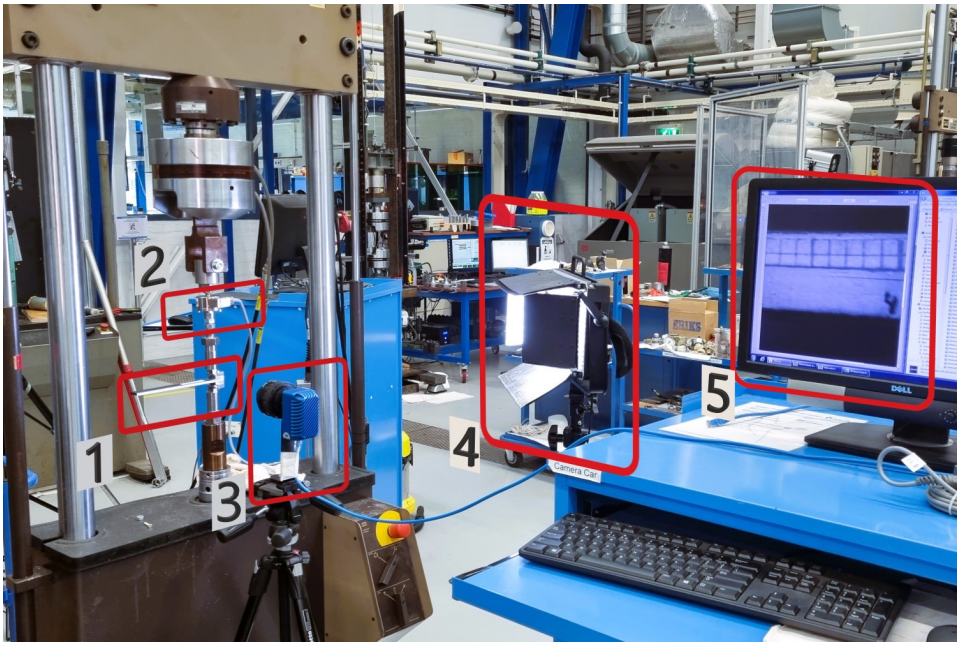

Figure 4.6: An overview of the DCB setup used for the fatigue tests:
1 - DCB specimen
2 - Loadcell (1 kN)
3 - Camera
4 - LED light
5 - Computer for storing images

Method I: Cutting Bridging Fibres

One of the methods for the exclusion of the fibre bridging effects involves the physical removal of bridging fibres whilst the composite specimen is still attached to the fatigue machine. The method, which is described in detail in relevant literature [34], makes use of a small glass fibre tow which is clamped in a jig saw frame. During the present research project, a similar setup is used. However, instead of a glass fibre tow, a wire made of stainless spring steel is used which has the same diameter as the glass fibre tow used in the paper [34], i.e. 0.1 mm. This type of wire provided similar results as in the literature, and its effect on removing fibre bridging is also nearly identical. In order to improve the cutting capabilities of the wire, it is carefully abraded using 120-grit sandpaper to slightly roughen the surface. Figure 4.7 shows the configuration in which the cutting of bridging fibres takes place. The composite specimen is held open at the maximum displacement during the cutting procedure to make it easier to reach as close to the delamination tip as possible. The fibres are removed by a sawing motion and putting light pressure in the direction of the crack tip.

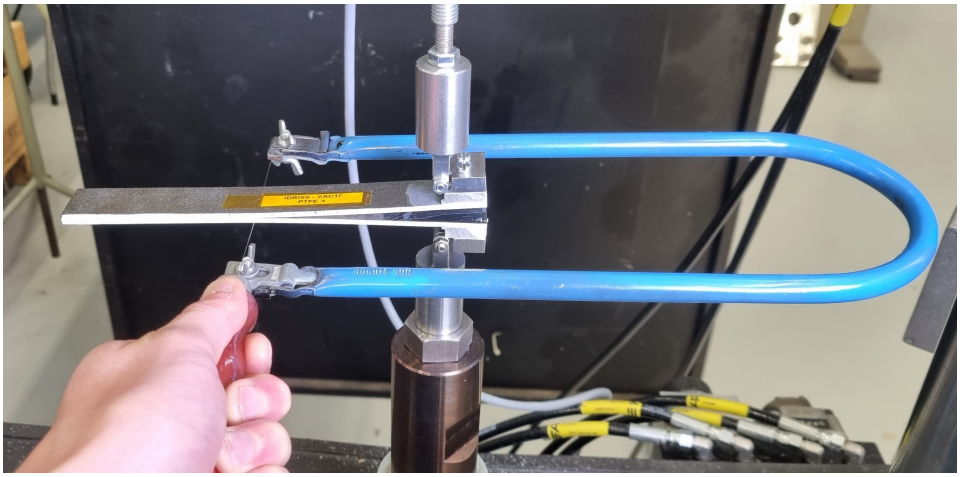

Figure 4.7: The procedure for removing the bridging fibres through a cutting method.

The findings of this method will indicate that the complete removal of all bridging fibres using the steel wire and jig saw frame is not possible. The steel wire has a limited reach of up to 5 mm behind the delamination tip. Following the methodology outlined in Khan's study [34], the load of the specimen is recorded both before and after the removal of bridging fibres. Additionally, the delamination length and cutting thread position is captured using the camera. Through the utilization of a power law fitting, the position of the cutting thread, and the delamination length, it becomes possible to extrapolate the load associated with the hypothetical scenario where all bridging fibres are successfully cut, see Equation 4.1.

Figure 4.8 presents the post-cut load and cutting thread position obtained from a fatigue test conducted on specimen "Vac17". The power law exponent m, determined through curve fitting, enables the extrapolation of the load for the hypothetical scenario where all bridging fibres have been cut. This load is required for calculating the fatigue loading parameter $\Delta\sqrt{G}$, which, in turn, can be utilized to construct a "zero-bridging" fatigue delamination resistance curve. The equation for extrapolating the theoretical "zero-bridging" load P_a in a composite specimen, as described by Khan et al. [34],

is given by:

$$P_a = P_{ac}\left(\frac{a}{a_c}\right)^m \tag{4.1}$$

Here, P_{ac} represents the load measured after cutting the bridging fibres, a_c is the position of the cutting thread, a denotes the total delamination length and m corresponds to the exponent of the power-law fitting obtained from Figure 4.8.

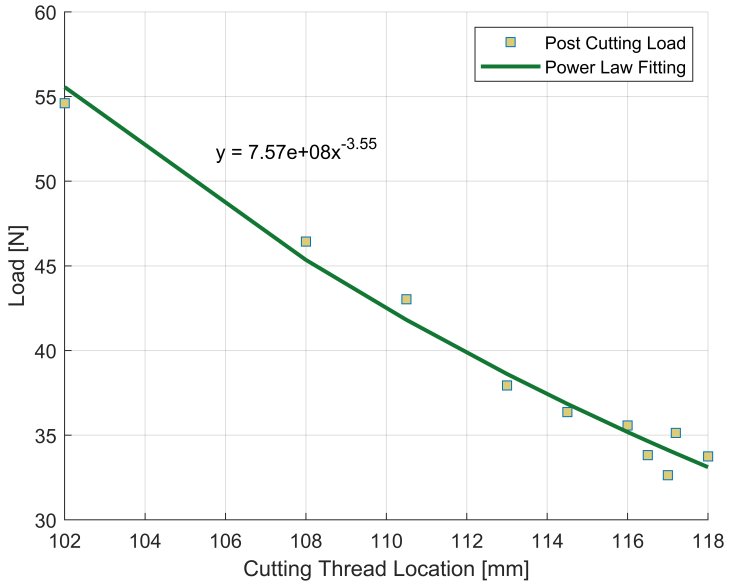

Figure 4.8: Load on the composite specimen versus the cutting thread position for specimen "Vac17".

Method II: Constant-$\Delta\sqrt{G}$

The next method employed in this study for excluding the fibre bridging effect in composite specimens involves maintaining a constant similitude parameter $\Delta\sqrt{G}$ throughout the fatigue test. This technique is described in the relevant literature and is covered in the Literature Study (page 14). However, in contrast to the approach described in the literature, a different similitude parameter is utilized in the experiments conducted in this thesis. Specifically, the aim is to maintain $\Delta\sqrt{G} = \left(\sqrt{G_{\text{max}}} - \sqrt{G_{\text{min}}}\right)^2$ constant, as opposed to solely G_{max} as described in the literature [21].

As previously mentioned, each composite DCB specimen undergoes testing with a selected $\Delta\sqrt{G}$ value. This involves using a force-controlled actuation of the fatigue machine, where the input loads are actively being altered to fit the desired $\Delta\sqrt{G}$ value. This requires implementing a feedback loop for determining the load, based on the measure compliance of the composite specimen. As the fatigue test progresses, the compliance of the specimen changes at the same applied load due to the growth of the delamination and the fibre bridging effect. The fatigue has to be initiated at a certain load, which also requires an input value of specimen compliance. To measure the initial compliance of the composite specimen, a step is added prior to fatigue loading. A load of 50 N is statically applied and the corresponding displacement is used for calculating the initial specimen compliance. At this load of 50 N, no delamination growth is yet to occur. To maintain a constant $\Delta\sqrt{G}$, the applied load is modified every 20 cycles, with the target load determined using the following equation:

$$P_{\text{Peak}} = \sqrt{\frac{2\alpha_1(2h)B^2G_{\text{max}}}{3(BC)^{2/3}}} \tag{4.2}$$

Here, α_1 represents a curve fitting parameter determined using Equation 5.1. This value of α_1 is specific to the experiment and should be determined during the post-test analysis. However, during the test, a value is also needed to be able to use Equation 4.2. A quasi-static test was used to produce a value of α_1, which is then used during the fatigue experiments with the constant-$\Delta\sqrt{G}$ method. This quasi-static α_1 differs from the fatigue α_1. This means that the selected value of $\Delta\sqrt{G}$ will actually not be precisely followed due to the difference between the quasi-static and fatigue α_1. The post-test analysis will therefore require the determination of the true $\Delta\sqrt{G}$.

Additionally, $2h$ and B denote the thickness and width of the specimen, respectively. The fatigue experiment is concluded when the saturation of the fibre bridging effect occurs. This happens at a delamination length of about 15 mm, the specimen compliance remains constant after this point. A simplified overview of the feedback loop which is implemented in this method can be found in Figure 4.9.

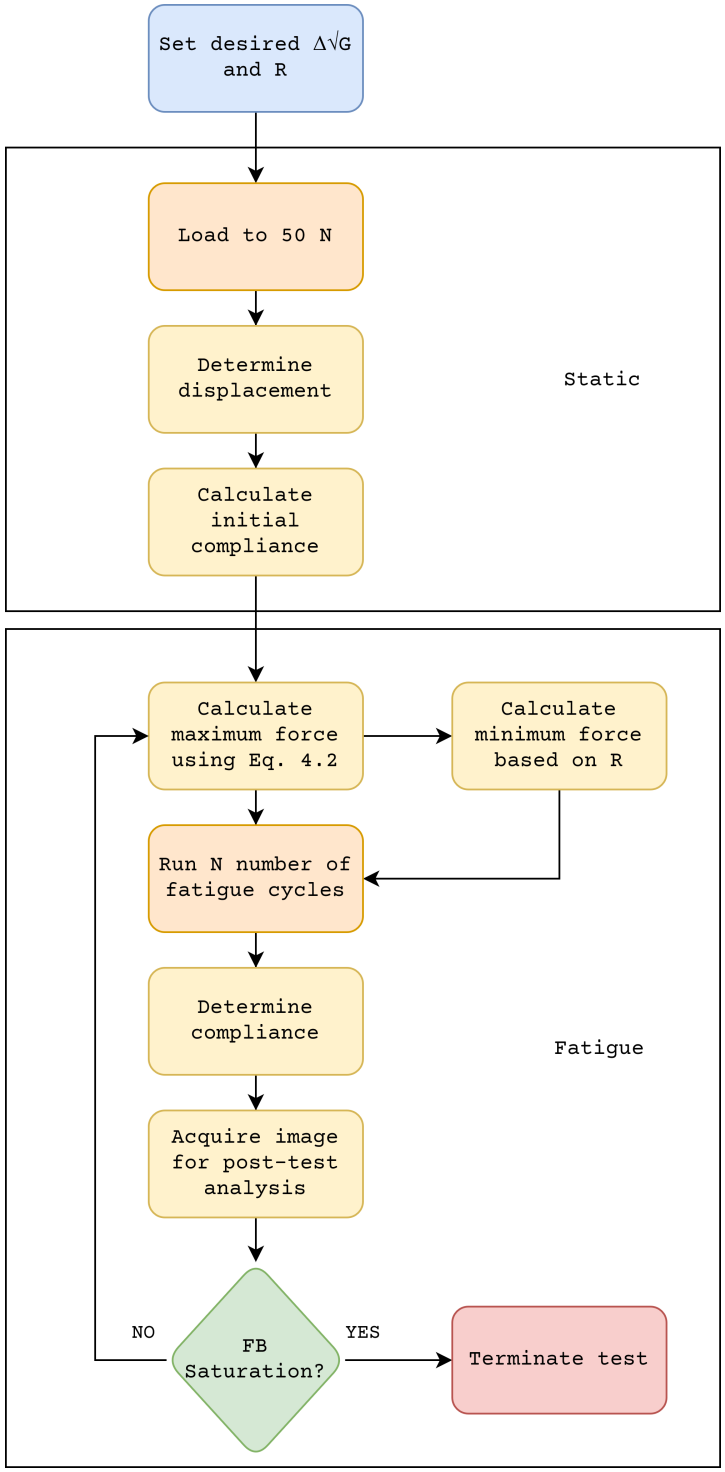

Figure 4.9: Flowchart displaying the feedback loop for the Constant-$\Delta\sqrt{G}$ fatigue experiments.

Method III and IV: Specimen Specific Extrapolation and Hartman-Schijve Equation

The fatigue data which will be used in the fibre bridging exclusion methods proposed by Alderliesten [2] (Method III) and Yao et al. [64] (Method IV) comes from the same specimen which was tested in a displacement-controlled configuration. Multiple fatigue experiments are performed on a single specimen in order to generate multiple fatigue delamination resistance curves. Alderliesten and Brunner [3] give a test protocol on fatigue delamination experiments on composite specimens.

The displacement-controlled tests are performed where the input of the maximum displacement is equal to about 80-90 % of the ultimate displacement for static delamination δ_{max}. The minimum displacement δ_{min} is calculated based on the displacement ratio $R_d = \delta_{min}/\delta_{max}$. At the start of the experiment the stress ratio R can be assumed to be equal to R_d, however, the minimum displacement δ_{min} might have to be altered to better follow the desired stress ratio R. To track the delamination length, an image is taken of the delamination tip location is taken with a selected interval. The recommended interval is every 100 cycles for the first 5000 cycles, then every 500 cycles for the following 15000 cycles, followed by an image every 1000 cycles until the test is terminated. The loads and corresponding SERR values will decrease as the delamination grows through the specimen. The fatigue experiment is continued until a crack growth rate da/dN of 10E-5 mm/cycle is reached. The maximum and minimum load, maximum and minimum displacement and cycle number are stored for each interval cycle. These values are used for calculating the SERR values.

4.3. Overview of Experiments

In this section, an overview is given of the experiments which were performed in this research. Table 4.1 shows the different fibre exclusion methods and which specimens are used to obtain the fatigue resistance curves where the fibre bridging effect is excluded. The cutting bridging fibres (CBF) and constant-$\Delta\sqrt{G}$ (C-$\Delta\sqrt{G}$) methods were used with respect to fatigue data obtained by testing specimens which were made during this thesis project. The fatigue data used for the specimen-specific extrapolation method (SSE) and the Hartman-Schijve (HS) equation method was gathered from the experiments conducted by Yao [63, 61, 62, 60], as per the testing protocol by Alderliesten and Brunner [3]. Due to the limited availability of the fatigue testing machines at the DASML, the choice was made to use Yao's data as a substitute. Importantly, the specimens used in Yao's experiments are identical to the ones made in this thesis in terms of pre-preg material, dimensions and fibre orientations.

Table 4.1: An overview of the experiments done over the course of the present research, including the data obtained from Yao [63, 61, 62, 60].

FB Exclusion Method	Specimen ID	Frequency [Hz]	Stress Ratio [-]	Displacement-/ force-actuated
I (CBF)	Vac17 (5.3 mm)	2	0.1	Displacement
I (CBF)	Vac17 (61.5 mm)	2	0.1	Displacement
II (C-$\Delta\sqrt{G}$)	Vac15 ($\Delta\sqrt{G}$ = 100.0)	2	0.1	Force
II (C-$\Delta\sqrt{G}$)	Vac7 ($\Delta\sqrt{G}$ = 114.2)	2	0.1	Force
II (C-$\Delta\sqrt{G}$)	Vac9 ($\Delta\sqrt{G}$ = 128.5)	2	0.1	Force
II (C-$\Delta\sqrt{G}$)	Vac10 ($\Delta\sqrt{G}$ = 142.8)	2	0.1	Force
II (C-$\Delta\sqrt{G}$)	Vac12 ($\Delta\sqrt{G}$ = 157.1)	2	0.1	Force
II (C-$\Delta\sqrt{G}$)	Vac5 ($\Delta\sqrt{G}$ = 171.3)	2	0.1	Force
II (C-$\Delta\sqrt{G}$)	Vac8 ($\Delta\sqrt{G}$ = 185.6)	2	0.1	Force
III (SSE)	Yao-Sp7-1 (3.1 mm)	5	0.1	Displacement
III (SSE)	Yao-Sp7-2 (15.1 mm)	5	0.1	Displacement
III (SSE)	Yao-Sp7-3 (28.0 mm)	5	0.1	Displacement
III (SSE)	Yao-Sp7-4 (40.2 mm)	5	0.1	Displacement
III (SSE)	Yao-Sp7-5 (53.7 mm)	5	0.1	Displacement
III (SSE)	Yao-Sp7-6 (68.3 mm)	5	0.1	Displacement
IV (HS)	Yao-Spec7-1 (3.1 mm)	5	0.1	Displacement
IV (HS)	Yao-Spec7-2 (15.1 mm)	5	0.1	Displacement
IV (HS)	Yao-Spec7-3 (28.0 mm)	5	0.1	Displacement
IV (HS)	Yao-Spec7-4 (40.2 mm)	5	0.1	Displacement
IV (HS)	Yao-Spec7-5 (53.7 mm)	5	0.1	Displacement

5

Data Analysis

The data obtained in the experimental campaign of the present project has to be analyzed before the research question can be answered. The goal of the data analysis is to consistently represent the fatigue data. To this end, the variables which are to be calculated are done so in a similar manner. Thus, the comparative nature of this experimental study can be ascertained.

5.1. Compliance and Delamination Length

The delamination length or crack length a is determined through images captured during the fatigue testing. The testing software makes it possible to send a pulse to the camera, triggering a snapshot which is subsequently saved. The delamination length a can be visually determined from these pictures using an imaging software called ImageJ. Since many images were gathered over the course of the fatigue testing, a less time-consuming method was used to gather the delamination length values for the recorded images.
The relationship between the specimen compliance C and the delamination length a can be approximately expressed in the following form:

$$\frac{a}{2h} = \alpha_0 + \alpha_1 (BC)^{1/3} \tag{5.1}$$

where $2h$ is the specimen thickness, B the specimen width, C the specimen compliance, and α_0 and α_1 are fitting coefficients. The specimen compliance is defined as the displacement divided by the load.

This relationship follows from the analysis of a cantilevered beam and the deflection associated with an applied load on the very end of such a beam. In essence, the double cantilevered beam (DCB) test consists of two such elementary beam structures. The length of the beam, which can be considered equal to the delamination length a is then a function of the cubed root of the inverse stiffness, i.e. the compliance: $a = f(C^{1/3})$.

Because the compliance can be found from the measurements of the 1 kN load cell and the displacement sensor in the fatigue machine, the fitting coefficients α_0 and α_1 can be determined if there are sufficient delamination length data points. Considering that there can be a large number of images to determine the crack length a from, it can be time efficient if these crack lengths are determined based on a fitted line using Equation 5.1 instead of determining all instances of a manually. Therefore, a small subset of images is chosen to establish the fitting coefficients α_0 and α_1. For every 0.5 mm of crack length extension, an image is chosen. In this manner, a delamination length a can be calculated using the established

fitting coefficients and Equation 5.1. The validity of this method of determining the delamination length based on specimen compliance is examined next.

To test the validity of determining crack length based on the measured compliance of the specimen, there are multiple points to take into account. Firstly, the assumption that the relationship between the crack length and the compliance is linear can be examined. As mentioned, Equation 5.1 is based on classical beam theory which does not assume the presence of the fibre bridging effect. Therefore, the manually determined crack length data can be plotted together with the corresponding specimen displacement. If a resulting linearly fitted line does not deviate much from the data points then it is possible to conclude that the fibre bridging effect has a negligible effect on the nature of Equation 5.1 over the course of a single fatigue test.

The second point of interest is understanding the specimen specificity of the aforementioned relationship between crack length and compliance. If the two fitting parameters α_0 and α_1 are not varying considerably per specimen then this would result in less work for determining the crack length for each obtained data point. Because specimens are made from a single composite panel, see Section 4.1, the initial hypothesis is that the fitting parameters will not vary between specimen to specimen.

Lastly, one might consider the effect of fibre bridging on the linearity of Equation 5.1 at different crack lengths. For instance, it is understood from the literature that the fibre bridging effect becomes more noticeable at larger delamination lengths. Thus, using a linear line fitting which is gathered using data with a pre-crack length of 50 mm and extrapolating crack length data for a fatigue test with a pre-crack length of 85 mm might be an invalid approach. This hypothesis is tested to display the effect of large-scale fibre bridging on the linearity of Equation 5.1.

Considering the first point of attention, a scatter plot is presented in Figure 5.1 for specimen ”Vac5” which was used in a constant-$\Delta\sqrt{G}$ test. About 50 data points are given, which amount to a total crack extension of about 25 mm. This means that after about 0.5 mm the crack length is noted down. Because the crack growth rate decreases as the fatigue tests proceed, more data points are gathered at the beginning stages of the test. Linearly fitting a line through the data points gives an acceptable coefficient of determination (R^2 = 0.996). This means that the linearity of Equation 5.1 is verified and the fitting parameters might be used for determining the crack length for points where the compliance is known through automatic data acquisition.

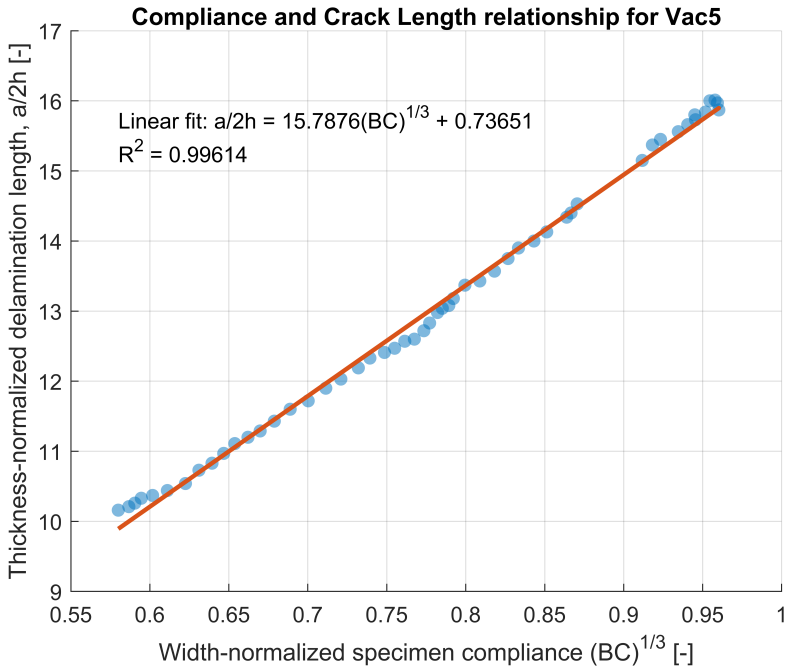

Figure 5.1: Linear fit of the compliance and the crack length for specimen "Vac5".

Determining the crack length based on the measured compliance is therefore a method which could yield time gained by not having to manually determine crack lengths from various images. This provides the opportunity to use more data points in the construction of a Paris-type power law for fatigue experiments which can eliminate scatter due to having a limited amount of data points. However, considering the second point mentioned above about the relationship of Equation 5.1 being specimen-specific, the following plot is presented. In Figure 5.2 the fitted line of specimen Vac5 (red line in Figure 5.1) is presented along with data points for specimen "Vac10". The data points of "Vac10" seem to be in accordance with the fitted line of "Vac5". It should be noted here that both tests on these specimens were started with the same initial crack length. However, it can be concluded that there is not a strict specimen-specificity of Equation 5.1 for specimens which are made from the same composite panel.

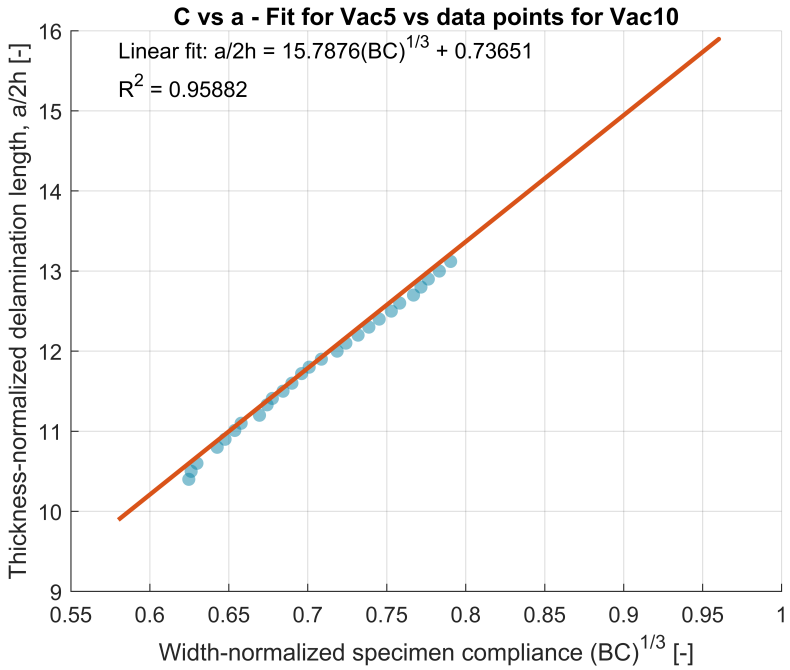

Figure 5.2: Crack length data points of Vac10 compared to the fitted line for "Vac5".

The effect of large-scale fibre bridging on the linearity of the compliance and crack length relationship still remains to be investigated. It is understood that for fatigue tests with different composite specimens, the crack lengths can be determined using a fitting of Equation 5.1 under the condition that these specimens share the same initial crack length, this method is also applied in this study. For testing procedures where multiple fatigue runs are conducted on a single specimen, it would also be beneficial to use the same method for obtaining crack lengths. Figure 5.3 shows how manually gathered crack length data (blue points) differs from the extrapolated linear fit for a smaller initial delamination length and that there is an unsatisfactory coefficient of determination between the extrapolated fit and the data of a different initial delamination length. It can be concluded that large-scale fibre bridging severely affects the linearity of Equation 5.1 over different initial crack lengths. Thus, one must not use a fit made for a certain crack length range and extrapolate it to crack lengths outside of this region, as it will likely provide inaccurate crack length values.

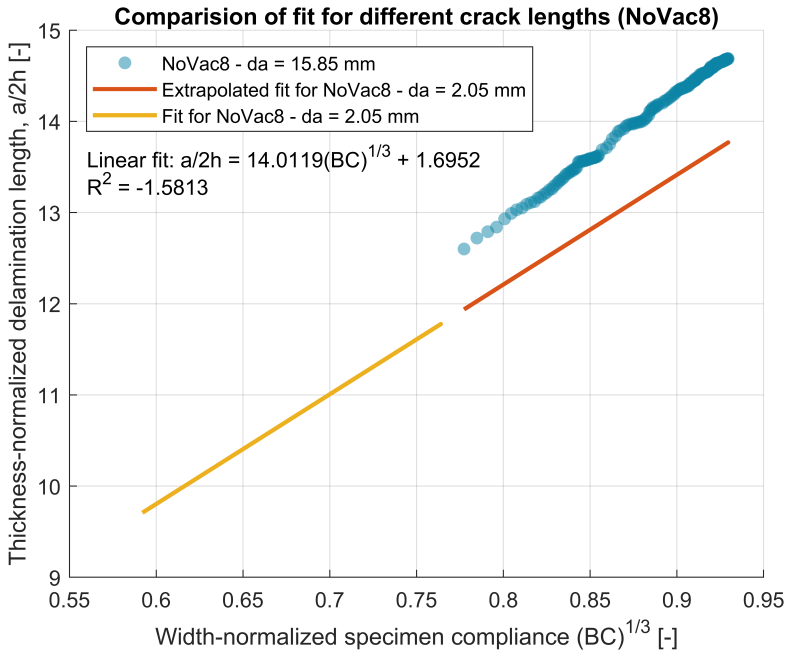

Figure 5.3: Comparison of relationships between crack length and compliance for two different initial crack lengths for specimen "NoVac8".

5.2. Crack Growth Rate

The rate at which delamination grows through a composite specimen during a fatigue test is called the crack growth rate, da/dN. The crack growth rate represents the length of delamination propagation in a single fatigue cycle. For accurately determining the crack growth rate da/dN at any given point during a fatigue test, multiple methods can be used.

5.2.1. Incremental Polynomial Method

The standard for the measurement of fatigue crack growth rates (ASTM E647) describes an incremental polynomial method through which da/dN may be calculated. It involves the fitting of a second-order polynomial through a set of successive data points. This set consists of $2n$ + 1 consecutive data points of a delamination length a vs fatigue cycle N curve. This method of determining the crack growth rates is not able to describe the delamination rates for the first and last n data points and therefore the da/dN values for these points should be calculated using lower values of n. Figure 5.4 visually shows how the first and last sets of data points can be used for determining their corresponding crack growth rates. The ASTM E647 takes a maximum of seven points at a time to calculate the value of da/dN. This implies that n = 3 for most data points, the 7-point-method in Figure 5.4.

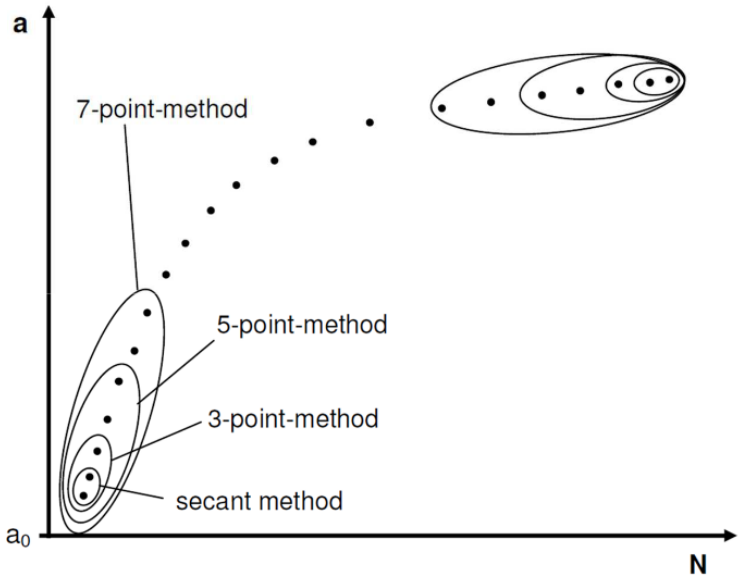

Figure 5.4: Schematic for a conventional a vs N-curve for the determination of the delamination growth rate, da/dN.

Regression parameters can be determined using a least square approach which minimizes the square of the deviation between the observed and fitted values of the delamination length a.

The fitted second-order polynomial which is used for determining da/dN has the following function:

$$\hat{a}_i = b_0 + b_1 \left(\frac{N_i - C_1}{C_2} \right) + b_2 \left(\frac{N_i - C_1}{C_2} \right)^2 \tag{5.2}$$

where b_0, b_1 and b_2 are the regression parameters from the least squares

method over the range of $a_{i-n} \leq a \leq a_{i+n}$. The parameters $C_1 = 1/2\,(N_{i-n} + N_{i+n})$ and $C_2 = 1/2\,(N_{i+n} - N_{i-n})$ are scaling parameters for the input data. The rate of crack growth at N_i is obtained by taking the derivative of the second-order polynomial (parabola) of Equation 5.2:

$$(\mathrm{d}a/\mathrm{d}N)_{\hat{a}_i} = (b_1)\,/\,(C_2) + 2b_2\,(N_i - C_1)\,/C_2^2 \tag{5.3}$$

5.2.2. Higher Order Polynomial Method

For experiments where a high number of data points is available for the crack length the method described above yields growth rate values with a high degree of scatter. For certain experiments, a compliance value was stored after every 20 fatigue cycles, which results in a large number of crack length values, calculated through the method described in Section 5.1. This data can get noisy, as shown in Figure 5.5. Applying the Incremental Polynomial Method to this noisy data gives unreliable results for the crack growth rate values with a large amount of scatter.

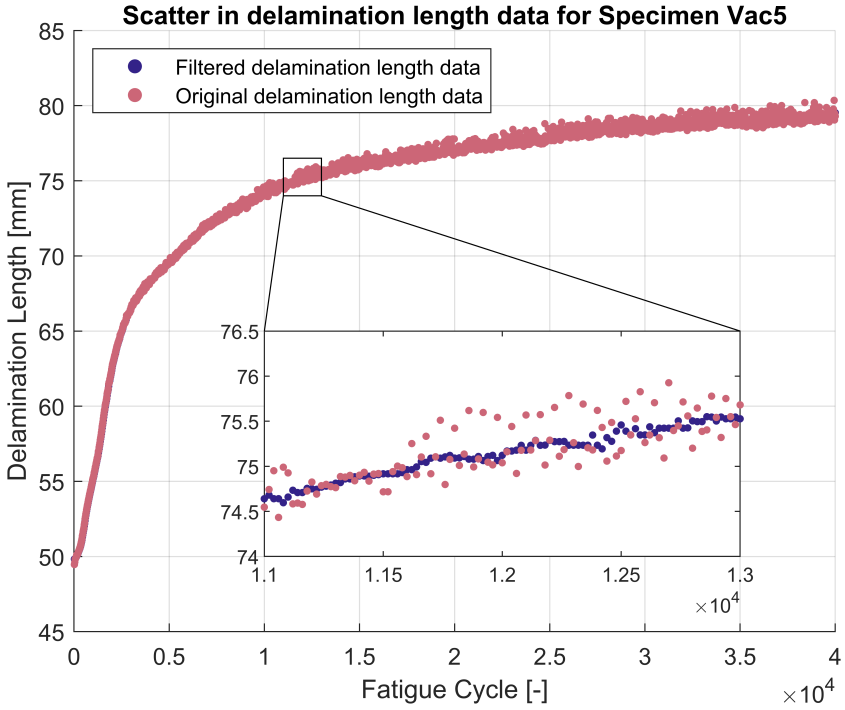

Figure 5.5: Noise in the delamination length data of Specimen "Vac5".

The undesirable scatter in the delamination length data can be countered with a variety of techniques. A choice could be made to include fewer data points and take a delamination length value every 500 fatigue cycles instead of 20 fatigue cycles. However, this would mean that a lot of valuable data points would be lost and for that reason, this approach was not taken. Another way of removing the noise from the data is to take a larger number of points over which a parabola is fitted with the Incremental Polynomial Method. The choice of taking n = 3 is quite arbitrary and one could choose to take a much higher number. Although this approach gives reasonable values for the crack growth rate, da/dN, it does take a lot of computational time to fit a parabola over a larger set of data points for each data point.

An approach for computing crack growth rate values from noisy data is to filter the data prior to analysis, which is computationally more feasible.

MATLAB provides the "smoothdata" function to reduce noise in data. A sliding window with a length of ten data points can be used to calculate a median value. The resulting delamination length data set is less noisy, enabling the fitting of a high-order polynomial ($n > 50$) to obtain a continuous curve in the a vs N figure. The derivative of this curve can be calculated to obtain the crack growth rate da/dN as a function of the fatigue cycle N. Figure 5.5 displays the filtered data. This method of filtering the noisy data prior to fitting a higher-order polynomial is used in the determination of the crack growth rates, da/dN, in this study.

5.3. Strain Energy Release Rate

To construct a fatigue delamination resistance curve for the experiments in this research, an expression for the strain energy release rate (SERR) is required. ASTM D5528 [5] recommends calculating the SERR using the modified compliance calibration (MCC) method, given by the following expression:

$$G_I = \frac{3}{2(2h)} \cdot \left(\frac{P}{B}\right)^2 \cdot \frac{(BC)^{2/3}}{\alpha_1} \cdot F \tag{5.4}$$

where G_I is the SERR for a Mode I (opening tensile) configuration, α_1 is given in Equation 5.1, P and B are the applied load and specimen width, respectively and F is a large-displacement correction factor (described below). The maximum and minimum SERR, G_{max} and G_{min} are calculated by substituting the maximum and minimum load into Equation 5.4.

A large-displacement correction factor F is to be applied to all the SERR calculations done during the data analysis. According to ISO 15024 [55], the factor F will contribute significantly when the quotient of the displacement and delamination length is larger than 0.4, i.e. δ/a > 0,4. The large-displacement correction factor F is expressed as:

$$F = 1 - \frac{3}{10}\left(\frac{\delta}{(a - a_{spec})}\right)^2 - \frac{2}{3}\left(\frac{\delta l_1}{(a - a_{spec})^2}\right) \tag{5.5}$$

where l_1 is defined as the distance from the piano hinge axis to the midplane of the DCB specimen. In this case, a_{spec} is defined as the horizontal distance between the piano hinge axis and the short edge of the DCB specimen at the side of the piano hinge. These two values are equal for all the specimens used in this study and are equal to 10 mm and 21 mm for l_1 and a_{spec} respectively. This typically leads to a negligible change (< 0.5%) in the calculated SERR value. Xu et al. [58] showed that the large-displacement correction factor F tends to be inaccurate for large deformations. However, the present research did not utilise the proposed re-formulation of the factor F as large deformations were not encountered during the delamination experiments in this work.

For characterizing delamination growth in composite specimens a number of similitude parameters may be chosen. To analyze growth behaviour under cyclic loading, Rans et al. [47] showed that using the SERR range defined as $\Delta G = G_{max} - G_{min}$ introduces a mean load dependency. Instead, the authors propose to use $\Delta\sqrt{G} = \left(\sqrt{G_{\max}} - \sqrt{G_{\min}}\right)^2$ as a similitude parameter in composite delamination growth characterization. Therefore, in the subsequent data analysis and resulting plots showing the fatigue delamination resistance curve this expression of the SERR range will be maintained.

6

Results & Discussion

This chapter presents the experimental findings of the current research, which focuses on the methods for excluding the fibre bridging effect and the influence it has on fatigue data. Each section of the current chapter is dedicated to a specific method for excluding this phenomenon. The methods have been introduced individually in Section 2.2. In the last section of this chapter, the results of the methods are compared in order to answer the posed research questions from Chapter 3.

6.1. Method I: Cutting Bridging Fibres

This section presents the findings of the method proposed by Khan [34] for mitigating the impact of the fibre bridging effect. The method aims to exclude the influence of bridging fibres on fatigue delamination resistance curves by physically cutting the bridging fibres while a composite specimen is positioned in the fatigue machine. To this end, a steel wire is securely clamped in a jig saw frame, allowing the cutting of bridged fibres trailing the delamination tip when the fatigue test is temporarily paused. Figure 6.1 illustrates the effectiveness of this method in removing a significant number of bridging fibres trailing with the delamination tip.

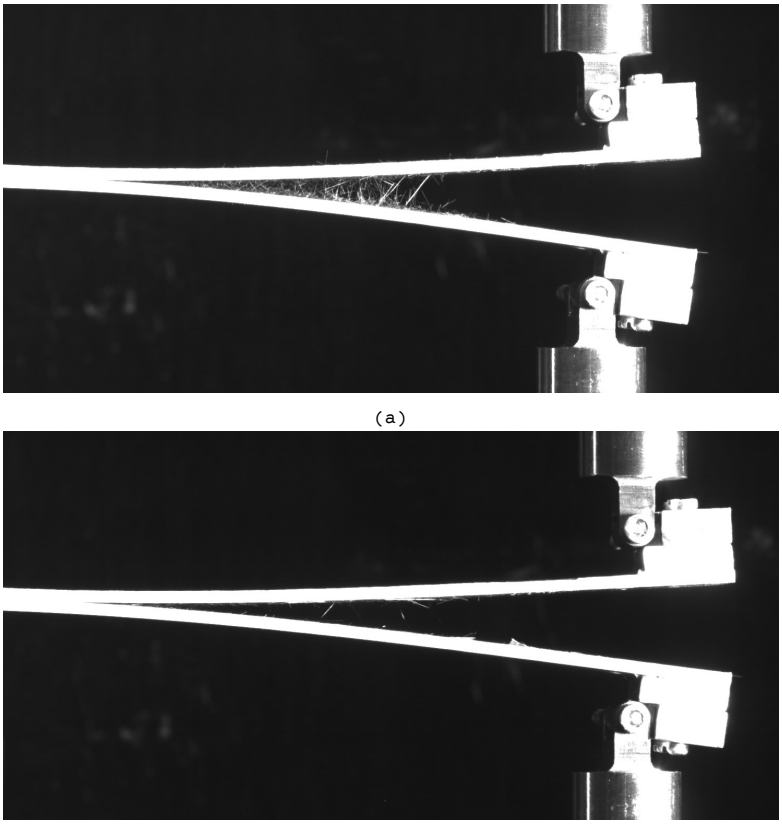

(a)

(b)

Figure 6.1: A composite DCB (Double Cantilever Beam) specimen, where the upper image (a) is taken before cutting the bridging fibres and the lower image (b) is taken after cutting the bridging fibres.

Two fatigue delamination experiments were performed on a single specimen, named "Vac17", using the cutting method introduced by Khan et al. [34]. Whilst one test was started at a higher pre-crack delamination length, close to $a - a_0$ = 61.5 mm, the other one was done at a lower pre-crack delamination length of 5.3 mm. The reason for doing this was to investigate if the resulting "zero-bridging" fatigue delamination curve of the two different tests showed accordance with each other as expected. If this is the case, then both fatigue data points where the fibre bridging effect is excluded could be used to construct a single fatigue delamination resistance curve. Figure 6.2 shows the load measured on the specimen after removing the bridging fibres plotted against the position of the cutting thread. As per the method [34], by fitting a power law to this dataset, the exponent m can be determined.

Equation 4.1 is used to extrapolate and obtain the load in the absence of the fibre bridging effect. In Figure 6.3 the loads on the specimens before and after cutting the bridging fibres as well as the extrapolated load for the zero-bridging case are plotted as a function of the delamination length for both delamination experiments. It is observed that there is a considerable difference between the pre/post-cutting loads and the "zero-bridging" load. The shortcoming of the cutting method is that the cutting thread does not fully reach the delamination tip and trails it by around 5 mm. Khan et al. [34] find a similar distance between the delamination tip and the cutting thread of 3 to 5 mm. In this short region, however, the contribution of the fibre bridging effect seems to be the largest. Inspecting this region visually, the density of bridging fibres is determined to be of a high nature.

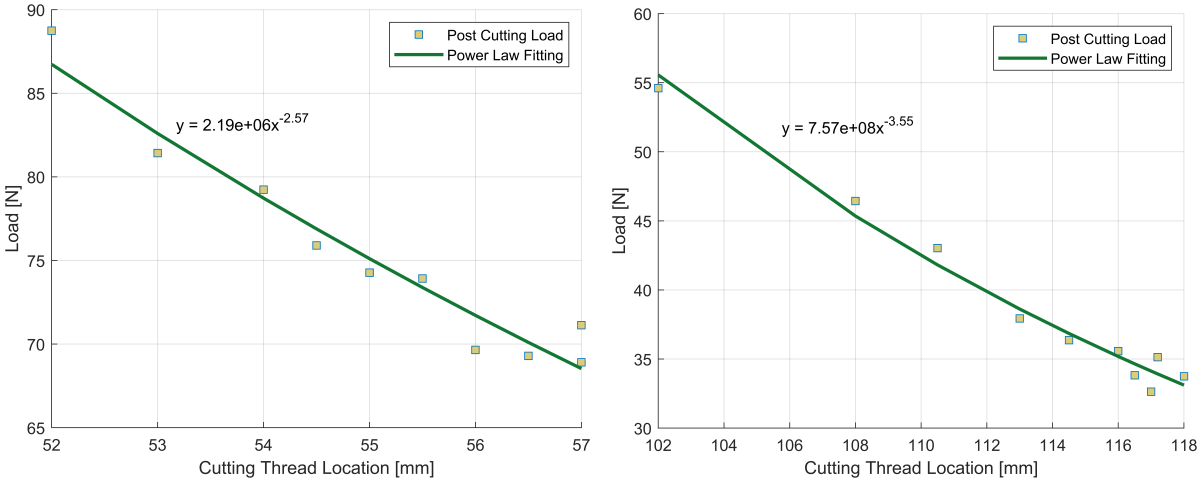

Figure 6.2: Loads on the specimen as a function of the cutting thread position for specimens "Vac17", for obtaining the power law exponent m.

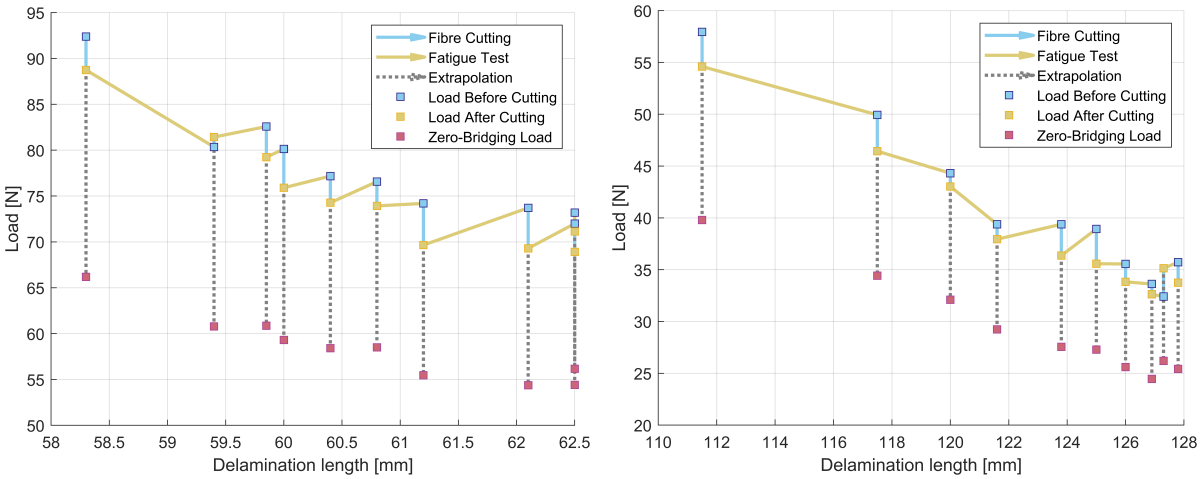

Figure 6.3: Loads on the specimens as a function of the delamination length for specimen "Vac17".

To obtain a "zero-bridging" delamination resistance curve the corresponding values for the maximum and minimum SERR may be found by using Equation 5.4. The SERR range, $\Delta\sqrt{G} = \left(\sqrt{G_{\max}} - \sqrt{G_{\min}}\right)^2$, is calculated. The method for finding the crack growth rate da/dN is described in Chapter 5.2.2. Figure 6.4 shows two fatigue delamination resistance curves. The right curve shows the values of $\Delta\sqrt{G}$ when the load measured after cutting the fibres is used as an input and the left curve uses the "zero-bridging" load values which were extrapolated. As expected, this yields a more conservative fatigue R-curve as the "zero-bridging" loads are lower and the corresponding SERR values are lower too.

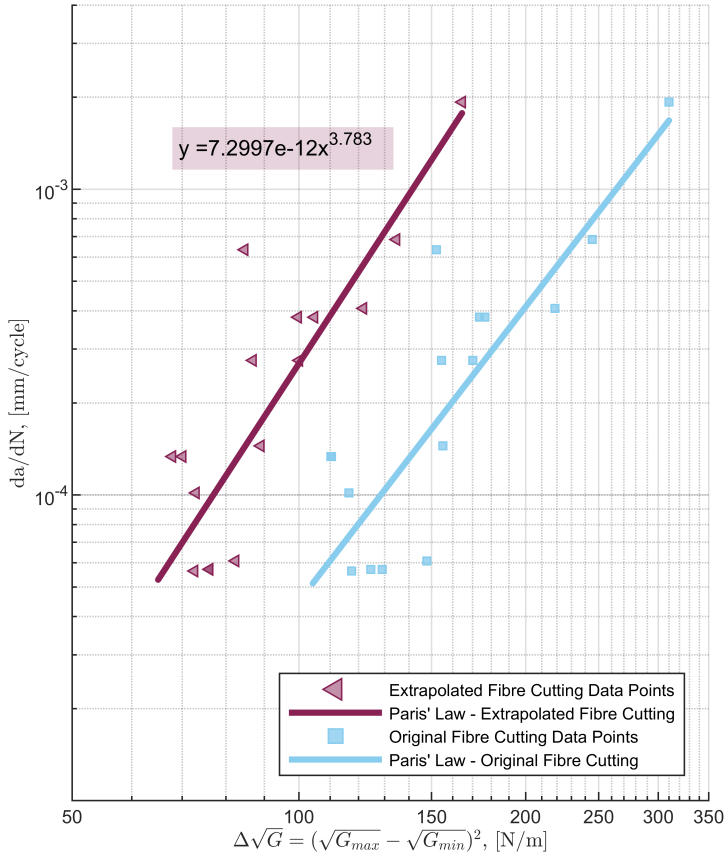

Figure 6.4: Delamination resistance curve for the fibre cutting method by Khan [34]. Data points for both the extrapolated, zero-bridging case and the non-extrapolated data points.

Cutting bridging fibres during the fatigue delamination experiments seems to be a method which is able to produce a fatigue R-curve where the delamination resistance contribution due to fibre bridging is excluded. Figure 6.4 not only shows the Paris-type power law for the "zero-bridging" case but also the individual fatigue data points which are used to construct this relationship. As mentioned before, the fatigue data points originated from two fatigue delamination experiments on the same composite specimen with different pre-crack delamination lengths. In Figure 6.5, the "zero-bridging" fatigue delamination resistance curve of Figure 6.4 is repeated but the data points are separated based on the two experiments. Instead of one Paris-type power law for the two experiments together, each test now has an individual power law fitting. The accordance between the two fitting functions suggests the possibility to use data from multiple fatigue experiments done on the same composite specimen with the intent of creating a "zero-bridging" fatigue delamination resistance curve. Performing multiple fibre-cutting experiments on the same specimen would also increase the size of the data set from which a single "zero-bridging" Paris-type power law could be made. This way the variance of the data set could be reduced, resulting in a more effective "zero-bridging" depiction.

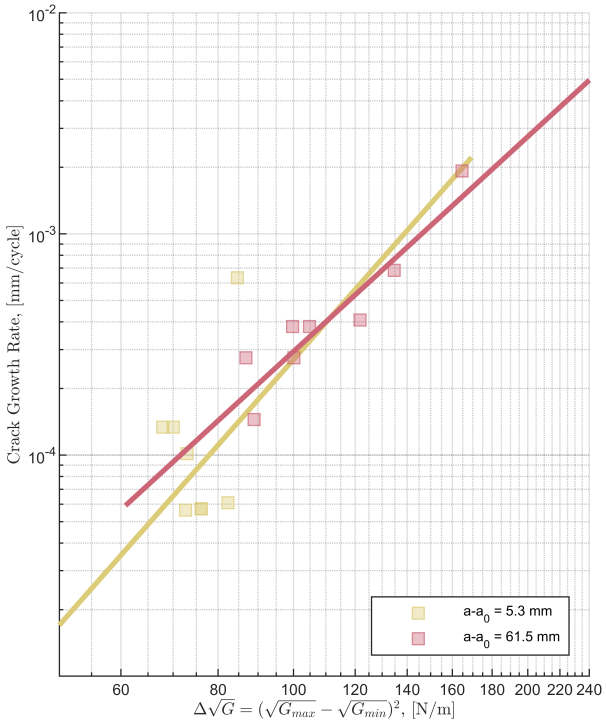

Figure 6.5: Two "zero-bridging" fatigue delamination resistance curves constructed for two fatigue tests done at different pre-crack delamination lengths.

The considerable scatter in the results associated with the fibre cutting method makes this method less suitable for standardized use. Developing this method to contain the spread of "zero-bridging" fatigue data points might be of interest to further investigate how this method compares to the other fibre bridging exclusion methods. In particular, the paper [34] describing this exclusion method leaves too much room for operator scatter because the fibre cutting protocol is not accurately described. This is essential and should be considered before this method can be used in a standardized testing protocol. Measures to contain the scatter associated with this method could be in the form of determining the horizontal load associated with the fibre cutting procedure. Applying too much force whilst performing the fibre cutting could induce unintended delamination propagation. Moreover, it might be beneficial to use a more accurate load-measuring device as compared to the 1 kN load cell used in this research. The difference in the pre-and post-cutting load was too small to be accurately determined using the measurement equipment used in this thesis.

6.2. Method II: Constant-$\Delta\sqrt{G}$

Next, the results of the fibre exclusion method where the similitude parameter $\Delta\sqrt{G}$ is kept constant throughout the fatigue test, are presented. The required alterations to the traditional, displacement-controlled fatigue tests are described in Section 4.2. This exclusion method involves a feedback loop where the applied load on the composite specimen is a function of the measured specimen compliance during the fatigue test. Figure 6.6 illustrates the outcomes of a fatigue experiment carried out with a corresponding value of $\Delta\sqrt{G}$ = 171.3 N/m. Due to the difference in the value of the quasi-static α_1 and fatigue α_1 in Equation 4.2, the true value of $\Delta\sqrt{G}$ (= 171.3 N/m) differs from the selected value $\Delta\sqrt{G}$ (= 300 N/m).

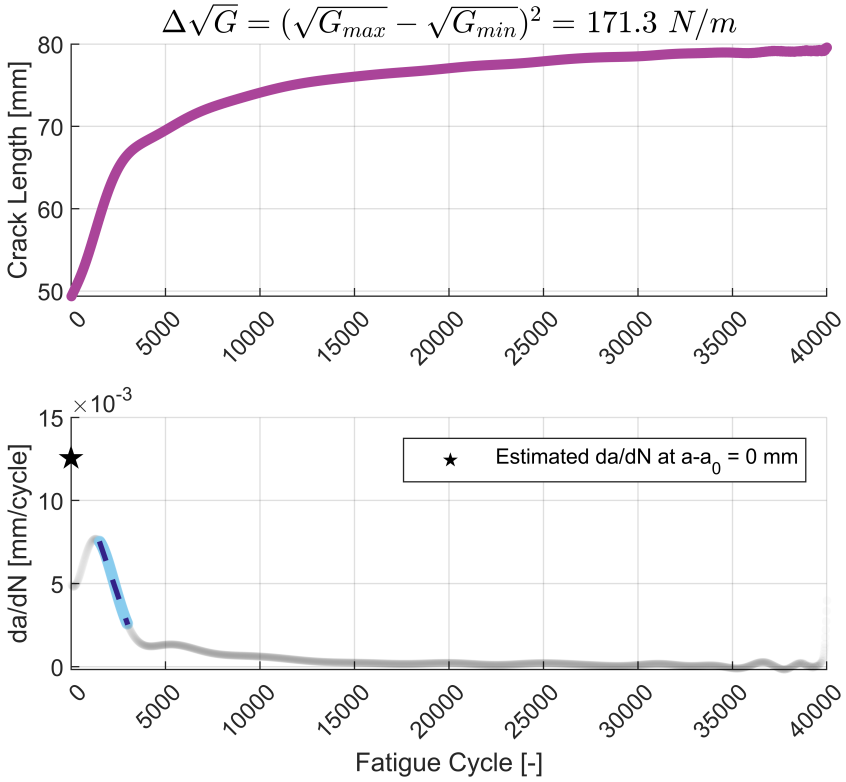

Figure 6.6: The delamination length and the delamination growth rate as a function of the fatigue cycle of a specimen used in a constant-$\Delta\sqrt{G}$ experiment.

In Figure 6.6, the upper plot demonstrates how the delamination length changes as the fatigue test progresses. The crack-shielding characteristic of composite specimens with fibre bridging can be observed, as the crack growth rate declines and eventually becomes almost constant. The decrease in the rate at which the delamination length changes is attributed to the creation of bridging fibres at the mid-plane of the composite specimens. Initially, only new bridging fibres form due to crack opening, but after roughly 15 mm, the steady-state of fibre bridging is observed. This steady state is also observed by Donough et al. [15] and Sato et al. [51].

The objective of this fibre bridging exclusion method is to determine a value for the crack growth rate where no fibre bridging is apparent. In the lower plot of Figure 6.6, the crack growth rate da/dN is displayed as a function of the fatigue cycle number N. The crack growth rate is computed by acquiring the derivative function of the line in the upper plot, according to the method described in Section 5.2.2. Several observations can be made upon

examination of the resulting crack growth rate and comparison to findings in comparable research.

The function shape in the present study exhibits similarities with the results of two previous studies [21, 15], as depicted in Figure 2.9. Initially, the crack growth rate increases until a maximum value is reached, followed by a linear decrease until the steady state for bridging fibre formation is reached. As in the previous studies [21, 15], the zero-bridging case, representing the absence of nucleated bridging fibres at the start of the fatigue test (N = 0), can be determined by linearly extrapolating the region with constant decrease and finding the point where the extrapolated line intersects the y-axis. The black pentagram in Figure 6.6 represents the zero-bridging crack growth rate value, which coincides with the extension of the blue dashed line, the linear fit of the light blue data points in the region of interest.

To construct a delamination resistance (R-curve) using this method, multiple tests were performed with different specimens, all tested at a selected value of $\Delta\sqrt{G}$. However, it is crucial to ensure that the specimens have not yet shown saturation of the fibre bridging effect. If saturation of fibre bridging is achieved, for instance at N > 3000 cycles in Figure 6.6, then it will not be possible to perform the linear extrapolation to a "zero-bridging" value of the crack growth rate. A slight propagation of the delamination is still allowable, as this will only conceal the initial increase of the crack growth rate. Thus, in this method, specimens without fibre bridging saturation are used where the delamination is solely caused by the PTFE insert at the mid-plane and not as a result of delamination growth during experiments.

Figure 6.7 displays a "zero-bridging" delamination resistance curve constructed using the constant-$\Delta\sqrt{G}$ method. This curve was generated using data from fatigue tests on seven different composite specimens, each with a unique value for $\Delta\sqrt{G}$. The black pentagrams on the curve indicate the zero-bridging crack growth rate values, which represent the crack growth rates at which no bridging fibres are present. The light blue data points represent the crack growth rates measured for each individual composite specimen.

To establish a Paris' law for the zero-bridging case, a power law was fitted through the pentagrams. The resulting relationship is shown in Figure 6.7, along with the relevant fitting parameters D and n. This power law relationship can be used to predict the delamination growth rate at a given SERR value, provided that no bridging fibres are present:

$$\frac{da}{dN} = D(\Delta\sqrt{G})^n = D\left[\left(\sqrt{G_{\max}} - \sqrt{G_{\min}}\right)^2\right]^n \tag{6.1}$$

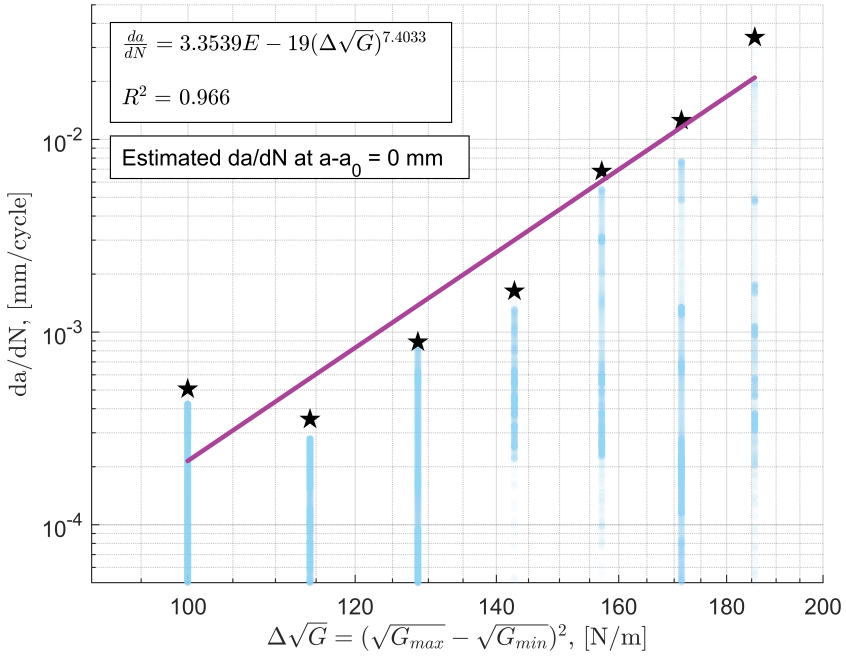

Figure 6.7: Relationship between rack growth rate da/dN and $\Delta\sqrt{G}$, a delamination resistance curve.

The obtained Paris-type power law curve describes a typical delamination resistance curve for this type of composite specimen. The expected value of the exponent n was around 6, based on earlier research found in literature [2] with similar material. Remarkably, the crack growth rate da/dN for the composite specimen tested at the lowest fatigue loading ($\Delta\sqrt{G}$ = 100 N/m) does not yet show any signs of a fatigue threshold where slow crack growth is observed. Therefore, it cannot yet be assumed that a slow crack growth regime of a delamination resistance curve was reached. Conversely, the crack growth rate for the zero-bridging case with this particular SERR value seems to be higher than that of the higher neighbouring fatigue loading which is not expected. For a better understanding of the behaviour of the delamination resistance in the slow growth regime, more fatigue tests may be executed with a denser range of $\Delta\sqrt{G}$ values to be kept constant. These slow-growth tests will naturally take up more time, which is the leading reason why they have not been considered in the present study. Overall, the fitted power law through the seven data points has a high coefficient of determination, i.e. $R^2 \approx 0.966$.

6.3. Method III: Specimen Specific Extrapolation

In this section, the methodology proposed by Alderliesten [2] to exclude the influence of the fibre bridging effect is applied and the results are presented. As highlighted in the Literature Study (see page 17), this approach involves extrapolating a fitted surface equation to approach a zero pre-crack delamination length. It emphasizes considering fatigue data solely related to a specific composite specimen. Employing this technique, the fatigue data from a single specimen utilized in the studies conducted by Yao et al. [63, 61, 62, 60] is analyzed. The fatigue delamination resistance curve obtained after eliminating the fibre bridging effect is presented in this section.

Six consecutive fatigue delamination resistance curves are generated and analyzed from a single composite specimen taken from the available fatigue data of Yao et al. [63, 61, 62, 60], referred to as "Spec7". By fitting a Paris-type power law through each of the curves and translating the corresponding SERR values along the slope of the power law to a value of $da/dN_T = 2 \times 10^{-7}$ m/cycle, an average can be taken of these translated SERR values. For each delamination resistance curve, a corresponding average translated SERR value is therefore calculated. By plotting these values along with their respective pre-crack delamination length values, it is possible to show how the saturation of bridging fibres occurs for longer delamination lengths. In Figure 6.8, it can be seen how a second-order polynomial curve fit through these data points approaches a constant value for the average translated SERR value.

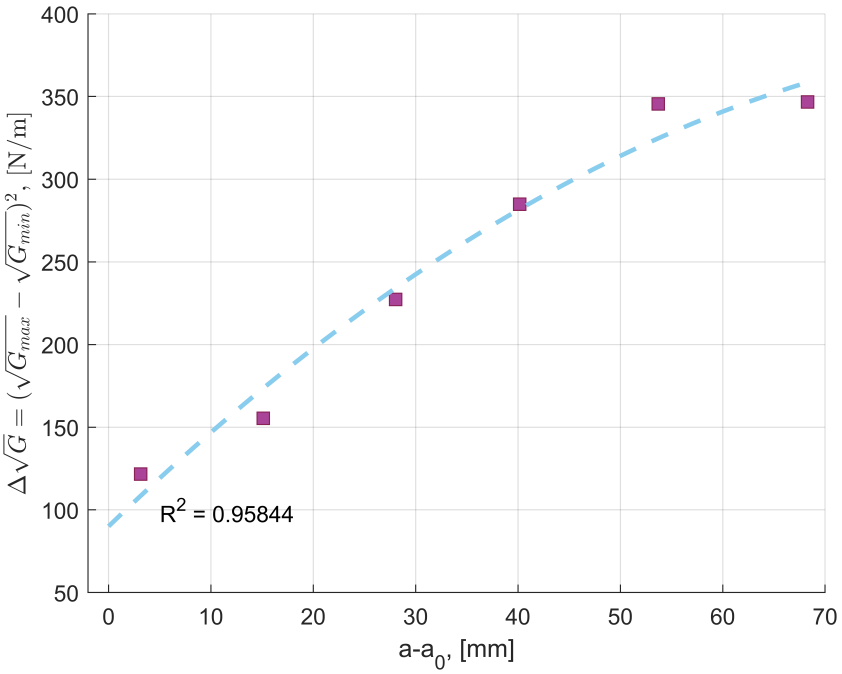

Figure 6.8: The average, translated SERR value for six fatigue delamination resistance curves with corresponding pre-crack delamination lengths.

Next, a regression analysis can be performed on the six delamination resistance curves according to the method [2]. By using Equation 2.4 and setting the pre-crack delamination to zero, an expression is obtained for a

"zero-bridging" resistance curve:

$$\log(\Delta\sqrt{G})_{avg,thr} = C_0 + C_2 \log\left(\frac{da}{dN}\right) + C_4 \left[\log\left(\frac{da}{dN}\right)\right]^2 \tag{6.2}$$

The determined values for C_0, C_2, and C_4 are 3.48, 0.321, and 0.0126, respectively.

Lastly, the scatter of the individual fatigue data points is projected onto this "zero-bridging" curve. The result is Figure 6.9, which displays a fatigue delamination resistance curve where the fibre bridging effect is excluded, yielding a more conservative curve.

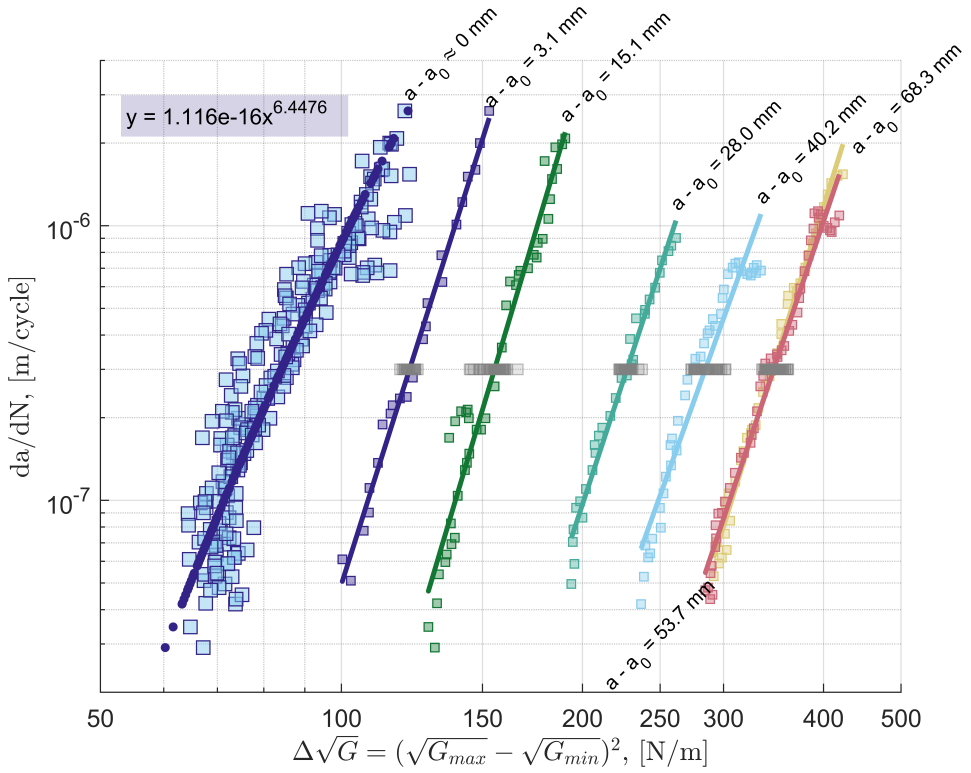

Figure 6.9: A "zero-bridging" fatigue delamination resistance curve along with original fatigue curves which are used in accordance with the method by Alderliesten [2], data obtained from Yao ("Spec7") [66, 67].

The robustness of the present method for the exclusion of the fibre bridging is analysed by performing the surface fitting of Equation 6.2 on data for which the development of bridging fibres has not yet reached a saturated state. To do this, three fatigue experiments on a single experiment are analyzed instead of six previously. In Figure 6.10, two Paris-type power laws are shown for three fatigue experiments done on specimen "NoVac8". Equation 6.2, which represents a fit using a second-order polynomial function is used and shown using the magenta line. Clearly, this line does not represent a "zero-bridging" case where the fibre bridging effect has no contribution, as the line fails to bind the fatigue data displayed by the scattered points.

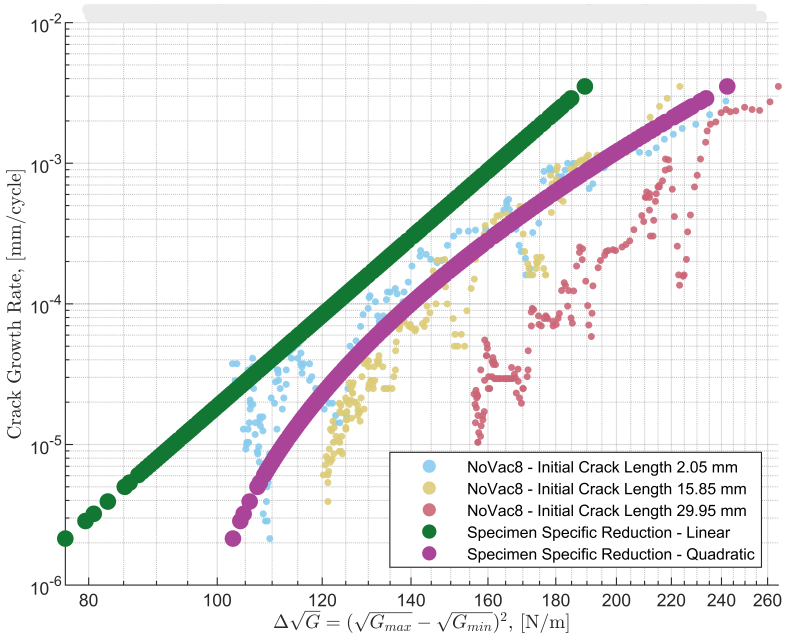

Figure 6.10: The "zero-bridging" fatigue delamination resistance curves generated as per the method of Ref. [2], where the data has not reached full fibre bridging saturation.

A more conservative and arguably more realistic approach for constructing a "zero-bridging" curve using data where the saturation of bridging fibres has not yet occurred, would be to use a linear relationship for Equation 6.2 instead. This can easily be achieved by simply excluding the second-order term from the equation and adopting the approach as is. The green line in Figure 6.10 displays such a linear relationship and compared to the second-order polynomial fitting which is described in the method [2] provides a more conservative "zero-bridging" which binds nearly all fatigue data points except a few outliers. It, therefore, offers a more conservative representation of the fatigue delamination behaviour of the composite specimen.

The difficulty of constructing a "zero-bridging" curve using fatigue data where the fibre bridging effect is not in a steady-state case can also be shown by reproducing Figure 2.13 for data where the saturation of fibre bridging has not yet happened. Figure 6.11 show the average, translated values of $\Delta\sqrt{G}$ where the selected crack growth rate for translation, da/dN_T is equal to 4.5×10^{-7} m/cycle. This figure plots the translated, average $\Delta\sqrt{G}$ value of each of the three fatigue R-curves against the corresponding pre-crack delamination length. Again, a linear and a quadratic fitting are shown in the figure which may be used to determine an average SERR value for the "zero-bridging" fatigue delamination resistance curve at a chosen value for da/dN. The linear fit produces a lower SERR value at the "zero-bridging" case, where $a - a_0$ equals zero. This leads to a more conservative estimate of the case where the fibre bridging effect is excluded and can be seen by the left-most curve of Figure 6.10. By assuming a linear fit instead of a quadratic one, it may be considered that the bi-linear model proposed by Yao et al. [62] is utilized.

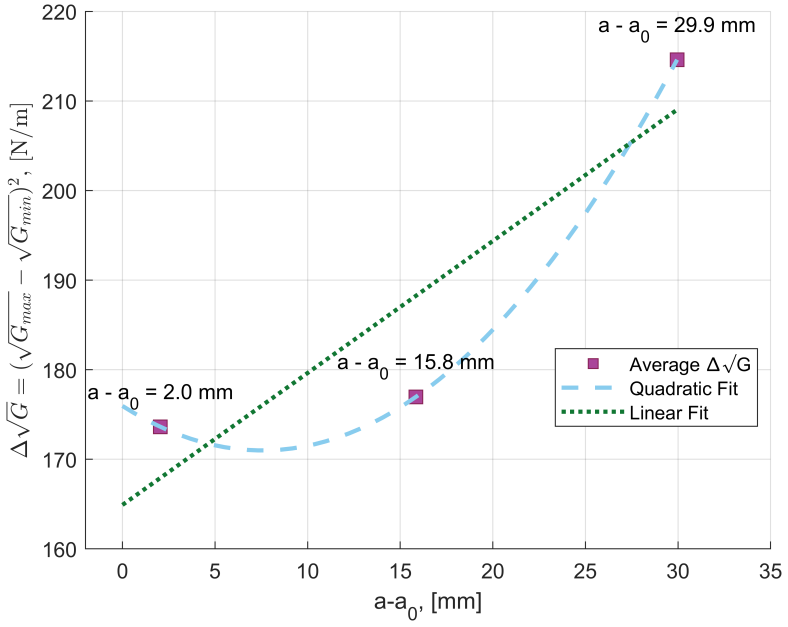

Figure 6.11: Average, translated $\Delta\sqrt{G}$ against the pre-crack delamination length, $a - a_0$ with both a linear and quadratic curve fitting for specimen "NoVac8".

Next, the case where a full saturation of fibre bridging is again considered, but now a third-order surface fit is assumed for Equation 6.2 instead of the second-order polynomial as per the method [2]. Based on the more conservative results using a linear equation, seen in the figure above, the expected "zero-bridging" fatigue delamination resistance curve using a third-order polynomial should yield a "zero-bridging" curve laying to the right of the original, second-order polynomial curve. Figure 6.12 shows how a typical second-order polynomial fitting relates to the same curve where a third-order is used. As expected, the third-order polynomial yields a less conservative "zero-bridging" fatigue delamination resistance curve.

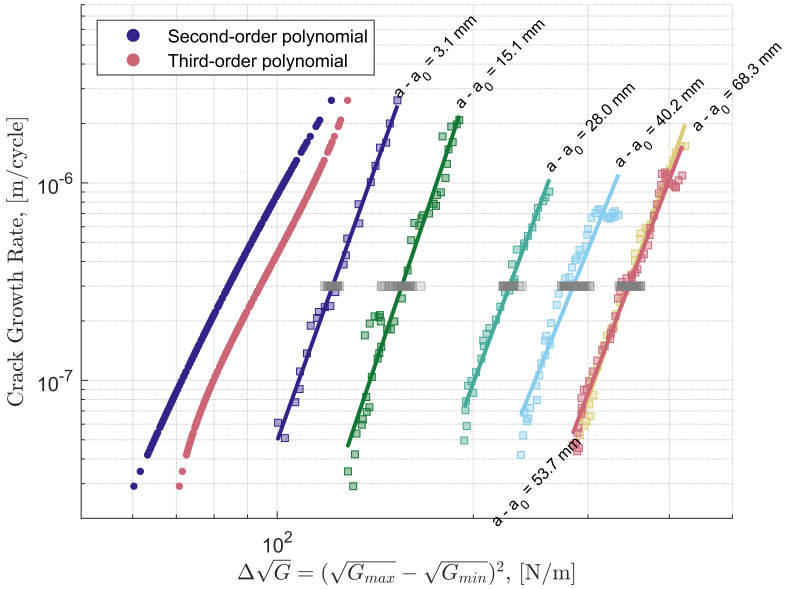

Figure 6.12: Comparision between a "zero-bridging" fatigue delamination resistance curve of a second-order and third-order surface fit for Equation 6.2 and the original fatigue data points.

6.4. Method IV: Hartman-Schijve Equation

This section discusses the results of the method for excluding the fibre bridging effect, based on the approach outlined by Yao et al. [64] and Jones et al. [30], as applied to the experimental data of "Spec7" by Yao [63, 61, 62, 60]. The objective of this method is to obtain a zero-bridging case for delamination growth in composite specimens. The first step of the method involves fitting the fatigue data to the Hartman-Schijve equation (Eq. 6.3) and selecting the values of the parameters A and $\Delta\sqrt{G_{thr}}$ such that the resulting data points collapse onto a single "master" line, as shown in Figure 2.15, enabling the fitting of a Paris-type power law:

$$\frac{da}{dN} = D\left[\frac{\Delta\sqrt{G} - \Delta\sqrt{G_{thr}}}{\sqrt{\left\{1 - \sqrt{G_{\max}}/\sqrt{A}\right\}}}\right]^n \tag{6.3}$$

Table 6.1: The values for the parameters A and $\Delta\sqrt{G_{thr}}$ for which a "master" relationship can be constructed by using the Hartman-Schijve equation, see Figure 6.13.

Pre-crack delamination length, $(a - a_0)$ in [mm]	R-ratio	$\Delta\sqrt{G_{thr}}$ in [$\sqrt{}$(N/m)]	A in [(N/m)]
2.7	0.1	9.2	240
14.8	0.1	10.5	350
28.0	0.1	12.9	570
40.0	0.1	14.5	680
53.6	0.1	16.4	700

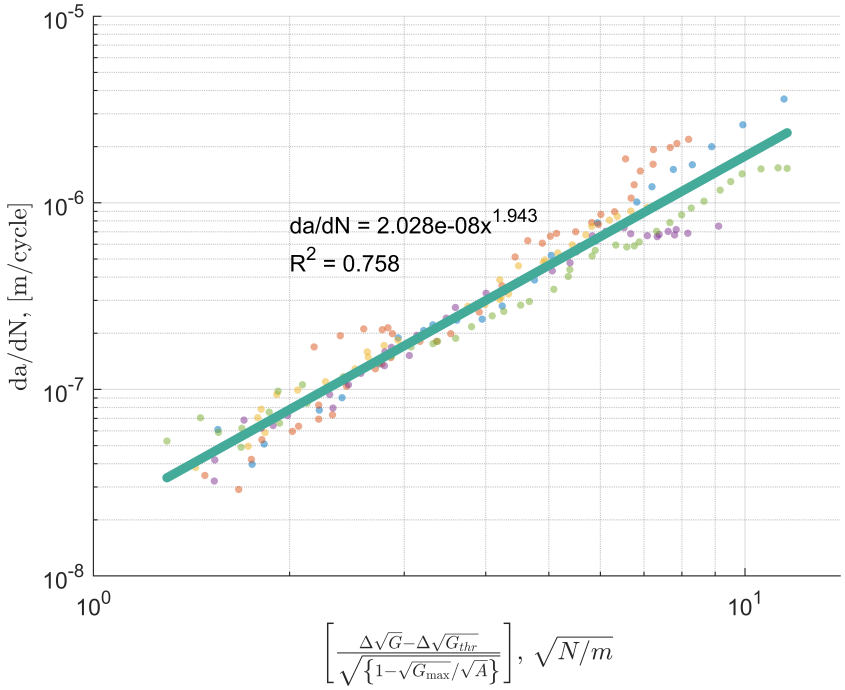

Figure 6.13: A linear "master" relationship which is obtained for multiple fatigue delamination tests ("Spec7" by Yao [63, 61, 62, 60]), of which the data is displayed using the Hartman-Schijve equation (Eq. 6.3) and the values of Table 6.1.

The data points in Figure 6.13, represented by different colours, correspond to multiple fatigue tests conducted on specimens with distinct pre-crack delamination lengths, $(a-a_0)$. As anticipated, it is possible to fit the data from these multiple tests onto a single "master" curve, yielding a satisfactory goodness of fit (R^2 = 0.76). It should be noted that only five fatigue tests were employed in this analysis, in contrast to the roughly 60 tests used in the work of Yao [64], which is depicted in Figure 2.15 resulting in a much higher goodness of fit (R^2 = 0.994). Nevertheless, the results of the present study are suitable for the development of an "upper-bound" fatigue resistance curve that eliminates the contribution of the fibre bridging effect.

To construct this "upper-bound" curve both the Paris' law fitting parameters D and n of Equation 6.3 are needed. Furthermore, the parameters A and $\Delta\sqrt{G_{thr}}$ are to be determined for the case where the pre-crack delamination length, $(a-a_0)$, is equal to zero. For this length, there is no opportunity for bridging fibres to have been nucleated and it may therefore be assumed that it represents a "zero-bridging" case. The values of A and $\Delta\sqrt{G_{thr}}$ are plotted against their corresponding pre-crack length values in Figure 6.14. Equivalent to the method [64] a second-order polynomial may be fitted through these data points. This polynomial fitting line is shown along with the confidence interval which represents a single standard deviation from the fit line.

The "zero-bridging" values for the curve fitting parameters of Equation 6.3, i.e. A_0 and $\Delta\sqrt{G_{thr,0}}$ are found by extrapolating the fitted polynomial and determining their values at $(a-a_0)$ = 0 mm. The confidence bound for the extrapolated region close to the Y-axis is larger because the confidence interval becomes greater for an extrapolated region, as the uncertainty associated with making predictions beyond the range of observed data is greater than the uncertainty associated with values within the observed range [14]. The found values and their standard deviations of A_0 and $\Delta\sqrt{G_{thr,0}}$ are 170 $\pm$ 69 N/m and 8.69 $\pm$ 0.41 $\sqrt{}$(N/m) respectively.

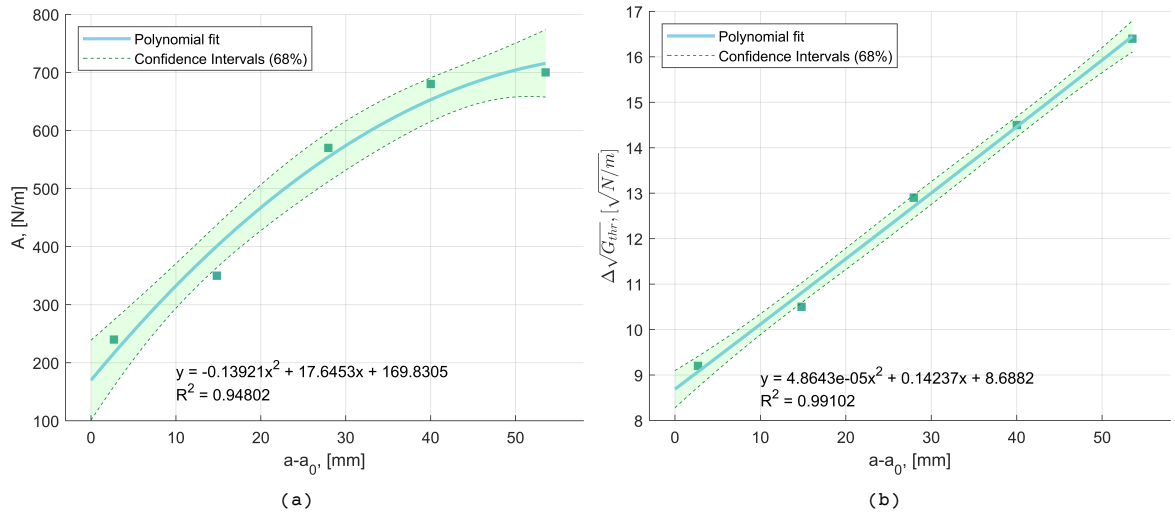

Figure 6.14: $\Delta\sqrt{G_{thr}}$ and A as a function of the pre-crack delamination length $(a-a_0)$. The values used for $\Delta\sqrt{G_{thr}}$ and A are taken from Table 6.1.

Using the determined "zero-bridging" parameters A_0 and $\Delta\sqrt{G_{thr,0}}$ along with the pre-determined Paris' law fitting parameters D and n, an "upper-bound" fatigue delamination resistance curve can be established. The values of the

relevant parameters are found in Table 6.2. The statistical approach [42] discussed in the Literature Study is utilized for this purpose. Specifically, the Hartman-Schijve equation (Eq. 6.3) is employed with the values A_0 and $\Delta\sqrt{G_{thr,0}}$ reduced by their corresponding standard deviation. This conservative estimation establishes the delamination resistance curve in the absence of any expected fibre bridging effect. Figure 6.15 illustrates the resulting "zero-bridging" curve in comparison to the original fatigue data points. The predicted "upper-bound" curve effectively bounds the experimental fatigue data, representing a worst-case scenario in terms of the conservativeness of the fatigue data. Therefore, this curve may be used to provide a designer of composite structures with allowable values for delamination growth rates, da/dN, for a given fatigue load.

Table 6.2: Values of terms used in Equation 6.3 for predicting an upper-bound "zero-bridging" fatigue delamination resistance curve.

Term	Value
D	2.028E-08 m/cycle
n	1.94
$\Delta\sqrt{G_{thr,0}}$ minus a standard deviation	8.28 $\sqrt{}$(N/m)
A_0 minus a standard deviation	101 N/m

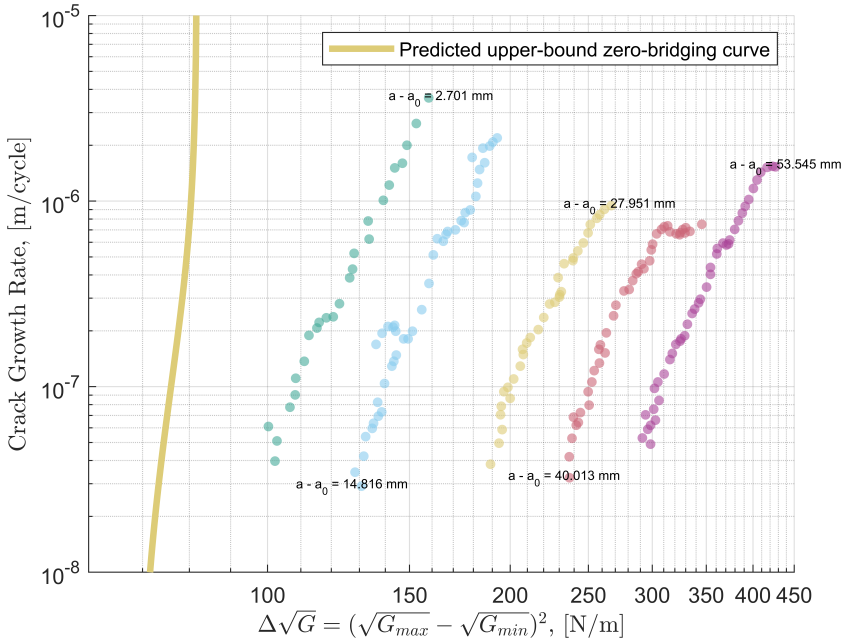

Figure 6.15: The original fatigue data points of "Spec7" by Yao [64] along with an "upper-bound" fatigue resistance curve constructed using Equation 6.3 with A_0 and $\Delta\sqrt{G_{thr,0}}$ based on their value minus their respective standard deviation.

As shown in figure 6.15 the method for excluding the fibre bridging effect from fatigue data using the Hartman-Schijve equation [30] provides a conservative "zero-bridging" case. As mentioned in the Literature Study (page 21) the choice of the order of polynomial for the line fitting to determine the values of both A_0 and $\Delta\sqrt{G_{thr,0}}$ has a significant effect on their outcome.

To determine the dependency on the order of polynomial for the fitting of Figure 6.14a the resulting values for A_0 are analyzed for two more polynomial

fitting functions which deviate from the second-order polynomial which is used in Figure 6.14a. Figure 6.16a shows how a third-order polynomial function is fitted to the data points for A. The result is a higher estimate for A_0 of 225 N/m, yielding a less conservative fatigue delamination resistance curve.

Moreover, if a fourth-order polynomial function is used (Figure 6.16b) then the intercept with $(a - a_0)$ = 0 mm, results in an even higher value for A_0 of 260 N/m, resulting in an extended shift towards the right of the upper-bound design curve of Figure 6.15, in other words towards un-conservativeness. The exact same issue is encountered when considering the determination of the zero-bridging parameter $\Delta\sqrt{G_{thr,0}}$ and it can therefore be concluded that one must take care to choose a curve fitting function which reflects the slope of the data points in the extrapolated zero-bridging region, close to $(a - a_0)$ = 0 mm.

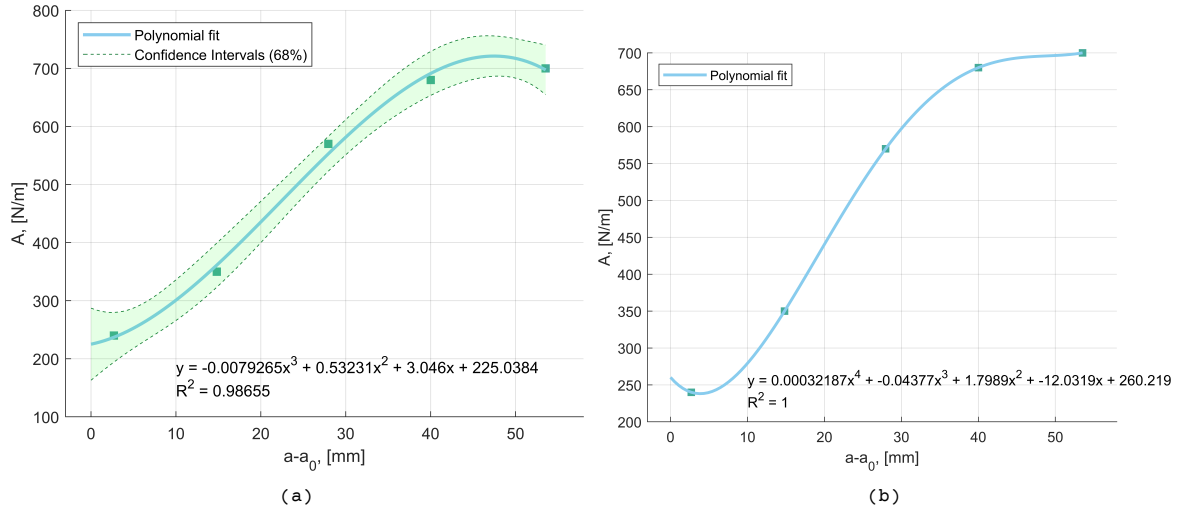

Figure 6.16: A as a function of the pre-crack delamination length $(a - a_0)$, where the fitted line is in (a) a third-order polynomial function and in (b) a fourth-order polynomial function.

The effect of the choice for order of fitting polynomial function on the "zero-bridging" fatigue delamination resistance curve is shown in Figure 6.17. Here, the original curve of Figure 6.15 is shown which is constructed using a second-order polynomial function to find the "zero-bridging" parameters A_0 and $\Delta\sqrt{G_{thr,0}}$. As expected, using a third-and fourth-order polynomial function decreases the conservative nature of the resulting "zero-bridging" fatigue delamination resistance curves. The curves constructed in Figure 6.17 are constructed using the curve fitting parameters A_0 and $\Delta\sqrt{G_{thr,0}}$ represented by their mean values and not the mean value minus a standard deviation. The fourth-order polynomial function used in Figure 6.16b does not have a standard deviation as the fitted line perfectly intercepts all the data points, resulting in overfitting [20]. Subsequently, the "zero-bridging" curve associated with this order polynomial lays to the right of the fatigue data for the shortest pre-crack delamination length, $a - a_0$ = 2.7 mm. This yields an inaccurate representation of a "zero-bridging" scenario.

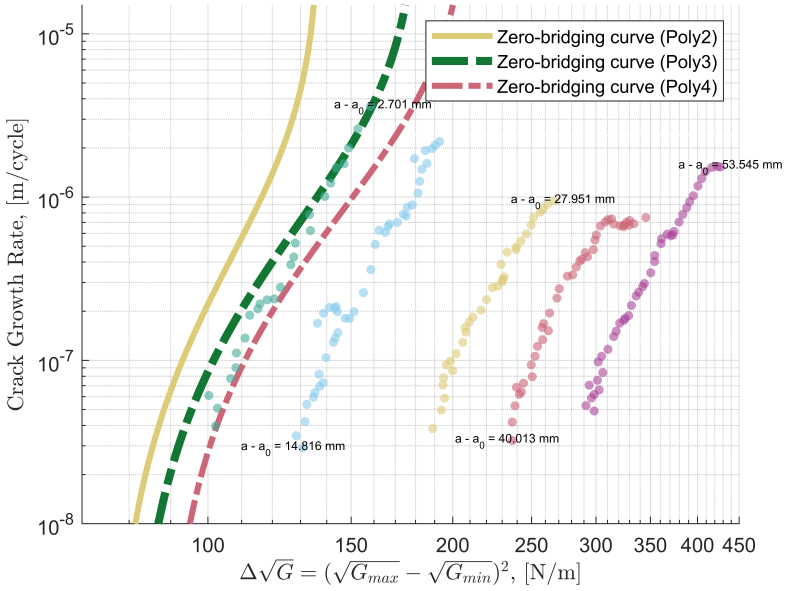

Figure 6.17: A ”zero-bridging” fatigue delamination resistance curve obtained by using the method involving the Hartman-Schijve equation [30] where the order of the fitting polynomial is varied.

6.5. Comparison of Methods

The resulting "zero-bridging" fatigue delamination resistance curves for each individual method are presented in the preceding section. However, to gain an understanding of the manner in which the methods relate to each other and to answer the posed research questions, they should be compared directly. Only then, conclusions can be made about for instance the conservative-ness of the results stemming from a fibre-bridging exclusion method. The most straightforward way to compare the methods would be to present their influence on the raw fatigue data in a single delamination resistance curve. In this section, such a fatigue R-curve is presented and discussed.

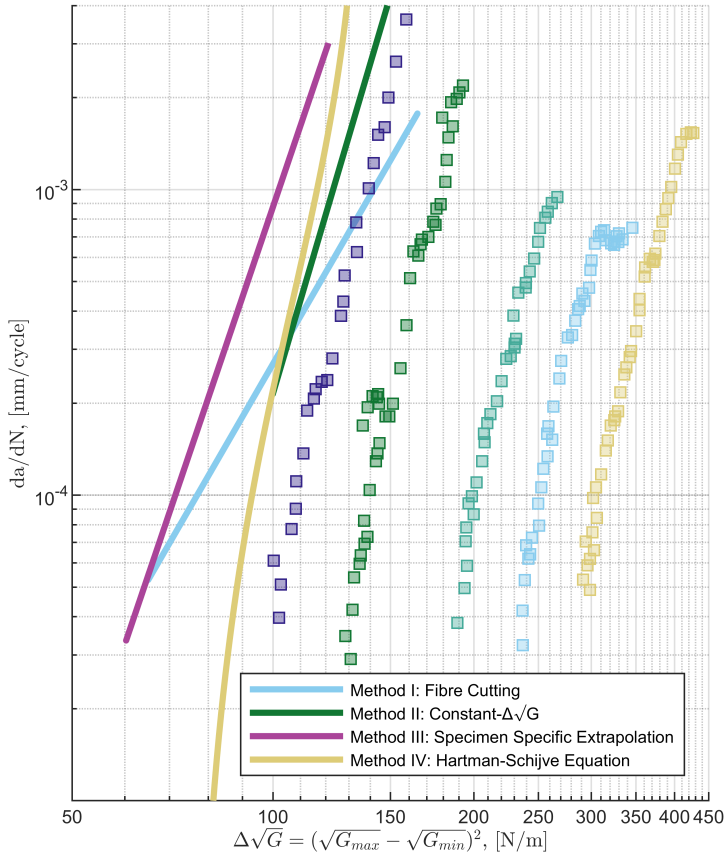

Figure 6.18: The "zero-bridging" fatigue delamination curves of four fibre bridging excision methods along with unaltered fatigue data

Figure 6.18 shows the four methods for fibre bridging exclusion along with the fatigue delamination resistance curves of a set of fatigue experiments where the fibre bridging was not accounted for. The data for this set of fatigue R-curves with the contribution of fibre bridging is obtained from the testing campaign of Yao ("Spec7") [66, 67]. This data was used in the methods of Alderliesten (Method III) [2] and Jones and Yao (Method IV) [64, 30]. All in all, the constructed "zero-bridging" fatigue delamination resistance curves for the four methods explored in this research show that they are all capable of predicting a "zero-bridging" scenario. This conclusion follows from the fact that all the curves are to the left of the original data. This showcases the ability of the methods to approach a more conservative case where the crack growth rates are expected to be higher due to the absence of the delamination-resisting fibre bridging effect. Figure 6.19 shows the resulting curves of the methods without the original fatigue data for a more

straightforward comparison.

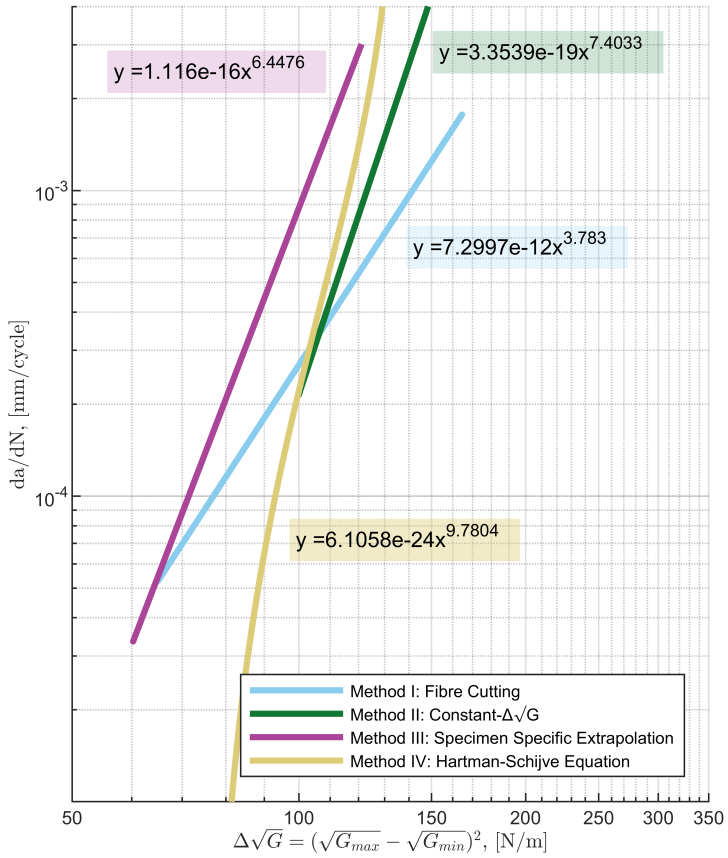

Figure 6.19: Comparison for various methods for the exclusion of the fibre bridging effect, a delamination resistance graph.

From the figure above, the accordance between Method IV, involving the Hartman-Schijve equation, and Method II, constant-$\Delta\sqrt{G}$ testing, can be seen for the Paris' law region. Moreover, the "zero-bridging" procedure proposed by Alderliesten [2] (Method III) shows a shift towards the left compared to the three other methods. This means that this method predicts a more conservative scenario when considering fatigue delamination in the absence of the fibre bridging effect.

The effect of removing or cutting the bridging fibres during the fatigue test according to the method by Khan [34] is evident. The slope of the Paris-type power law associated with this method deviates from the slope of the other methods for fibre bridging exclusion. It is now well established that the fibre bridging effect leads to lower propagation rates during fatigue delamination because of its delamination-resisting nature. Whilst fatigue data obtained in the other three methods do not specifically account for the fibre bridging effect during the experiment, the fatigue data associated with Khan's fibre cutting method [34] provides results that explicitly account for this effect during the test. In displacement-controlled fatigue experiments, the fatigue curve originates from the top right and progresses towards the bottom left. However, when conducting a fatigue test involving the active cutting of bridging fibres, the resulting curve tends to exhibit this reduced slope. It can primarily be attributed to the absence of fibre bridging during the later stages of the fatigue test, at the bottom left

region, where a higher rate of crack growth is observed due to the absence of fibre bridging. Consequently, the fibre cutting method yields a flatter ”zero-bridging” curve, characterized by a lower slope.

7

Conclusion

This study investigated different methods to eliminate the fibre bridging effect in composite structures under cyclic Mode I loading. The objective of this research was to assess and compare the effectiveness of these methods in excluding the increased resistance against delamination caused by fibre bridging. To accomplish this goal, a primary research question was formulated, accompanied by three subquestions, which can be found in Chapter 3. In this chapter, the subquestions are reintroduced and after a short discussion are answered. The main research question is subsequently answered.

1. Which method for the exclusion of the fibre bridging effect in cyclic Mode I loading of UD composite laminates is feasible to be integrated into a standardized framework for describing fatigue delamination growth in composite specimens?

In order to better understand and predict fatigue delamination behaviour in composite structures, it is recommended to develop a standardized method that encompasses this [9]. The standardization industry should adopt a straightforward method for accounting for unrealistic delamination resistance caused by fibre bridging, without relying on extensive expertise from test operators. A primary objective of a standard is to achieve reproducible results under the same conditions. This study explored four fibre bridging exclusion methods, which yielded more conservative fatigue data but varied in terms of ease of use. The fibre-cutting method proved to be time-consuming and relied on the operator's discretion during the cutting procedure. This aspect, not described in the paper [34], introduced more scatter compared to other methods, as shown in Figure 6.4. The "zero-bridging" fatigue resistance curve of the $\Delta\sqrt{G}$-constant method exhibited less scatter but required multiple specimens and wasted much delamination length, with the test concluding upon reaching bridging saturation, typically after around 15 mm. The remaining two methods did not require multiple specimens and were less susceptible to operator-induced scatter than the fibre-cutting method. However, the Hartman-Schijve equation method required careful selection of appropriate fitting parameters. Consequently, it can be concluded that the specimen-specific extrapolation method minimizes the potential for scatter introduced by the operator during fatigue testing or during data analysis. This observation, along with the overall straightforwardness and no requirement for active supervision of the test, makes the specimen-specific extrapolation method the most feasible for standardized use.

2. Which method for the exclusion of the fibre bridging effect in cyclic Mode I loading yields the most conservative outcome?

The most conservative fibre bridging exclusion method is defined as having the ”zero-bridging” fatigue delamination resistance curve laying to the left of all the other curves. Design engineers should abide by a ”worst-case” scenario for the material properties, therefore a conservative curve should be chosen. The comparison of the ”zero-bridging” fatigue delamination resistance curves of Figure 6.19 showed that the specimen-specific extrapolation method yields a curve which lies to the left of all the other curves. At the fatigue threshold, where slow crack growth is expected to happen ($< 1 \times 10^{-4}$ mm/cycle), the ”zero-bridging” curves of Method III and Method I seemed to intersect. Therefore, it cannot be determined which of these methods provides a conservative ”zero-bridging” curve at the fatigue threshold.

3. Which method for the exclusion of the fibre bridging effect in cyclic Mode I accurately captures a zero-bridging fatigue delamination scenario?

Figure 6.19 illustrates the impact of different fibre bridging exclusion methods on fatigue resistance curves, revealing a consistent leftward shift across all curves. Notably, the fibre-cutting method exhibited a lower slope of the Paris-type power law. Conversely, the other exclusion methods did not display such a decrease in the slope. The hypothesis here is that because the fibre-cutting method accounted for fibre bridging during the fatigue experiment, the decrease in crack growth rate failed to occur. In the other three methods, the onset of fibre bridging caused an increasing resistance against delamination.

For displacement-controlled tests, the SERR range decreases during the fatigue test. For the lower values of the SERR range a lower crack growth rate is thus expected if the contribution of the fibre bridging effect increases during the test. This results in a higher slope of the Paris-type power law if fibre bridging is not excluded during the test. Therefore, the lower slope of a ”zero-bridging” fatigue resistance curve seems to best capture the fatigue delamination behaviour in the absence of the fibre bridging effect. From the covered methods, this could only be achieved with the fibre-cutting method [34].

Finally, addressing the main research question:

- How can the fibre bridging effect be excluded in a suitable manner from data obtained during the cyclic Mode I loading of UD composite specimens?

The answer to the main research question is supported by the conclusions made concerning the three posed sub-questions. This study showed that all four examined methods for fibre bridging exclusion are able to exclude the contribution of fibre bridging to the delamination resistance to some extent. This study also showed that by assuming the fibre bridging effect to be a specimen-specific phenomenon, an exclusion method could be applied under the condition that the full saturation of fibre bridging has occurred. This method produced the most conservative prediction of the ”zero-bridging” case. It also provides a suitable manner to exclude the fibre bridging effect in a straightforward method, requiring little additional data analysis and no active supervision of the experiment. Furthermore, this methodology effectively preserves the observed scatter during multiple consecutive delamination experiments, enabling the construction of A-basis or B-basis

upper bounds for strength predictions. Hence, this method offers a suitable approach for excluding the fibre bridging effect during the cyclic Mode I loading of UD composite specimens.

8

Recommendations

Based on the findings of this study on the exclusion of fibre bridging in composite structures, several recommendations are proposed. Firstly, it is recommended to revise the existing standards [55, 5] to acknowledge the presence of fibre bridging in multidirectional delamination interfaces of composite structures. The current portrayal of fibre bridging in the standards does not accurately reflect its occurrence in real-world scenarios. Furthermore, the relationship between the delamination-resisting phenomenon in multidirectional and unidirectional laminates remains unclear. Hence, it is advisable to exclude the fibre bridging effect unless a thorough investigation is conducted to understand the delamination resistance behaviour specific to the interface orientation of a given multidirectional structure. To achieve this, one could use the specimen-specific exclusion method proposed by Alderliesten [2], which yields a conservative ”zero-bridging” prediction in a straightforward manner as was concluded in this research.

Moreover, a point can be made concerning the fibre bridging effect itself and the reasons and assumptions for excluding it from fatigue delamination data. The toughening nature of the fibre bridging effect is assumed to not occur in real-life composite structures which typically consist of MD laminates. Contrary to ASTM D5528 [5], Gong et al. [19] have shown how toughening of an MD composite laminate occurs for extended delamination propagation. It might therefore be possible for fibre bridging or any other toughening phenomenon to occur in real-life composite structures. Further research related to the fatigue delamination behaviour of multidirectional composite structures could give insight into the predictability of delamination retardation in these types of structures. Specifically, to determine the magnitude of the fibre bridging effect in real-life composite structures, larger components such as composite panels should be tested under fatigue loading. Such research should be able to determine to what extent the fibre bridging effect could be used as an additional resistance against fatigue-induced delamination. A ”slow-growth” concept [45] could allow for structural design to harness the increased material properties related to the fibre bridging effect if they can be classified as ”slow, stable and predictable” [1].

The effect of the manufacturing process of composite laminates on the fibre bridging effect during fatigue delamination has not been covered extensively in the literature. To the author’s knowledge the only source discussing the manufacturing process and the development of fibre bridging during delamination is by Hu et al. [23]. This source [23], however, solely looked at the effect of changing the curing temperature and curing time. It would be of interest to investigate how curing pressure influences the development of bridging fibres in a composite laminate. Fibre nesting has typically been

seen as the root cause of subsequent bridging fibres. A view concerning this topic could be that maintaining a lower curing pressure would result in less fibre nesting and, in turn, less fibre bridging during delamination. This hypothesis could be tested by performing delamination experiments on composite specimens which are cured at different pressures.

Finally, it is worth noting the considerable scatter observed in the data collected from cyclic Mode I experiments conducted on composite specimens. Various factors possibly contribute to this scatter, including the testing setup and the presence of fibre bridging. However, before the raw data is transformed into the conventional Paris-type power law, data analysis precedes. This particular step may also introduce additional scatter. While standardized methods exist for determining parameters such as the SERR, certain aspects of fatigue experiment data analysis remain subjective. For instance, different individuals assessing imagery to determine the delamination length may yield different results, consequently influencing crack growth rates. The operator-dependent process of accurately identifying the location of the delamination tip is the reason for this potential bias. To evaluate the impact of the data analysis step on scatter, further research is needed. Multiple researchers could independently analyze raw data acquired from fatigue delamination experiments to assess the extent of scatter introduced during the data analysis process.

References

[1] European Aviation Safety Agency. AMC 20-29 : Composite Aircraft Structure. 2010. URL: https://www.easa.europa.eu/en/downloads/1698/en.

[2] René Alderliesten. “Fatigue delamination of composite materials - approach to exclude large scale fibre bridging”. en. In: IOP Conference Series: Materials Science and Engineering 388 (July 2018), p. 012002. ISSN: 1757-8981, 1757-899X. DOI: 10.1088/1757-899X/388/1/012002. URL: https://iopscience.iop.org/article/10.1088/1757-899X/388/1/012002 (visited on 06/07/2022).

[3] René Alderliesten and Andreas J Brunner. Determination of Mode I Fatigue Delamination Propagation in Unidirectional Fibre-Reinforced Polymer Composites. en. Tech. rep., p. 14.

[4] J. Andersons, M. Hojo, and S. Ochiai. “Empirical model for stress ratio effect on fatigue delamination growth rate in composite laminates”. en. In: International Journal of Fatigue 26.6 (June 2004), pp. 597-604. ISSN: 0142-1123. DOI: 10.1016/j.ijfatigue.2003.10.016. URL: https://www.sciencedirect.com/science/article/pii/S0142112303002718 (visited on 05/09/2023).

[5] ASTM. Standard Test Method for Mode I Interlaminar Fracture Toughness of Unidirectional Fiber-Reinforced Polymer Matrix Composites - ASTM D5528 - 13. en. Tech. rep. Jan. 2013. URL: https://www.nen.nl/en/astm-d5528-13-en-1086343 (visited on 09/01/2022).

[6] J. Aveston and J. M. Sillwood. “Synergistic fibre strengthening in hybrid composites”. en. In: Journal of Materials Science 11.10 (Oct. 1976), pp. 1877-1883. ISSN: 1573-4803. DOI: 10.1007/BF00708266. URL: https://doi.org/10.1007/BF00708266 (visited on 05/23/2023).

[7] C. Blondeau, G. Pappas, and J. Botsis. “Influence of ply-angle on fracture in antisymmetric interfaces of CFRP laminates”. en. In: Composite Structures 216 (May 2019), pp. 464-476. ISSN: 0263-8223. DOI: 10.1016/j.compstruct.2019.03.004. URL: https://www.sciencedirect.com/science/article/pii/S0263822319303307 (visited on 06/20/2022).

[8] A. J. Brunner et al. “Cyclic fatigue delamination of carbon fiber-reinforced polymer-matrix composites: Data analysis and design considerations”. en. In: International Journal of Fatigue 83 (Feb. 2016), pp. 293-299. ISSN: 0142-1123. DOI: 10.1016/j.ijfatigue.2015.10.025. URL: https://www.sciencedirect.com/science/article/pii/S0142112315003722 (visited on 11/01/2022).

[9] Andreas J. Brunner, Laurent Warnet, and Bamber R. K. Blackman. “35 years of standardization and research on fracture of polymers, polymer composites and adhesives in ESIS TC4: Past achievements and future directions”. en. In: Procedia Structural Integrity. 26th International Conference on Fracture and Structural Integrity 33 (Jan. 2021), pp. 443-455. ISSN: 2452-3216. DOI: 10.1016/j.prostr.2021.10.051. URL: https://www.sciencedirect.com/science/article/pii/S2452321621001463 (visited on 10/07/2022).

[10] N. Choi, Anthony Kinloch, and J. Williams. “Delamination Fracture of Multidirectional Carbon-Fiber/Epoxy Composites under Mode I, Mode II and Mixed-Mode I/II Loading”. In: Journal of Composite Materials - J COMPOS MATER 33 (Jan. 1999), pp. 73-100. DOI: 10.1177/002199839903300105.

[11] Roberta Cumbo et al. “Design allowables of composite laminates: A review”. In: Journal of Composite Materials 56 (Sept. 2022). ADS Bibcode: 2022JCoMa..56.3617C, pp. 3617-3634. ISSN: 0021-9983. DOI: 10.1177/00219983221117216. URL: https://ui.adsabs.harvard.edu/abs/2022JCoMa..56.3617C (visited on 05/16/2023).

[12] G. A. O. Davies and J. Ankersen. “Virtual testing of realistic aerospace composite structures”. en. In: Journal of Materials Science 43.20 (Oct. 2008), pp. 6586-6592. ISSN: 1573-4803. DOI: 10.1007/s10853-008-2695-x. URL: https://doi.org/10.1007/s10853-008-2695-x (visited on 06/16/2023).

[13] Nelson De Carvalho and Gretchen Murri. “A Novel Method for Characterizing Fatigue Delamination Growth Under Mode I Using the Double Cantilever Beam Specimen”. In: Sept. 2014.

[14] FM Dekking et al. A modern introduction to probability theory and statistics. Vol. Springer texts in statistics. London: Springer, 2005. ISBN: 978-1-85233-896-1. URL: http://www.springer.com/sgw/cda/pageitems/document/cda_downloaddocument/0,11855,0-0-45-166677-p34951942,00.pdf (visited on 05/16/2023).

[15] M. J. Donough et al. “Scaling parameter for fatigue delamination growth in composites under varying load ratios”. en. In: Composites Science and Technology 120 (Dec. 2015), pp. 39-48. ISSN: 0266-3538. DOI: 10.1016/j.compscitech.2015.10.011. URL: https://www.sciencedirect.com/science/article/pii/S0266353815301081 (visited on 09/15/2022).

[16] K. E. Evans, B. D. Caddock, and K. L. Ainsworth. “Statistical changes during the corrosion of glass fibre bundles”. en. In: Journal of Materials Science 23.8 (Aug. 1988), pp. 2926-2930. ISSN: 1573-4803. DOI: 10.1007/BF00547471. URL: https://doi.org/10.1007/BF00547471 (visited on 05/23/2023).

[17] Amar C. Garg. “Delamination—a damage mode in composite structures”. en. In: Engineering Fracture Mechanics 29.5 (Jan. 1988), pp. 557-584. ISSN: 0013-7944. DOI: 10.1016/0013-7944(88)90181-6. URL: https://www.sciencedirect.com/science/article/pii/0013794488901816 (visited on 06/16/2023).

[18] Yu Gong, Bing Zhang, and Stephen R. Hallett. “Delamination migration in multidirectional composite laminates under mode I quasi-static and fatigue loading”. en. In: Composite Structures 189 (Apr. 2018), pp. 160-176. ISSN: 0263-8223. DOI: 10.1016/j.compstruct.2018.01.074. URL: https://www.sciencedirect.com/science/article/pii/S0263822317331355 (visited on 05/29/2023).

[19] Yu Gong et al. “R-curve behaviour of the mixed-mode I/II delamination in carbon/epoxy laminates with unidirectional and multidirectional interfaces”. en. In: Composite Structures 223 (Sept. 2019), p. 110949. ISSN: 0263-8223. DOI: 10.1016/j.compstruct.2019.110949. URL: https://www.sciencedirect.com/science/article/pii/S0263822318345604 (visited on 05/29/2023).

[20] Douglas M. Hawkins. “The Problem of Overfitting”. In: Journal of Chemical Information and Computer Sciences 44.1 (Jan. 2004). Publisher: American Chemical Society, pp. 1-12. ISSN: 0095-2338. DOI: 10.1021/ci0342472. URL: https://doi.org/10.1021/ci0342472 (visited on 05/28/2023).

[21] Masaki Hojo and Takahira Aoki. “Characterization of Fatigue R-curves based on Gmax-constant Delamination Tests in CF/PEEK Laminates”. en. In: ICCM20. Copenhagen, Danemark: Aalborg University, Fredrik Bajers Vej 5, 9100 Aalborg, Denmark, 2015, p. 8.

[22] Masaki Hojo, Kazuro Kageyama, and Kiyoshi Tanaka. “Prestandardization study on mode I interlaminar fracture toughness test for CFRP in Japan”. en. In: Composites 26.4 (Apr. 1995), pp. 243–255. ISSN: 0010-4361. DOI: 10.1016/0010-4361(95)93668-A. URL: https://www.sciencedirect.com/science/article/pii/001043619593668A (visited on 10/12/2022).

[23] Ping Hu et al. “Influence of curing processes on the development of fiber bridging during delamination in composite laminates”. en. In: Composites Part A: Applied Science and Manufacturing 149 (Oct. 2021), p. 106564. ISSN: 1359-835X. DOI: 10.1016/j.compositesa.2021.106564. URL: https://www.sciencedirect.com/science/article/pii/S1359835X21002852 (visited on 05/24/2023).

[24] X. Hu and F.H. Wittmann. “Experimental method to determine extension of fracture-process zone”. English. In: Journal of Materials in Civil Engineering 2.1 (1990), pp. 15–23. ISSN: 0899-1561. DOI: 10.1061/(ASCE)0899-1561(1990)2:1(15).

[25] Xiao-Zhi Hu and Yiu-Wing Mai. “Mode I delamination and fibre bridging in carbon-fibre/epoxy composites with and without PVAL coating”. en. In: Composites Science and Technology 46.2 (Jan. 1993), pp. 147–156. ISSN: 0266-3538. DOI: 10.1016/0266-3538(93)90170-L. URL: https://www.sciencedirect.com/science/article/pii/026635389390170L (visited on 06/27/2022).

[26] X. N. Huang and D. Hull. “Effects of fibre bridging on GIC of a unidirectional glass/epoxy composite”. en. In: Composites Science and Technology 35.3 (Jan. 1989), pp. 283–299. ISSN: 0266-3538. DOI: 10.1016/0266-3538(89)90040-7. URL: https://www.sciencedirect.com/science/article/pii/0266353889900407 (visited on 10/14/2022).

[27] D. L. Hunston et al. “Matrix Resin Effects in Composite Delamination: Mode I Fracture Aspects”. en-US. In: Toughened Composites. ASTM International, pp. 74–94. DOI: 10.1520/STP24372S. URL: https://www.astm.org/stp24372s.html (visited on 05/30/2023).

[28] W Johnson and Prakash Mangalgiri. “Investigation of Fiber Bridging in Double Cantilever Beam Specimens”. In: Journal of Composites Technology and Research 9 (Feb. 1987). DOI: 10.1520/CTR10421J.

[29] R. Jones, W. Hu, and A. J. Kinloch. “A convenient way to represent fatigue crack growth in structural adhesives”. en. In: Fatigue & Fracture of Engineering Materials & Structures 38.4 (2015). _eprint: https://onlinelibrary.wiley.com/doi/pdf/10.1111/ffe.12241, pp. 379–391. ISSN: 1460-2695. DOI: 10.1111/ffe.12241. URL: https://onlinelibrary.wiley.com/doi/abs/10.1111/ffe.12241 (visited on 11/01/2022).

[30] R. Jones et al. “Application of the Hartman-Schijve equation to represent Mode I and Mode II fatigue delamination growth in composites”. en. In: Composite Structures 94.4 (Mar. 2012), pp. 1343–1351. ISSN: 0263-8223. DOI: 10.1016/j.compstruct.2011.11.030. URL: https://www.sciencedirect.com/science/article/pii/S0263822311004454 (visited on 06/22/2022).

[31] R. Jones et al. “Delamination growth in polymer-matrix fibre composites and the use of fracture mechanics data for material characterisation and life prediction”. en. In: Composite Structures 180 (Nov. 2017), pp. 316–333. ISSN: 0263-8223. DOI: 10.1016/j.compstruct.2017.07.097. URL: https://www.sciencedirect.com/science/article/pii/S0263822317316720 (visited on 10/14/2022).

[32] Rafiullah Khan. “Delamination Growth in Composites under Fatigue Loading”. PhD thesis. Oct. 2013.

[33] Rafiullah Khan. “Fiber bridging in composite laminates: A literature review”. en. In: Composite Structures 229 (Dec. 2019), p. 111418. ISSN: 0263-8223. DOI: 10.1016/j.compstruct.2019.111418. URL: https://www.sciencedirect.com/science/article/pii/S0263822318346051 (visited on 05/31/2022).

[34] Rafiullah Khan et al. “Crack closure and fibre bridging during delamination growth in carbon fibre/epoxy laminates under mode I fatigue loading”. en. In: Composites Part A: Applied Science and Manufacturing 67 (Dec. 2014), pp. 201–211. ISSN: 1359-835X. DOI: 10.1016/j.compositesa.2014.08.028. URL: https://www.sciencedirect.com/science/article/pii/S1359835X14002693 (visited on 06/22/2022).

[35] Weiling Liu and Puhui Chen. “Theoretical analysis and experimental investigation of the occurrence of fiber bridging in unidirectional laminates under Mode I loading”. en. In: Composite Structures 257 (Feb. 2021), p. 113383. ISSN: 0263-8223. DOI: 10.1016/j.compstruct.2020.113383. URL: https://www.sciencedirect.com/science/article/pii/S0263822320333092 (visited on 05/30/2023).

[36] J. J. M. Machado et al. “Mode II fracture toughness of CFRP as a function of temperature and strain rate”. en. In: Composites Part B: Engineering 114 (Apr. 2017), pp. 311–318. ISSN: 1359-8368. DOI: 10.1016/j.compositesb.2017.02.013. URL: https://www.sciencedirect.com/science/article/pii/S1359836816329808 (visited on 05/29/2023).

[37] Micah Cl McCrary-Dennis and Okenwa I Okoli. “A review of multiscale composite manufacturing and challenges”. en. In: Journal of Reinforced Plastics and Composites 31.24 (Dec. 2012), pp. 1687–1711. ISSN: 0731-6844, 1530-7964. DOI: 10.1177/0731684412456612. URL: http://journals.sagepub.com/doi/10.1177/0731684412456612 (visited on 06/14/2023).

[38] Mária Mrázová. “Advanced composite materials of the future in aerospace industry”. In: INCAS BULLETIN 5 (Sept. 2013), pp. 139–150. DOI: 10.13111/2066-8201.2013.5.3.14.

[39] Gretchen B Murri. “Effect of data reduction and fiber-bridging on Mode I delamination characterization of unidirectional composites”. en. In: Journal of Composite Materials 48.19 (Aug. 2014). Publisher: SAGE Publications Ltd STM, pp. 2413–2424. ISSN: 0021-9983. DOI: 10.1177/0021998313498791. URL: https://doi.org/10.1177/0021998313498791 (visited on 06/17/2022).

[40] Gretchen B Murri. “Evaluation of Delamination Growth Characterization Methods Under Mode I Fatigue Loading”. en. In: (Jan. 2012), p. 21.

[41] NASGRO® Fracture Mechanics & Fatigue Crack Growth Software. en. Sept. 2016. URL: https://www.swri.org/consortia/nasgro (visited on 05/09/2023).

[42] Chunyun Niu and Michael Chun-Yung Niu. Composite airframe structures: practical design information and data. Adaso Adastra Engineering Center, 1992.

[43] T. Kevin O’Brien. “Interlaminar fracture toughness: the long and winding road to standardization”. en. In: Composites Part B: Engineering 29.1 (Jan. 1998), pp. 57–62. ISSN: 1359-8368. DOI: 10.1016/S1359-8368(97)00013-9. URL: https://www.sciencedirect.com/science/article/pii/S1359836897000139 (visited on 05/29/2023).

[44] Mike van der Panne. “Effect of different fibre orientations at the interface on fatigue delamination growth”. Jan. 2022.

[45] John-Alan Pascoe. “Slow-growth damage tolerance for fatigue after impact in FRP composites: Why current research won’t get us there”. en. In: Procedia Structural Integrity 28 (2020), pp. 726–733. ISSN: 24523216. DOI: 10.1016/j.prostr.2020.10.084. URL: https://linkinghub.elsevier.com/retrieve/pii/S2452321620305862 (visited on 05/30/2022).

[46] J. N. Price and D. Hull. “Propagation of stress corrosion cracks in aligned glass fibre composite materials”. en. In: Journal of Materials Science 18.9 (Sept. 1983), pp. 2798–2810. ISSN: 1573-4803. DOI: 10.1007/BF00547597. URL: https://doi.org/10.1007/BF00547597 (visited on 05/23/2023).

[47] Calvin Rans, René Alderliesten, and Rinze Benedictus. “Misinterpreting the results: How similitude can improve our understanding of fatigue delamination growth”. en. In: Composites Science and Technology 71.2 (Jan. 2011), pp. 230–238. ISSN: 0266-3538. DOI: 10.1016/j.compscitech.2010.11.010. URL: https://www.sciencedirect.com/science/article/pii/S0266353810004495 (visited on 06/22/2022).

[48] J. Rouchon and M.J. Bos. Fatigue and Damage Tolerance Evaluation of Structures: The Composite Materials Response. Tech. rep. NLR-TP-2009-221. National Aerospace Laboratory NLR, Jan. 2009.

[49] Alan J. Russell. “A Constant dG Test for Measuring Mode I lnterlaminar Fatigue Crack Growth Rates”. In: Composite Materials: Testing and Design Eighth Conference (1988), pp. 259–577.

[50] Mototsugu Sakai, Tatsuya Miyajima, and Michio Inagaki. “Fracture toughness and fiber bridging of carbon fiber reinforced carbon composites”. en. In: Composites Science and Technology 40.3 (Jan. 1991), pp. 231–250. ISSN: 0266-3538. DOI: 10.1016/0266-3538(91)90083-2. URL: https://www.sciencedirect.com/science/article/pii/0266353891900832 (visited on 05/30/2023).

[51] N. Sato, M. Hojo, and M. Nishikawa. “Intralaminar fatigue crack growth properties of conventional and interlayer toughened CFRP laminate under mode I loading”. en. In: Composites Part A: Applied Science and Manufacturing 68 (Jan. 2015), pp. 202–211. ISSN: 1359-835X. DOI: 10.1016/j.compositesa.2014.09.031. URL: https://www.sciencedirect.com/science/article/pii/S1359835X14003194 (visited on 07/13/2022).

[52] N. Sela and O. Ishai. “Interlaminar fracture toughness and toughening of laminated composite materials: a review”. en. In: Composites 20.5 (Sept. 1989), pp. 423–435. ISSN: 0010-4361. DOI: 10.1016/0010-4361(89)90211-5. URL: https://www.sciencedirect.com/science/article/pii/0010436189902115 (visited on 07/13/2022).

[53] B.F. Sørensen. “Microscale testing and modelling for damage tolerant composite materials and structures”. English. In: vol. 942. ISSN: 1757-8981 Issue: 1. 2020. DOI: 10.1088/1757-899X/942/1/012004.

[54] Bent F Sørensen and Torben K Jacobsen. “Large-scale bridging in composites: R-curves and bridging laws”. en. In: Composites Part A: Applied Science and Manufacturing 29.11 (Nov. 1998), pp. 1443–1451. ISSN: 1359-835X. DOI: 10.1016/S1359-835X(98)00025-6. URL: https://www.sciencedirect.com/science/article/pii/S1359835X98000256 (visited on 06/17/2022).

[55] International Organization for Standardization. Fibre-reinforced plastic composites Determination of mode I interlaminar fracture toughness, GIC, for unidirectionally reinforced materials - ISO 15024:2001. Tech. rep. International Organization for Standardization, Jan. 2001. URL: https://connect.nen.nl/standard/openpdf/?artfile=429934&RNR=69853&token=ef885c48-3852-4143-a1f7-b01f301afcbb&type=pdf#pagemode=bookmarks (visited on 10/17/2022).

[56] Z. Suo, G. Bao, and B. Fan. “Delamination R-curve phenomena due to damage”. en. In: Journal of the Mechanics and Physics of Solids 40.1 (Jan. 1992), pp. 1–16. ISSN: 0022-5096. DOI: 10.1016/0022-5096(92)90198-B. URL: https://www.sciencedirect.com/science/article/pii/002250969290198B (visited on 06/22/2022).

[57] Anastasios P. Vassilopoulos and Thomas Keller. “Introduction to the Fatigue of Fiber-Reinforced Polymer Composites”. en. In: Fatigue of Fiber-reinforced Composites. Ed. by Anastasios P. Vassilopoulos and Thomas Keller. Engineering Materials and Processes. London: Springer, 2011, pp. 1–23. ISBN: 978-1-84996-181-3. DOI: 10.1007/978-1-84996-181-3_1. URL: https://doi.org/10.1007/978-1-84996-181-3_1 (visited on 05/29/2023).

[58] W. Xu and J. C. Ding. “Correction of the large displacement effect on determination of mode I interlaminar fracture toughness of composite”. en. In: Engineering Fracture Mechanics 238 (Oct. 2020), p. 107279. ISSN: 0013-7944. DOI: 10.1016/j.engfracmech.2020.107279. URL: https://www.sciencedirect.com/science/article/pii/S0013794420308626 (visited on 05/26/2023).

[59] Liaojun Yao. “Mode I fatigue delamination growth in composite laminates with fibre bridging”. PhD thesis.

[60] Liaojun Yao, R. C. Alderliesten, and R. Benedictus. “Interpreting the stress ratio effect on delamination growth in composite laminates using the concept of fatigue fracture toughness”. en. In: Composites Part A: Applied Science and Manufacturing 78 (Nov. 2015), pp. 135–142. ISSN: 1359-835X. DOI: 10.1016/j.compositesa.2015.08.005. URL: https://www.sciencedirect.com/science/article/pii/S1359835X15002766 (visited on 05/15/2023).

[61] Liaojun Yao, René Alderliesten, and R. Benedictus. “The effect of fibre bridging on the Paris relation for mode I fatigue delamination growth in composites”. In: Composite Structures 140 (Apr. 2016), pp. 125–135. DOI: 10.1016/j.compstruct.2015.12.027.

[62] Liaojun Yao et al. “A modified Paris relation for fatigue delamination with fibre bridging in composite laminates”. en. In: Composite Structures 176 (Sept. 2017), pp. 556–564. ISSN: 0263-8223. DOI: 10.1016/j.compstruct.2017.05.070. URL: https://www.sciencedirect.com/science/article/pii/S0263822317308656 (visited on 06/17/2022).

[63] Liaojun Yao et al. “Bridging effect on mode I fatigue delamination behavior in composite laminates”. en. In: Composites Part A: Applied Science and Manufacturing 63 (Aug. 2014), pp. 103–109. ISSN: 1359-835X. DOI: 10.1016/j.compositesa.2014.04.007. URL: https://www.sciencedirect.com/science/article/pii/S1359835X14001092 (visited on 06/07/2022).

[64] Liaojun Yao et al. “Delamination fatigue growth in polymer-matrix fibre composites: A methodology for determining the design and lifing allowables”. en. In: Composite Structures 196 (July 2018), pp. 8–20. ISSN: 0263-8223. DOI: 10.1016/j.compstruct.2018.04.069. URL: https://www.sciencedirect.com/science/article/pii/S0263822318312017 (visited on 07/08/2022).

[65] Liaojun Yao et al. “Discussion on the use of the strain energy release rate for fatigue delamination characterization”. en. In: Composites Part A: Applied Science and Manufacturing 66 (Nov. 2014), pp. 65–72. ISSN: 1359-835X. DOI: 10.1016/j.compositesa.2014.06.018. URL: https://www.sciencedirect.com/science/article/pii/S1359835X14001973 (visited on 06/15/2022).

[66] Liaojun Yao et al. “Fibre bridging effect on the Paris relation for Mode I fatigue delamination growth in composites with consideration of interface configuration”. In: Composite Structures 159 (Jan. 2017), pp. 471–478. DOI: 10.1016/j.compstruct.2016.09.082.

[67] Liaojun Yao et al. “Stress ratio dependence of fibre bridging significance in mode I fatigue delamination growth of composite laminates”. en. In: Composites Part A: Applied Science and Manufacturing 95 (Apr. 2017), pp. 65–74. ISSN: 1359-835X. DOI: 10.1016/j.compositesa.2016.11.030. URL: https://www.sciencedirect.com/science/article/pii/S1359835X16304249 (visited on 06/17/2022).

[68] Jianyu Zhang et al. “Fatigue delamination growth rates and thresholds of composite laminates under mixed mode loading”. en. In: International Journal of Fatigue 40 (July 2012), pp. 7–15. ISSN: 0142-1123. DOI: 10.1016/j.ijfatigue.2012.01.008. URL: https://www.sciencedirect.com/science/article/pii/S0142112312000254 (visited on 05/29/2023).

9

Appendix A

Constant-$\Delta\sqrt{G}$ - Experimental Results

In this appendix, the results of the experiments involving the constant-$\Delta\sqrt{G}$ fatigue delamination experiments are presented. Each data point in Figure 1 represents a single test conducted at a specific $\Delta\sqrt{G}$ value.

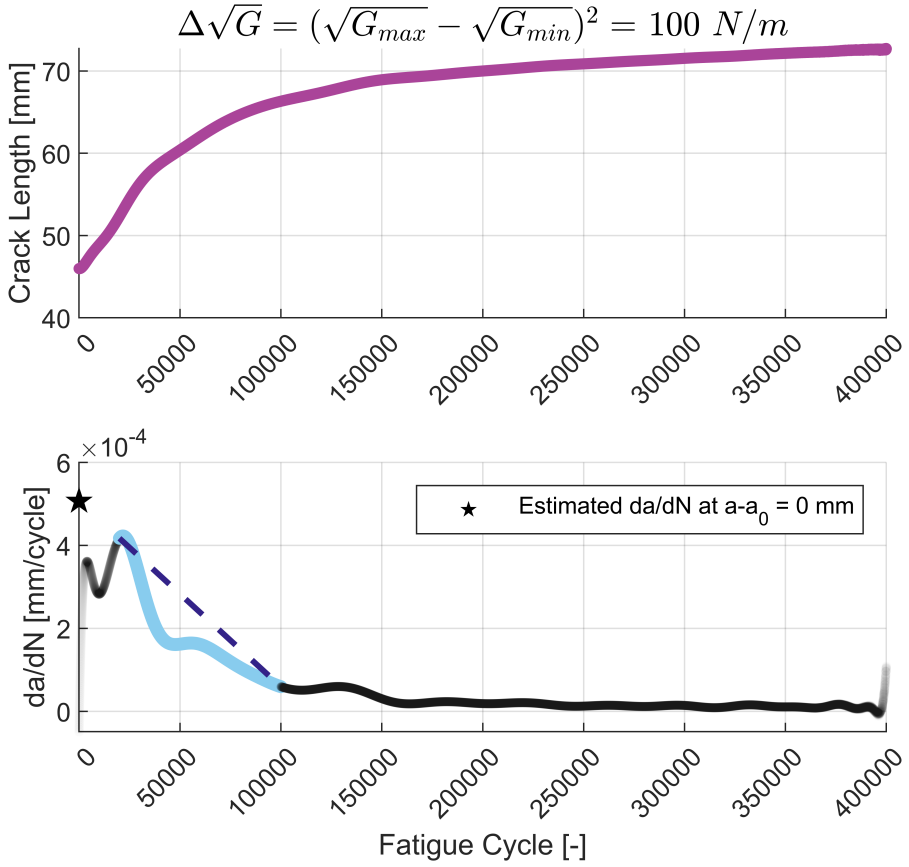

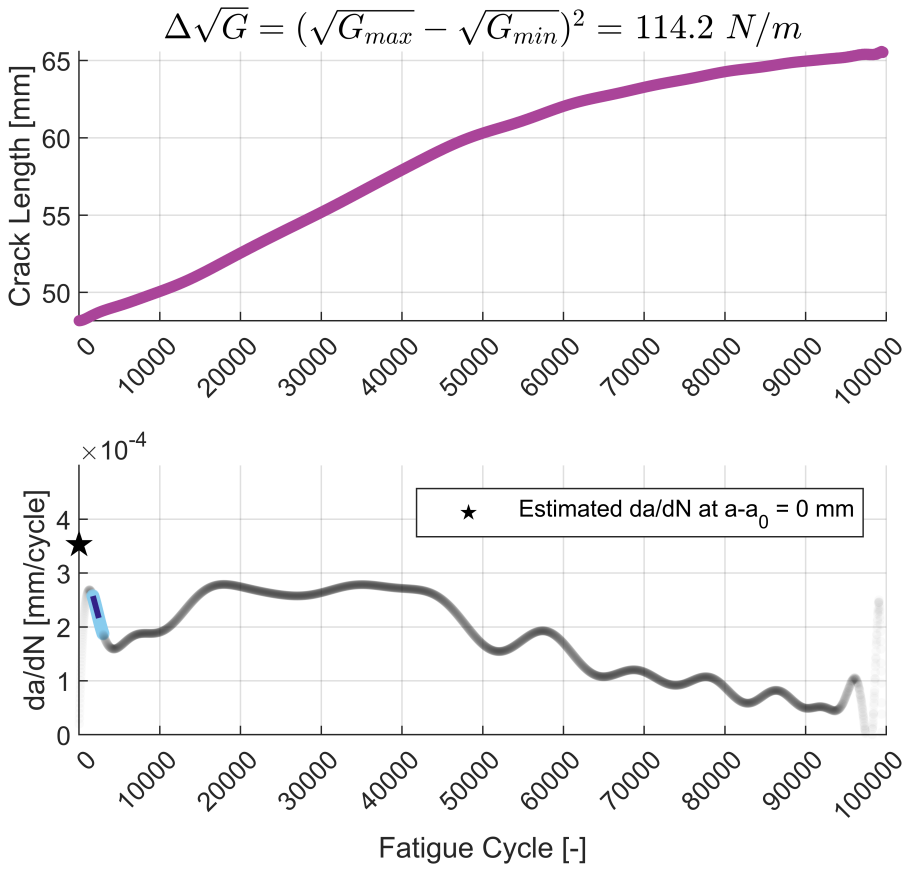
$\Delta\sqrt{G} = (\sqrt{G_{max}} - \sqrt{G_{min}})^2 = 114.2\ N/m$
Crack Length [mm]
65
60
55
50
0
10000
20000
30000
40000
50000
60000
70000
80000
90000
100000
×10-4
da/dN [mm/cycle]
4
3
2
1
0
Estimated da/dN at a-a0 = 0 mm
Fatigue Cycle [-]

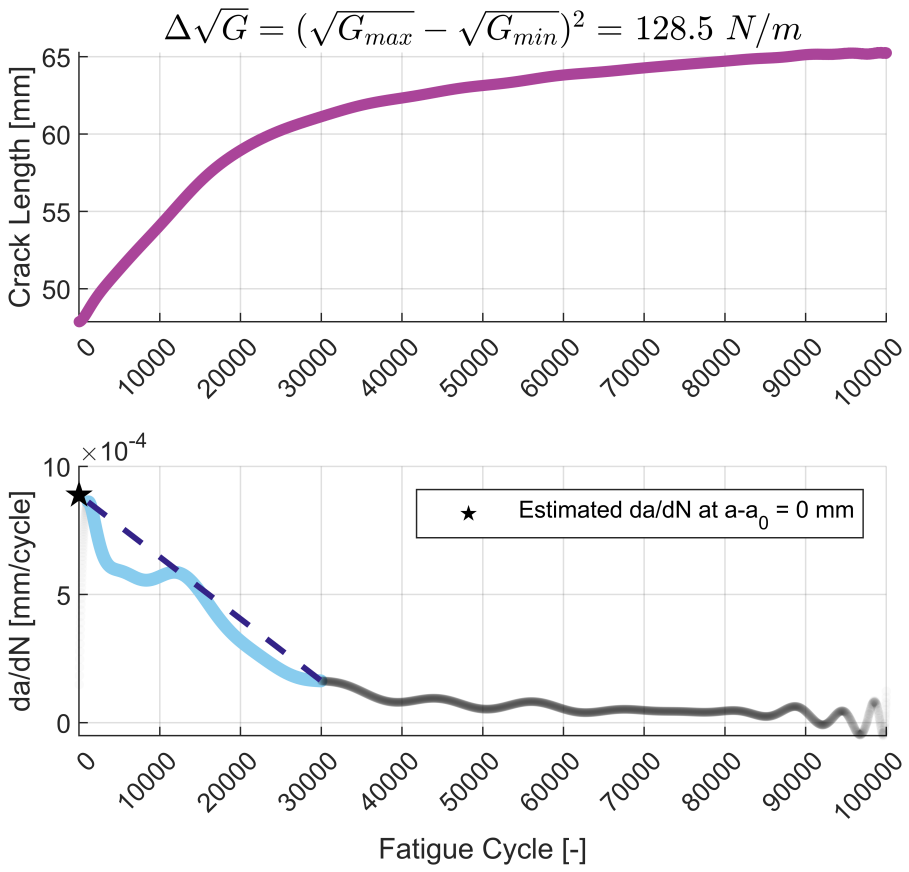
$\Delta\sqrt{G} = (\sqrt{G_{max}} - \sqrt{G_{min}})^2 = 128.5\ N/m$
Crack Length [mm]
65
60
55
50
0
10000
20000
30000
40000
50000
60000
70000
80000
90000
100000
×10-4
da/dN [mm/cycle]
10
5
0
Estimated da/dN at a-a0 = 0 mm
Fatigue Cycle [-]

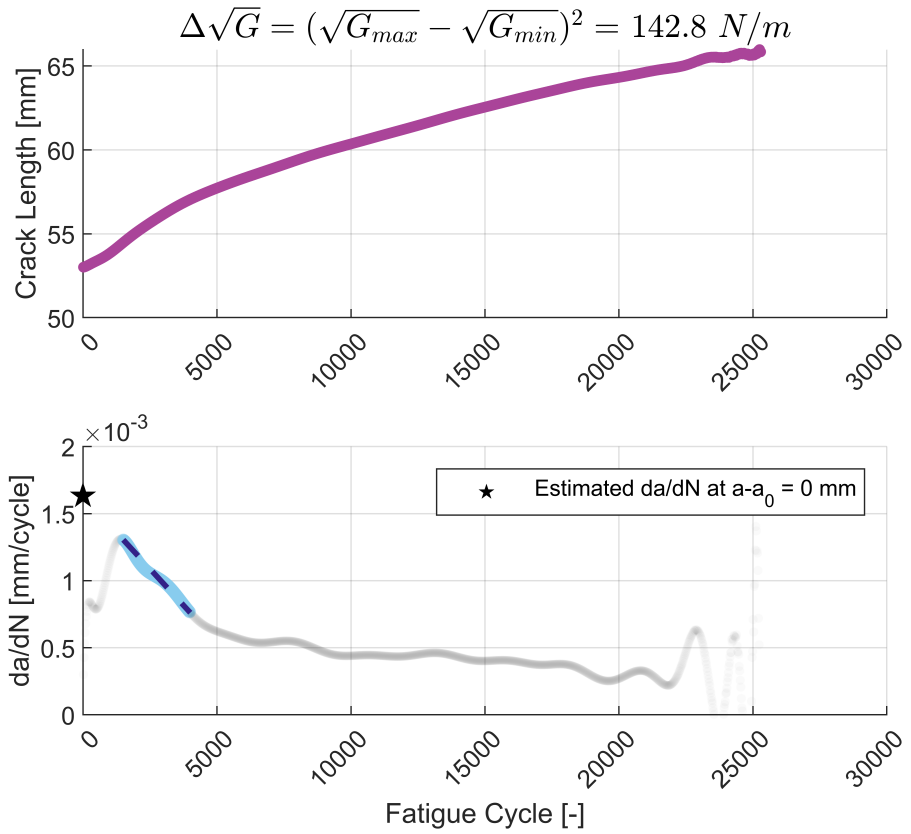
$\Delta\sqrt{G} = (\sqrt{G_{max}} - \sqrt{G_{min}})^2 = 142.8\ N/m$
Crack Length [mm]
65
60
55
50
0
5000
10000
15000
20000
25000
30000
$\times 10^{-3}$
2
1.5
1
0.5
0
da/dN [mm/cycle]
Estimated da/dN at a-a$_0$ = 0 mm
Fatigue Cycle [-]

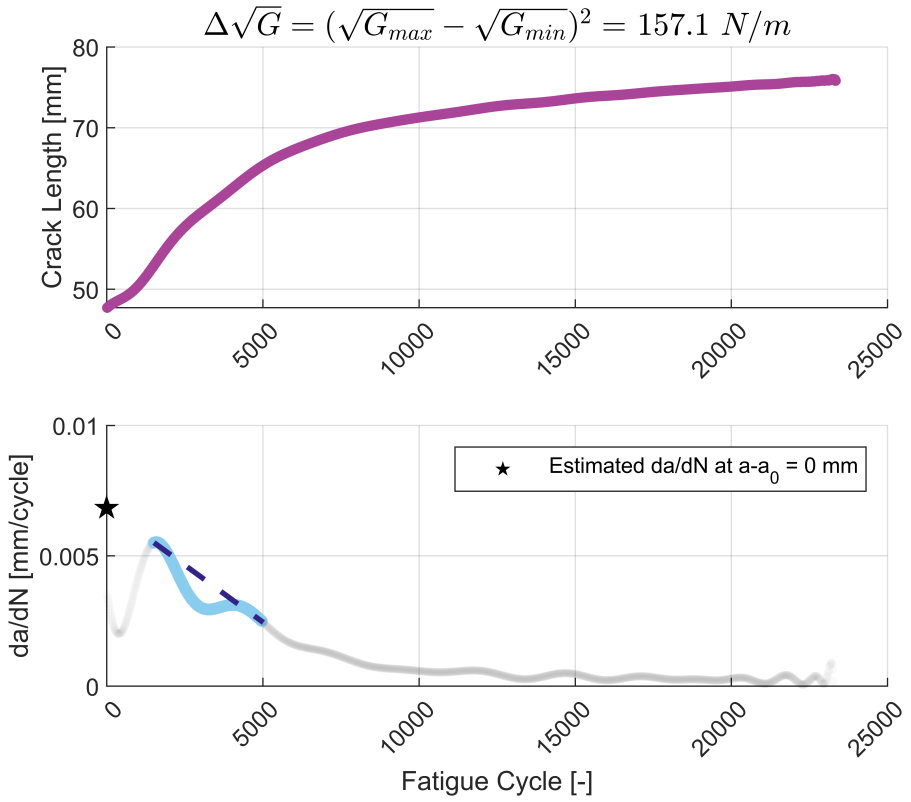
$\Delta\sqrt{G} = (\sqrt{G_{max}} - \sqrt{G_{min}})^2 = 157.1\ N/m$
Crack Length [mm]
80
70
60
50
0
5000
10000
15000
20000
25000
0.01
0.005
0
da/dN [mm/cycle]
Estimated da/dN at a-a$_0$ = 0 mm
Fatigue Cycle [-]

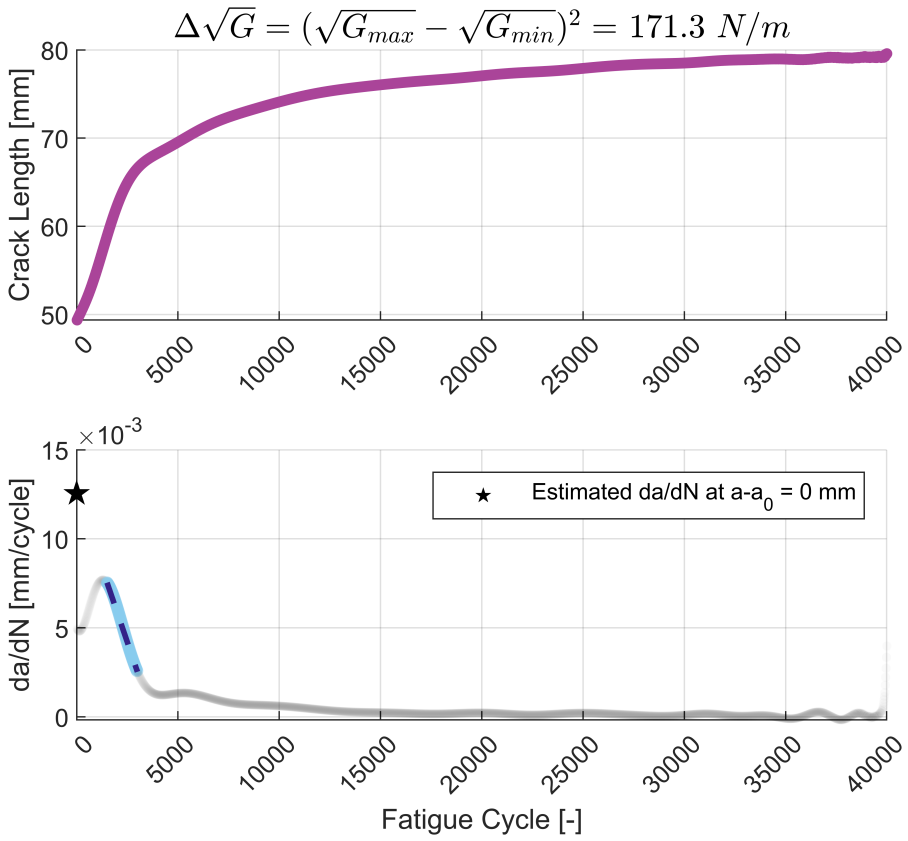
$\Delta\sqrt{G} = (\sqrt{G_{max}} - \sqrt{G_{min}})^2 = 171.3\ N/m$
Crack Length [mm]
80
70
60
50
0
5000
10000
15000
20000
25000
30000
35000
40000
×10-3
15
10
5
0
da/dN [mm/cycle]
Estimated da/dN at a-a0 = 0 mm
Fatigue Cycle [-]

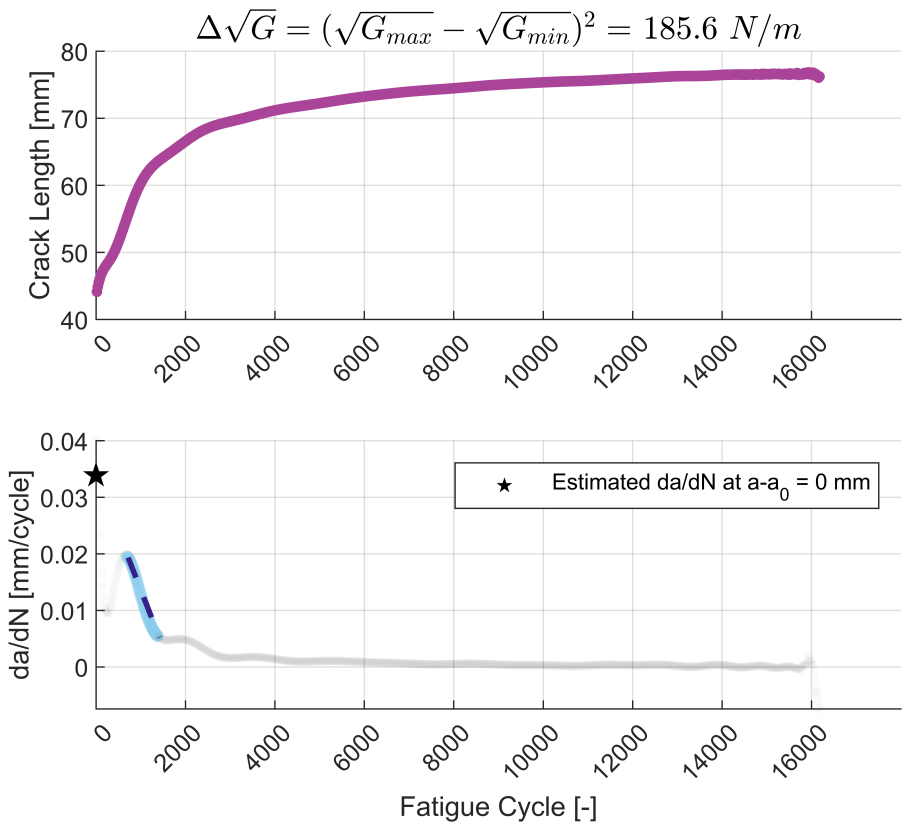
$\Delta\sqrt{G} = (\sqrt{G_{max}} - \sqrt{G_{min}})^2 = 185.6\ N/m$
Crack Length [mm]
80
70
60
50
40
0
2000
4000
6000
8000
10000
12000
14000
16000
0.04
0.03
0.02
0.01
0
da/dN [mm/cycle]
Estimated da/dN at a-a0 = 0 mm
Fatigue Cycle [-]

10

Appendix B

Fibre Cutting - Experimental Results

In this appendix, the results of the experiments involving the fibre cutting method fatigue delamination experiments are presented.

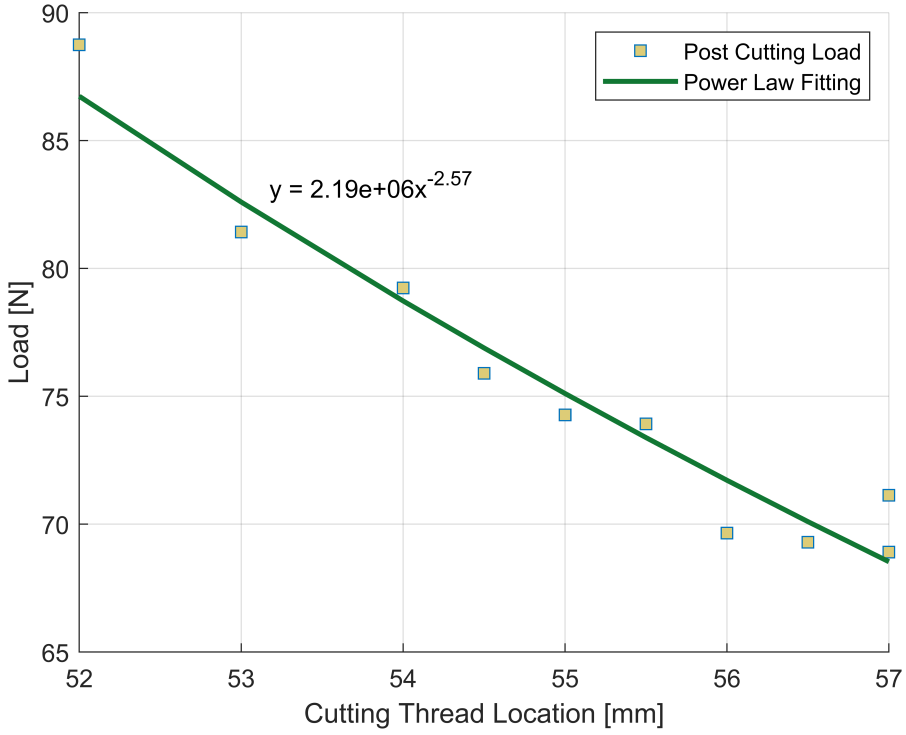

Figure 10.1: Load on the composite specimen versus the cutting thread position for specimen "Vac17".

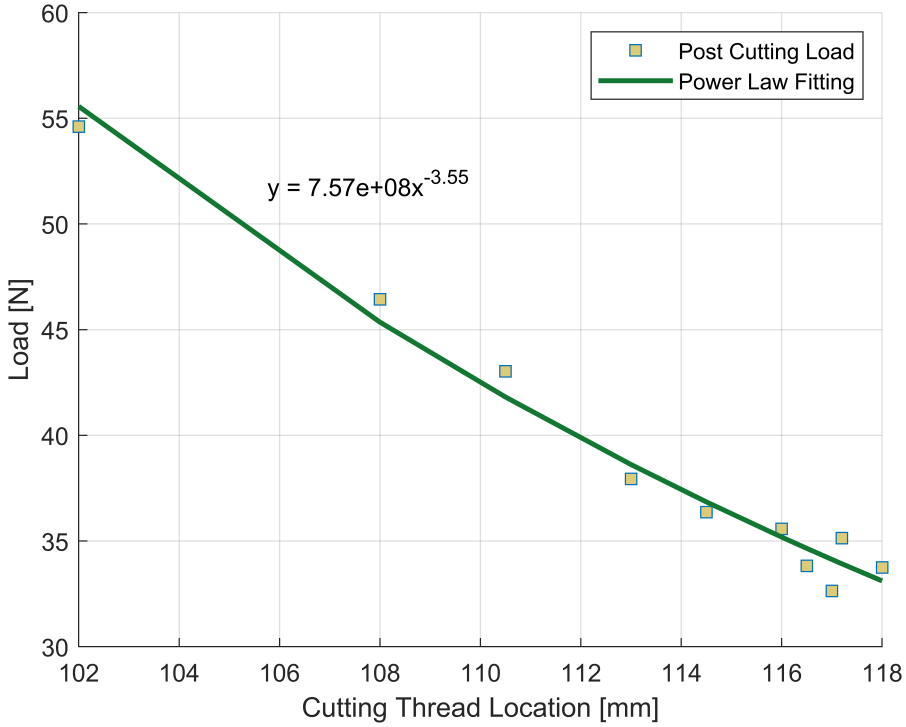

Figure 10.2: Load on the composite specimen versus the cutting thread position for specimen "Vac17".

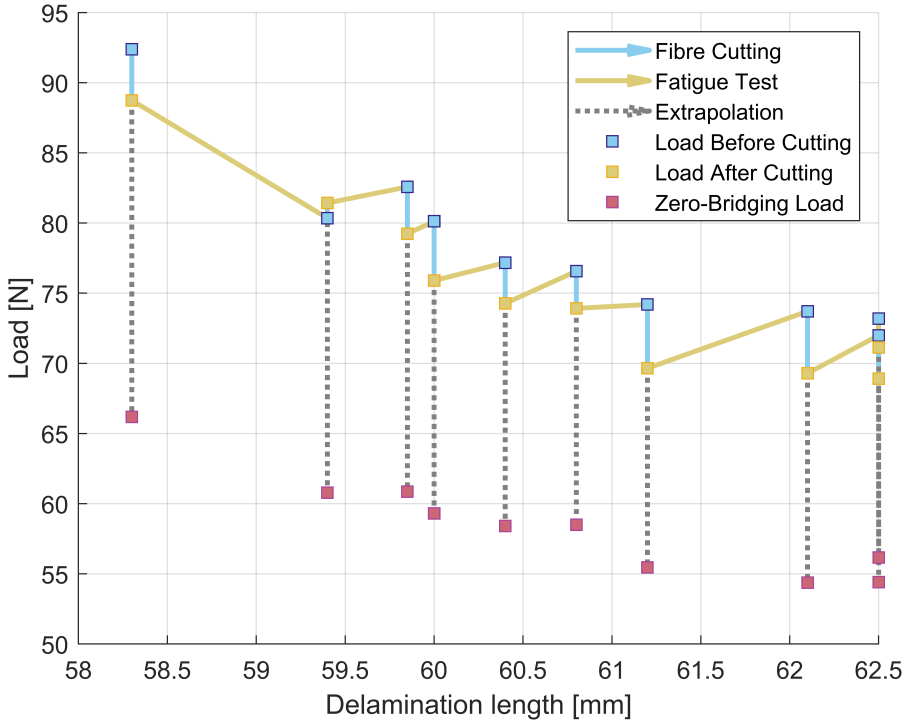

Figure 10.3: Loads on the specimens as a function of the delamination length for specimen "Vac17".

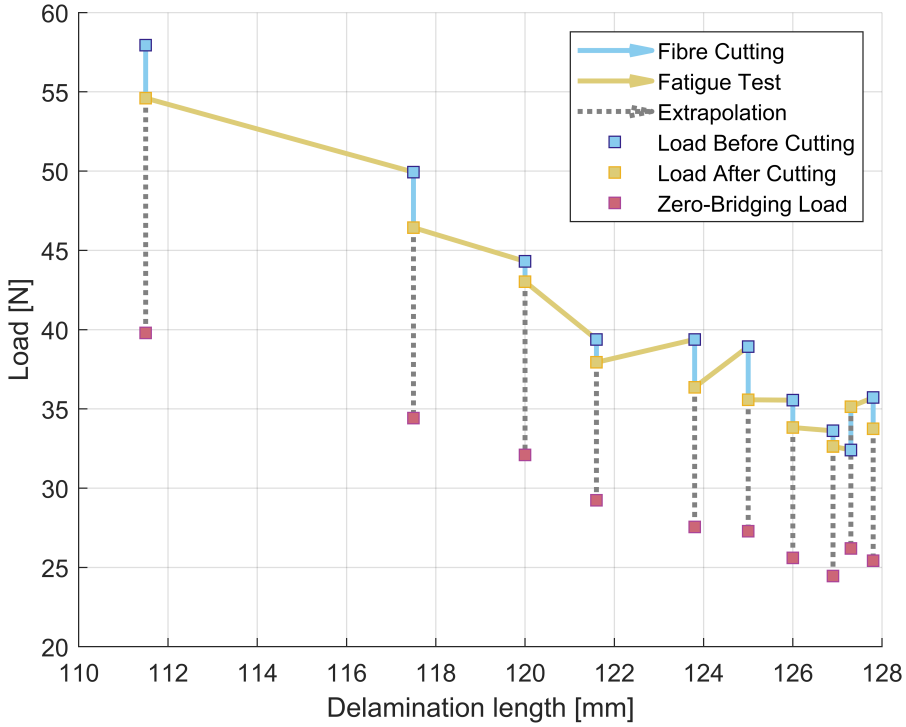

Figure 10.4: Loads on the specimens as a function of the delamination length for specimen "Vac17".

11

Appendix C

Manufacturing Documents

This appendix shows the engineering drawing for a double-cantilevered beam (DCB) composite specimen. It also gives a checklist which was used during the manufacturing of the composite panel from which the DCB specimens were cut.

Checklist:

- ☐ Aluminium mould preparation [H]
- ☐ Apply release agent/film [H]
- ☐ 1st prepreg layer [H]
  - ☐ Cut to size
  - ☐ Debulking
    - ☐ Vacuum bagging
    - ☐ Apply vacuum 3 minutes
- ☐ Prepreg up to mid-plane
- ☐ Apply Teflon strip [H]
- ☐ Remainder of prepreg plies
  - ☐ Debulking after max 3 layers
- ☐ Apply the non-perforated release film
  - ☐ Cut to size (Specimens size)
- ☐ Apply Peel Ply
  - ☐ Cut to size (larger than specimens)
- ☐ Apply breather [H]
  - ☐ Cut to size
  - ☐ Add patch for vacuum coupler
  - ☐ Seal to mould edge with tape
- ☐ Vacuum bagging [H]
  - ☐ Cut to size
  - ☐ Stick to tacky tape around mould perimeter
  - ☐ Make hole for vacuum coupler
  - ☐ Attach coupler counterpart
  - ☐ Test vacuum
- ☐ Curing [H]
  - ☐ Place into autoclave
  - ☐ Cure with correct cycle
- ☐ Demoulding [H]
- ☐ Cutting specimens from plate [H]

Figure 11.1: Checklist for composite panel manufacturing.

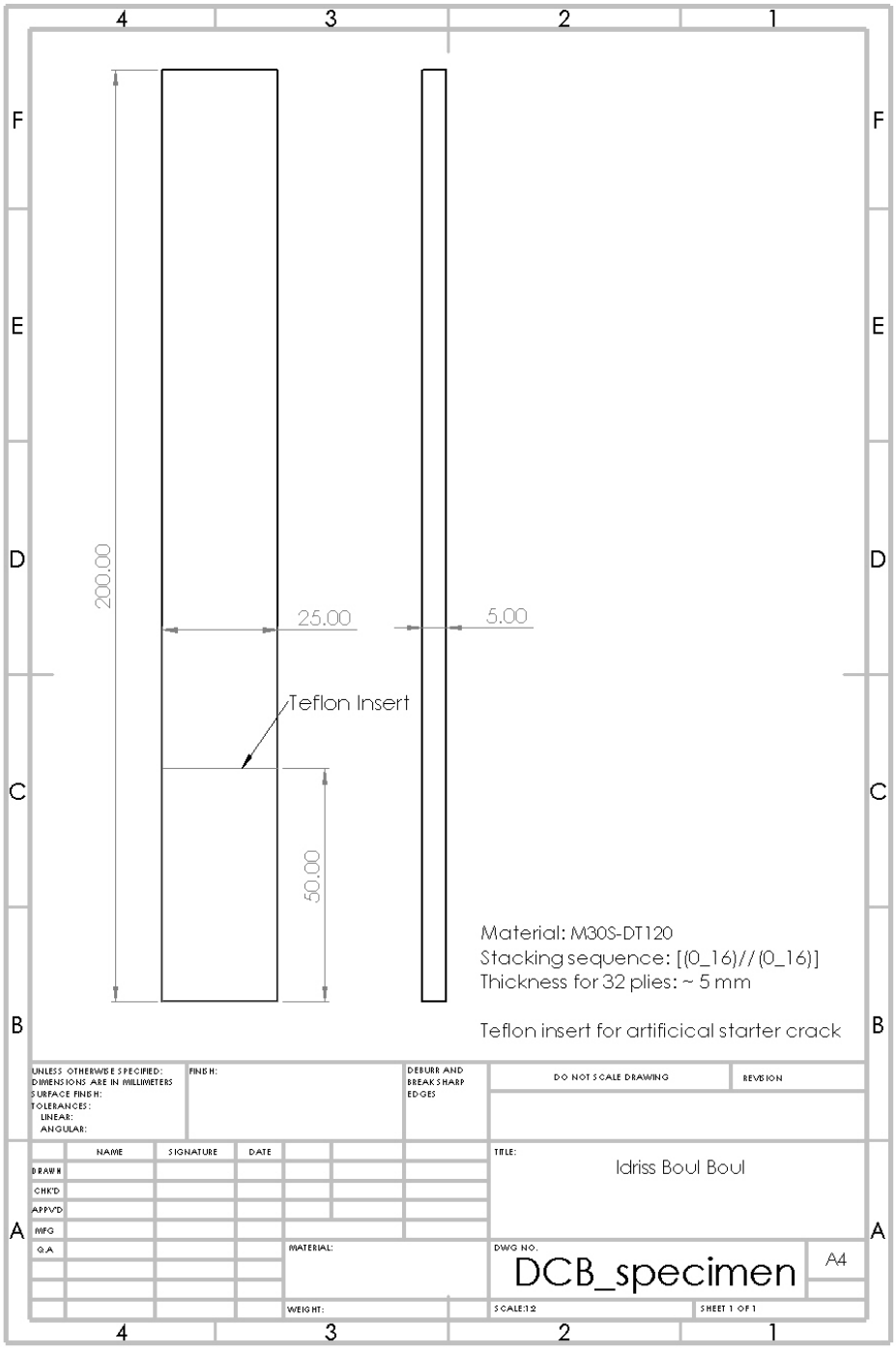

Figure 11.2: SOLIDWORKS engineering drawing of a DCB composite specimen.